Purdue University
Purdue e-Pubs

Open Access Dissertations | Theses and Dissertations

January 2015

Enabling New Functionally Embedded Mechanical Systems Via Cutting, Folding, and 3D Printing

Wei Gao
Purdue University

Follow this and additional works at: https://docs.lib.purdue.edu/open_access_dissertations

Recommended Citation
Gao, Wei, "Enabling New Functionally Embedded Mechanical Systems Via Cutting, Folding, and 3D Printing" (2015). *Open Access Dissertations*. 1300.
https://docs.lib.purdue.edu/open_access_dissertations/1300

This document has been made available through Purdue e-Pubs, a service of the Purdue University Libraries. Please contact epubs@purdue.edu for additional information.

Graduate School Form 30
Updated 1/15/2015

PURDUE UNIVERSITY
GRADUATE SCHOOL
Thesis/Dissertation Acceptance

This is to certify that the thesis/dissertation prepared

By Wei Gao

Entitled

ENABLING NEW FUNCTIONALLY EMBEDDED MECHANICAL SYSTEMS VIA CUTTING, FOLDING, AND 3D PRINTING

For the degree of Doctor of Philosophy

Is approved by the final examining committee:

Karthik Ramani
Co-chair

Raymond J. Cipra
Co-chair

David Cappelleri

C. S. George Lee

To the best of my knowledge and as understood by the student in the Thesis/Dissertation Agreement, Publication Delay, and Certification Disclaimer (Graduate School Form 32), this thesis/dissertation adheres to the provisions of Purdue University's "Policy of Integrity in Research" and the use of copyright material.

Approved by Major Professor(s): Karthik Ramani and Raymond J.Cipra

Approved by: Anil K. Bajaj 10/13/2015

Head of the Departmental Graduate Program Date

ENABLING NEW FUNCTIONALLY EMBEDDED MECHANICAL SYSTEMS VIA CUTTING, FOLDING, AND 3D PRINTING

A Dissertation

Submitted to the Faculty

of

Purdue University

by

Wei Gao

In Partial Fulfillment of the

Requirements for the Degree

of

Doctor of Philosophy

December 2015

Purdue University

West Lafayette, Indiana

To the Almighty.

To my parents Zhimin Gao & Peili Xu, and Aihe Chen for their constant love and support through this journey.

ACKNOWLEDGMENTS

This thesis is the culmination of years of pleasant association with the School of Mechanical Engineering at Purdue University. Foremost, I am very grateful to my advisors Dr. Karthik Ramani and Dr. Raymond Cipra for their guidance, discussions and support throughout the duration of my research.

My sincere thanks also go to my committee members, Dr. David Cappelleri and Dr. C.S. George Lee for their valuable guidance and discussions. I would also like to thank Dr. Rebecca Kramer, Dr. Xinyan Deng, Dr. Thomas Siegmund, Dr. Justin Seipel and Mike Sherwood for helping me throughout the modeling, prototyping and testing.

My discussions with my colleagues, especially Yunbo Zhang, Hairong Liu, Ke Huo, Diogo Nazzetta, Jasjeet Seehra, Sang Ho Yoon, Ayan Sinha, Senthil Chandrasegaran, William Bernstein and Vinayak, on issues of life and research will always be cherished.

To all my friends at Purdue, and particularly, Yunfei, Libo, Yuchen, Pengfei and Lixing, thanks for the good memories and making West Lafayette bearable.

Most of all, I would like to thank my parents, Zhiming Gao and Peili Xu, for their "long distance" care and encouragement. I would never be here without them and without their undying support. Thanks for everything!

TABLE OF CONTENTS

Page

LIST OF TABLES vi

LIST OF FIGURES vii

ABSTRACT xi

1. INTRODUCTION 1
   1.1 The Background of Paper Folding (Origami) & Cutting (Kirigami) 1
   1.2 The Background of Current FDM-Based 3D Printing 3
   1.3 Research Goals and Key Contributions 6
   1.4 Thesis Organization 7

2. FOLDING FRAMEWORK AND DESIGN THEORY OF "KINETOGAMI" 9
   2.1 Related Work of Building Polyhedral Mechanisms 9
   2.2 Basic Structural Units (BSU) 10
   2.3 2D Crease-Cut-Attachment Pattern Synthesis 11
      2.3.1 Tetrahedral BSU patterns 12
      2.3.2 Cuboidal BSU patterns 14
      2.3.3 Prismatic and pyramidal BSU patterns 17
   2.4 Design for Self-Overlapping Avoidance 18
   2.5 Concluding Remarks 18

3. EULERIAN CYCLE, FABRICATION PRINCIPLES AND CONSTRUCTION RULES 19
   3.1 Introduction to Fundamental Layout Planning and Folding Scheme 19
      3.1.1 Finding an Eulerian cycle 20
      3.1.2 Case studies on folding a BSU string to final construct . . . 24
   3.2 Ameliorated Process for Compact Layout Planning 27
   3.3 Design for Intersection-Free Folding Motion 29
   3.4 Representation of Combinatorial & Hierarchical Building Architecture 30
   3.5 Prototypical Results 31
   3.6 Concluding Remarks 35

4. GEOMETRIC AND KINEMATIC INTERPRETATION OF RECONFIGURATION USING TETRAHEDRAL BSU 37
   4.1 The Geometric Synthesis of Reconfigurability 37
   4.2 Mobility Analysis and Discussions 42
      4.2.1 Interpretation using $\Phi - T$ transformation system 42
      4.2.2 Single-loop analysis 44

Page
4.2.3 Multi-loop topological representation and analysis 46
4.3 Concluding Remarks 48

5. MECHANICAL APPLICATIONS DERIVED FROM KINETOGAMI . . 49
5.1 Material Selection for Substrate and Hinge 49
5.1.1 Applying multi-material additive manufacturing 50
5.1.2 Vision of integration of substrate-hinge-electrical network . . 51
5.2 HexaMorph: A Reconfigurable and Foldable Hexapod Robot Inspired by Kinetogami 53
5.2.1 Comparison of HexaMorph and existing modular robotic systems 53
5.2.2 Substrate and electronics design 55
5.2.3 Reconfiguration design and motion control 57
5.2.4 Simulation results of other locomotive gaits 61
5.3 Concluding Remarks 63

6. REVOMAKER: ENABLING FUNCTIONALLY-EMBEDDED PROTOTYPING USING MULTI-DIRECTIONAL 3D PRINTING 65
6.1 Related Work 68
6.1.1 Hollowing and optimizing support generation 68
6.1.2 Multi-axis manufacturing 69
6.1.3 Fast fabrication of 3D objects 70
6.1.4 Printing with functional effect 70
6.2 How RevoMaker Works 70
6.2.1 Objective function 71
6.2.2 Overhang-aware Cuboidization framework 73
6.2.3 Optimization of printing sequence 75
6.2.4 Mechanical implementation behind RevoMaker 77
6.3 Prototypical Results and Use Cases from RevoMaker 80
6.3.1 Sculptural objects 80
6.3.2 Use case 1: Custo “Mice”, customizable mice 82
6.3.3 Use case 2: wind-up Pokémon 83
6.4 Concluding Remarks 84

7. SYSTEM LIMITATION, CONCLUSION AND FUTURE WORK 89
7.1 Conclusion 89
7.2 Future Work 90
7.2.1 Various foldable construction enabled by digital fabrication . 90
7.2.2 Integration of Kinetogami and RevoMaker 91
7.2.3 Modular-based form and function embedded design 92

LIST OF REFERENCES 94

VITA 103

LIST OF TABLES

Table		Page
3.1	Finding an Eulerian cycle inside any structure derived by Kinetogami.	22
3.2	Spatial hinge-hinge relation of a single cubic BSU.	27
6.1	Algorithm of cuboid generation.	72
6.2	Comparison of time and total material reduction using RevoMaker and Ultimaker 2.	81

LIST OF FIGURES

Figure — Page

2.1 Four representative (a: tetrahedral; b: cuboidal; c: prismatic; d: pyramidal) BSUs folded from a single sheet. 11

2.2 (a) 2D - 3D formation of a single tetrahedral unit (a, b, c denote the edges of each triangular facet; α, β, γ denote the adjacent vertex angles of a tetrahedron). (b) Self-overlapping on a unfolded tetrahedral BSU pattern. 12

2.3 (a) Isosceles tetrahedral BSU; (b) Skew tetrahedral BSU; (c) Isos-equal tetrahedral BSU (*red*: overall cuts; *black*: folds; *blue*: the fold that functions as a common hinge; *shaded area*: attachments). 13

2.4 54 unique 2D crease patterns with attaching facets for a cuboidal unit (6 parent patterns with a corresponding child pattern are shown). 15

2.5 Net patterns of cuboidal BSU using 3 different edges as hinges (*red*: overall cuts; *black*: folds; *blue*: the common hinge). 16

2.6 (a) Triangular prismatic BSU; (b) Rectangular pyramidal BSU; (c) Pentagonal pyramidal BSU. 17

3.1 (a) Elementary-single-loop with n basic-structural-units $B_1, B_2, \cdots, B_n$. (b) Multi-loop that contains single and compound hinge joints. 20

3.2 Eulerian cycle generation for a hexagram-like mechanism. 23

3.3 Fabrication and construction rules for building a hexagram-like mechanism. (a) linearly duplicating the single unfolded skew tetrahedral BSU pattern along a strip of sheet. (b) folding each BSU pattern up into a BSU string. (c) threading the BSU string throughout an Eulerian cycle for the overall mechanism. (d) reconfiguring the mechanism among two different configurations. 25

3.4 Fabrication and hinge selection for cubic derivatives. (a) a single folded cube with 6 facets. (b) unfolded cubic pattern and possible hinge-hinge selection on pattern (*orange*: the hinge that couples the previous BSU; *blue*: the hinge that couples the next BSU). (c) 9 variations of different hinge-hinge combination. (d) 4 variations of different mountain-valley folding at the common hinge. (e) a folded ring with 3 cubic BSUs. . . . 26

Figure Page

3.5 Ameliorated processes for a compact 2D pattern layout. (a)-(b) overall pattern planning and arrangement for the skew tetrahedral BSU and cubic BSU (the symmetric green-red-purple areas are the turning areas that fold 3 times). (c) attaching 3 sheets together (top layer remains turning areas, while the rest two layers without the turning areas). (d) sequences of unfolding the rectangular pattern into a linear strip. 28

3.6 Kinematical combinatorics of tetrahedral BSUs. (a) a single-closed-loop containing 3 skew tetrahedral BSUs. (b) a multi-serial-loop containing 6 single-closed-loop. (c) a multi-parallel-loop containing 8 single-closed-loop. 32

3.7 Prototypical Kinetogamic derivatives from 4 BSUs: (a)-(h) constructs using tetrahedral BSUs. (i)-(o) constructs using cubic / cuboidal BSUs. (p)-(q) constructs using prismatic BSUs.(r)-(s) constructs using pyramidal BSUs. 34

4.1 Geometric parameters for determining variation of configuration states. 38

4.2 Prototypical demonstration of fully, limited reconfigurable and rigid-body state: single ring (a) with 3 isosceles tetrahedral BSUs. (b) with 4 isosceles tetrahedral BSUs. (c) with 5 isosceles tetrahedral BSUs. 40

4.3 Thresholds of fully, limited reconfigurable and rigid-body state. 41

4.4 The joint constraint matrix and shape matrix definition in $\Phi - T$ transformation system. 42

4.5 $\Phi - T$ transformation matrices for a skew tetrahedral ring. 44

4.6 Topology graph of the hexagram-like mechanism (42 revolute joints and 36 tetrahedral links). 47

5.1 (a) 3D Printed multi-material sheet. (b) compactly flat-folded configuration. (c) folded into 6 tetrahedral BSUs in a ring. (d) morphed among configurations. (e) flexure hinge. 50

5.2 Different substrate-hinge fabrication: (a) carbon fiber composites. (b) tile/elastomer assembly. (c) tile/fabric assembly. (d) multi-material 3D printed. (e) interlock assembly. (Figures (a) and (b) provided by Professor Rebecca Kramer). 52

5.3 A foldable and reconfigurable starfish-like robot, “HexaMorph”. (a) standing configuration. (b) ”huddled” towards the center. (c) fully-deployed configuration. 54

5.4 Electronics layout on a single skew tetrahedral BSU pattern. 55

Figure Page

5.5 (a) Overall 2D pattern with all the electronic components. (b) system pipeline and wireless control strategy. 56

5.6 Sequences of self-deploying motion. (a)-(b) moves from initial standing configuration to the fully-deployed configuration. (c)-(d) closes up to a smaller envelope volume. 58

5.7 Sequences of locomotive squirming motion. (a-c) opens its body till all limbs are stretched. (c-d) drives one limb while anchoring another one in order to squirm. 59

5.8 (a) The displacement of the robot front tip "A". (b) the velocity of the robot front tip "A". 60

5.9 Squatting and rising gait proposed for HexaMorph. (a) three alternative limbs flip while the other three stretch. (b) six limbs reach the same configuration to lower the robot height. (c) previous flipped and stretched limbs alternate with each other and lift the robot height. 61

5.10 Inchworming gait proposed for HexaMorph. (a) driving hindlimbs forward while anchoring the forelimbs (robot body contracted). (b) moving forelimbs forward while anchoring the hindlimbs (robot body stretched). (c)-(d) converting the motion direction by rearranging the function of each limb. 62

5.11 Slithering gait proposed for HexaMorph. (a) driving the right middle limb to linearly slide forward. (b) alternating the left middle limb to slide forward. 63

6.1 For instance, in order to print a sphere, traditional material extrusion process (a) generates sacrificial material to support printed overhanging features, and (b) has limited printing space if one intends to print around an enclosure. 66

6.2 (a)-(d) revolving a cuboidal base about the out-of-plane central axis and printing four partitioned geometries around the base. A pair of handles are added to the opposite facets, allowing the cuboid to be gripped for the next run of rotation. (e)-(g), revolving the cuboid about the in-plane central axis and printing the rest two partitioned geometries. (h), snapping off two extra handles when the print is completed. 67

6.3 (a) Inapplicable cases where overhanging features can not be largely reduced. For instance, (a) a 3D shape with high topological genus such as a ring of genus one, or (b) with long and branched protruding features such as a tree. 73

6.4 (a) sampling the unit vector $\mathbf{w}_i$ (b) sampling the unit vectors $\mathbf{u}_i$ and $\mathbf{v}_i$. 74

Figure Page

6.5 (a) partitioning based on above-facet regions and corner regions (b) printing sequence 1 generates support material (c) printing sequence 2 generates no support material. 76

6.6 We extend a standard low-cost FDM printer, UltiMaker2, with mechanical, electrical and pneumatic devices. 77

6.7 (a) a flattened cuboidal net pattern using laser-cut facets and slots; (b) a folded cuboid. 78

6.8 Each gripper from both sides has 3 degrees-of-freedom: (1) translation to fixate and release the cuboidal base, (2) rotation to revolve the cuboid facets around, and angular motion to apply gripping force to the handles. 80

6.9 (a)Cuboidal generation and partitioned results of a small Hexacronic Icositetrahedron with the "UIST 2015" logo. (b)-(g) printing 6 partitioned geometries intermittently around a revolving cuboidal base using our method. (h) final print. 85

6.10 first row: visualization of support generation for a sphere ball, Max Planck, French bulldog and Mickey Mouse head using existing FDM printing process in Ultimaker2 (the model is oriented where less support structures are created. second row: partitioned results of each model. third row: prototypical results of each model. 86

6.11 (a) user interaction to tailor the shape of his/her ergonomical-fitting mouse using Play Doh. (b) 3D scanning (c) hollowing the digital model with slot-cuts to separate out three button areas. (d) six partitioning geometries around an embedded cuboid. (e) enclose buttons, printed circuit board and optical components inside the laser-cut cuboid. 87

6.12 Revomaker prints the partitioned geometries around the cuboidal enclosure and delivers a functional and ergonomical computer mouse right after printing. 87

6.13 shows (a) support generation for Bulbasaur (b) six partitioning geometries around an embedded cuboid. (c) pre-assembling the wind-up motor and batteries onto flattened laser-cut facets and close the cuboid as a printing base. (d) printing the Bulbasaur shape around the cuboid. (e) winding the Bulbasaur up to trigger tail-waggling and eye-blinking. 88

ABSTRACT

Gao, Wei. Ph.D., Purdue University, December 2015. Enabling New Functionally Embedded Mechanical Systems via Cutting, Folding, and 3D Printing. Major Professors: Karthik Ramani and Raymond J. Cipra, School of Mechanical Engineering.

Traditional design tools and fabrication methods implicitly prevent mechanical engineers from encapsulating full functionalities such as mobility, transformation, sensing and actuation in the early design concept prototyping stage. Therefore, designers are forced to design, fabricate and assemble individual parts similar to conventional manufacturing, and iteratively create additional functionalities. This results in relatively high design iteration times and complex assembly strategies.

Stemmed from an ancient paper craft originating from Japan, Origami has been naturally contextualized in a variety of applications in the fields of mathematics, engineering, food packaging, and biological design. The computational and manufacturing capabilities today urge us to develop significantly new forms and processes of folding to create "functional enclosures", where full functionalities can be easily pre-synthesized and pre-embedded on flat. Furthermore, The external skin shapes are allowed to be "coated" over enclosures using 3D printing process. In the first phase of this thesis, by introducing line cuts into crease patterns and creating folded hinges across *"Basic Structural Units" (BSUs)*, typically not done in origami, we achieve a new multi-primitive folding framework using tetrahedral, cuboidal, prismatic, and pyramidal components, called "Kinetogami". The mathematical and folding theories are established to construct closed-loop(s) polyhedral mechanisms with multi-degree-of-freedom and self-deployable characteristics using a single sheet of material. The explicit 2D fabrication layout and construction rules are visually parameterized for geometric properties to ensure a continuous and intersection-free folding motion. Next, the study presents the prototypical results from a variety of foldable polyhedral mech-

anisms to the locomotive hexapod robots, using the tetrahedral module derived from Kinetogami. We also investigate the kinematic interpretation of reconfiguration between the folds and material selection of substrates and hinges. The last phase of this thesis focuses on combining functionally-embedded design along with the shape creation by embedding components during 3D printing. By modifying a standard low-cost FDM printer with a revolving and foldable cuboidal platform, and printing partitioned geometries around cuboidal facets, we achieve a multi-directional additive prototyping process, called "RevoMaker". A wide range of customized and fully-functional product prototypes, such as computer mice and wind-up toys are demonstrated in our prototyping results. Therefore, via integrating dimensions of folding, cutting and 3D printing, we achieve a shape-to-form-to-function design and prototyping framework that provides affordance for a new genre of functionally-embedded mechanical products and systems.

1. INTRODUCTION

The process of mechanical prototyping not only includes designing individual parts, but also includes encapsulating the integrated functionalities such as mobility, articulation, transformation, sensing and actuation through assembly. For instance, creating a prosthetic arm from scratch and prototyping enclosures can be an iterative and daunting task. It requires 3D modeling, molding/tooling design, physical assembly and calibration to be integrated seamlessly to fit all individual components inside an exterior shell. Besides, traditional computer-aided design tools are highly procedural and usually require elaborate training and practice before they can be effectively utilized. As a result, it is cognitively too difficult for novice designers, who lack specialized knowledge to technically design and prototype functionally-embedded mechanical systems.

Fortunately, current origami-inspired design theories and methodologies provide an elegant and simple folding strategy using flat surfaces to create foldable joints [1,2] and transformable 3D structures [3, 4]. In addition, the priori foldable platforms and voids can be utilized to embed functionalities such as enclosing circuits, sensors and motors, etc. These open the opportunities for the democratization of fabricating functional mechanisms, assemblies, smart structures and robots [5–8].

1.1 The Background of Paper Folding (Origami) & Cutting (Kirigami)

Origami originally was developed as a paper craft in the 17th century AD that allowed the diversity of representative 3D objects with individual unit arrangements and explicit folding processes from 2D sheets of paper. Artistic origami designs reveal the rudimentary characteristics of paper folding: inexpensive, lightweight, compact and combinatorial. During the last 40 years, “Why’s, What’s and How’s” of

different origami tessellations and structures have been geometrically and symbolically described by the underlying mathematical rules governing the creases, such as flat foldability [9] and "folding any polygonal shape" [10]. With the marriage of computational geometry and origami, systematic studies have been carried out recently (TreeMaker [11], Origamizer [12] and foldable-programmable-matter-editor (FPME) [13]).

Modern origami explorations can be generally classified into two categories: artistic compositions and systematic tessellation patterns. The former provides a guide to the origami artists while allowing the artist to express his or her own personality through interpretation and variation. Like a musical composer, the origami folder works with patterns and relationships within the paper and arranges those patterns into something that sparks from human's aesthetic, spontaneity and serendipity. On the other side, mathematicians, physicists and engineers have been seeking to design the systematic crease and tessellation patterns applied in multidisciplinary fields. The complexity and richness of the folded structures arise from simply repeating sub-patterns of crease lines and symmetries of polygonal shapes.

Our analysis of past work in origami and folding structures shows that its applications are limited by the following characteristics: (1) A number of developments have the typical goal of achieving a desired folding-state that renders functionality, i.e., the extended solar panel or the wrapped gift package. (2) In the previous work, continuous skin-based models and patterns are achieved by task-oriented operations (Miura folding [14] as well as patterns represented in airbag [15, 16], stent [17], sandwich core structures [18], honeycomb core structures [19, 20] and cartons [21]). (3) Recent advances in modular origami [22] [23] for polyhedral models use separate pieces of paper for each component or function.

Kirigami, as a variation of origami, originates from the art of paper cutting using scissors and knifes (from Japanese "kiru" refers to cut and "gami" means paper). Typically, kirigami starts with a folded base and then allows the cutting to achieve pictorial and figurative 2D patterns. Recently, the work of modular kirigami [24]

use the identical paper modules and assembles them into larger and more complex symmetric sculptures. Each paper module, however, is cut individually and separately while the design rationale of how and where to connect these modules happens in the late assemblage stage. Like the modular origami, the designers still face the uncertainties of building combinatorial systems embedded inside a single folded sheet, and of placing material where they desire it.

1.2 The Background of Current FDM-Based 3D Printing

Current additive manufacturing (AM) technologies, also referred to 3D printing, provide the freedom to a designer in the layer-wise realization of fabricating complex geometric shapes. The term additive manufacturing was ultimately chosen by the ASTM F42 committee as it clearly distinguishes the processes from subtractive manufacturing techniques wherein material is removed from a workpiece (e.g., cutting, milling, grinding) [25]. The significant amount of recent interest and investment towards AM technologies does not come as a surprise, as this layer-wise additive method is an elegant concept that can build complex shapes using a wide variety of materials. The reducing cost of programmable controllers, lasers, ink jet printing and computer-aided design (CAD) software has democratized the design process, allowing individuals to utilize, tinker with, and improvise these technologies. The main market driver for such systems has been consumers and industries that rely on lowmedium fidelity prototyping in the early stages of product design. Several startup companies are creating innovative and low-cost 3D printers for thermoplastics. As a result, plastics-based 3D printing has captured the imagination of the general public through platforms such as Do-It-Yourself (DIY) and the Maker Movement. Supply chain and retail businesses such as Staples, Shapeways and Sculpteo are taking advantage of the popularity of such platforms and bringing commercial printing and shipping services directly to customers. These companies are also supporting hobbyist communities by providing them with simple online 3D modelers allowing them

to create or tailor designs and turn them into customized products. Many roadmaps and reports have been carried out recently, including NIST roadmap [26], America Makes roadmap [27–30], CSC report [31], Wohlers reports [32–34], etc., to provide research and industry perspectives on AM technologies.

From the industry perspective, AM technologies have the potential for significantly impacting traditional production models in terms of industrial machinery, assembly processes, and supply chains. For example, multi-nationals such as General Electric (GE) are investing in research for commercializing metal-based AM technologies for remanufacturing. If successful, such technologies can simplify their manufacturing value chain by giving them independence from third-party suppliers, improve performance, and extend useful life of their engines. AM can also positively impact smaller corporations and end-customers by changing their roles into self-sufficient designers and manufacturers that can develop innovative products and production systems. The rapid proliferation of AM technologies is driven by the increase in the variety of materials, low-cost machines, and potential for new application areas. This has resulted in a lack of fundamental design guidelines or standardization of best practices. For example, the same digital input (3D model) may give rise to parts that can be different in surface finish and geometric torlerance. These effects are due to differences in manufacturing techniques (material extrusion, jetting, deposition, curing, lamination, etc.), materials (thermoplastics, photopolymers, epoxy resin, metal powder, conductive composition, etc.), and the geometric positioning/orientation of the geometries. As a result, designers often waste building and support material due to the multiple trial-and-error iterations required for fixing unqualified feature requirements, surface resolution and clearances of mechanical parts and assemblies. The use of electronics and circuits at macro- and micro-levels, both by embedding and integrating materials and sensors, is another trend that adds functionality, but threatens to complicate the design process for AM technologies.

When employing AM, this complexity comes at no additional cost, as there is no need for additional tooling, re-fixturing and increased operator and assembly exper-

tise. Other traditional manufacturing processes, including formative techniques (e.g., pressing, casting, forming), impose additional design constraints to those inherited by the subtractive techniques used to fabricate the required tools and patterns. Fundamentally, AM technologies impose only a few constraints and thus provide a designer the ability to selectively place (multi-)material precisely where it is needed to achieve the designed functionality.

Modern 3D printing techniques have their foundations in four key patents: vat photopolymerization, powder bed fusion, material extrusion, and binder jetting [35–38]. In the early 1990s, Kruth [39] categorized various additive manufacturing processes from three perspectives: liquid-based, powder-based and solid-based systems according to different material creation; and direct-3D and 2D-layers techniques according to different shape building. A whole family tree and AM process classification, including research and commercial methods, were presented by Helsinki University of Technology [40] and in the German production process standard (DIN8580) and (DIN8581). A functional classification schema of AM systems has also been presented by Williams [41]. Most recently, ASTM International has classified AM technologies into seven categories: (1) material extrusion, (2) powder bed fusion, (3) vat photopolymerization, (4) material jetting, (5) binder jetting, (6) sheet lamination, and (7) directed energy deposition [25]. Among these, the inexpensive and flexible extrusion systems are gaining an extensive popularity among the DIY crowds. The method, popularly referred to as Fused Deposition Modeling (FDM), generates layers by mechanically extruding molten thermoplastic material (e.g., ABS or PLA) onto a substrate.

Current FDM-based 3D printing is more suitable for fabricating the decorative models, design concept prototypes and customized products. Even though by pausing the build, one can embed foreign objects into a priori designed voids, which are then fully encapsulated into the part once printing is resumed [42–44]. Placing functional enclosures ahead on the print bed, unfortunately, will not allow continuous layer-wise fabrication since the printhead intersects with the enclosure and any geometry

beneath is infeasible to print. How to seamlessly and quickly combine functional design along with the shape creation becomes our motivation to design enabling methods and technologies via folding, cutting and printing.

1.3 Research Goals and Key Contributions

In this thesis, we combine the elegant art forms using the dimensions of cutting, folding and 3D printing to create foldable polyhedral enclosures. We use these enclosures as the foundation of our thesis to design functional prototypes since the functionalities can be pre-embedded easily and directly onto the flat, and then encapsulated inside when folded.

The main research goal in this thesis is twofold: (1) we connect a series of polyhedral building blocks (basic structural units) to build up closed-loop(s) polyhedral mechanisms that create the complexity of reconfiguration. This multi-primitive folding framework is called "Kinetogami". (2) We further enhance the shape complexity by 3D printing the skin geometries around each polyhedral primitive. A multi-directional additive prototyping process, called "RevoMaker", is proposed to produce direct out-of-the-printer functional prototypes.

In this thesis, we discuss the schemes of folding and prototyping framework for achieving the following key contributions:

1) We designed a class of elementary basic-structural-units (BSU), including tetrahedral, cubic, prismatic and pyramidal components, in order to fold up self-deployable polyhedral mechanisms using single sheet of material;

2) We synthesized the overall scheme of 2D crease-cut-attachment patterns for each BSU, and developed a generalized algorithm for finding an Eulerian cycle throughout each BSU and constructing single and multi-loop structures / mechanisms using tetrahedral BSU. We further designed a geometric predictor to achieve different stage of reconfiguration, and investigate the overall topological representation and mobility boundary of the mechanisms.

3) We developed a locomotive hexapod robotics, called HexaMorph. In terms of manufacturability, our design methodology enables the robot fabrication and assembly in 2D, folding and reconfiguring in 3D.

4) We developed a multi-directional 3D printing system that is capable of inherently reducing build and support consumption. The system enables the design space of 3D printing to go beyond simple parts using the volume within the 3D printed shape itself to encase the direct-out-of-printer functionalities.

Hence, by synthesizing and modifying the geometric features embedded in the 2D crease-cut-attachment patterns, we hierarchically change the kinematic performance of the single / multi-closed-loop reconfigurable polyhedral mechanisms to be folded, and provide the capacities for rendering different functionalities by changing locking/unlocking, and locomotive behaviors from a mechanical engineering design point of view. An augmented additive prototyping system using low-cost FDM printer is further developed to print exterior geometries around foldable primitive volumes.

1.4 Thesis Organization

We begin this thesis by discussing previous research, current state-of-the-art and limitations of folding, cutting and printing techniques. Chapter 2 introduces the reader to design and folding theories of building the basic structural units (BSU). In Chapter 3, the explicit 2D fabrication layout and construction rules are visually presented for geometric properties to ensure a continuous folding motion free of intersection. Chapters 4 and 5 discuss the prototypical results and kinematic interpretation of mechanisms derived from Kinetogami. Chapter 6 demonstrates a different material selection using additive manufacturing and the locomotive robotic application using skew tetrahedral units. In Chapter 7, we further explore a multi-directional 3D printing process that creates direct out-of-the-printer functional prototypes. Finally, Chapter 8 proposes our future work and the potential mechanical systems to be designed with our functionally-embedded prototyping framework. It is our hope that

these chapters will serve to motivate the research that is discussed in the proceeding chapters of this thesis.

2. FOLDING FRAMEWORK AND DESIGN THEORY OF "KINETOGAMI"

In this chapter, we discuss a new folding framework, called "Kinetogami", which encompasses multi-primitive, structural and foldable units including tetrahedral, cuboidal, prismatic, and pyramidal BSUs. We coined the word "Kinetogami" inspired by the Greek root "Kinetikos" and the Japanese word "kami", literally meaning that the polyhedral mechanisms and structures in motion are made by a single sheet of paper. With regards to any Origami design, it is necessary to understand the design motivation as well as corresponding crease patterns and folding sequences. To this end, we discuss the following topics on the fundamentals of "Kinetogami": (1) related work of constructing polyhedral mechanisms using traditional methods, (2) our design theory of folding multi-primitive units including tetrahedral, cuboidal, prismatic, and pyramidal BSUs, (3) synthesis of 2D crease-cut-attachment for each BSU, and (4) design rationale to avoid self-overlapping facets on the 2D pattern.

2.1 Related Work of Building Polyhedral Mechanisms

Polyhedral mechanisms are spatial mechanisms where vertices, edges and facets of the polyhedra are embedded into fundamental kinematic linkages and closed chains [45]. The pioneering work of the expandable polyhedral structures, named "Jitterbug transformers, was developed by Verheyen [46,47]. The proposed polyhedral structures contain rigid pairs of polygonal elements in a double-layer framework. Later on, a number of mechanisms with various polyhedral geometries were carried out such as "Heureka-polyhedron [48], "Hoberman switch-pitch ball [49], Platonic, Archimedean and Johnson solids [50,51]. In physical kinematic linkage design, each link is modeled as a rigid body and these individual links are jointed together in closed form(s) to provide a particular determinate motion. In this thesis, we specifically investigate

sets of periodic polyhedral pairs with reflectional symmetry and adjacent hinge axes with skew perpendicularity in the kinematic chain(s). Recent literature has shown and proved that a linear chain of polygonal or polyhedral modules can be folded into any arbitrary 3D shape [52, 53] and reach many general families of hinged dissection [54, 55].

In an analogous manner, we fold and close polyhedral facets to construct *"Basic Structural Units" (BSUs)* in a way that each individual polyhedron can be represented as a rigid link while maintaining the hinge axes orientations. These folded "links" are structural with empty volume enclosed instead of solid rods. The resulting mechanisms can reconfigure and manifest different functions afforded by the new configuration. Our design methodology allows manufacturing in 2D and folding in 3D. Hence, by synthesizing and modifying the geometric features embedded in the 2D crease-cut-attachment patterns, we hierarchically change the kinematic performance of the single / multi-closed-loop reconfigurable polyhedral mechanisms to be folded. To the best of our knowledge, such hierarchical and multi-scale mechanism constructions through folding and reconfiguration have not been envisioned or explored earlier.

2.2 Basic Structural Units (BSU)

In the past, the nature of paper sheets was deterministic with regard to the conventional rules of origami such as when folding without cutting. We strive towards exploring the heterogeneous, structural and reconfigurable characteristics of paper by allowing preplanned cuts with crease patterns and creating folded hinges across basic structural units, typically not done in Origami.

Generally speaking, a BSU consists of a pair of mirror-image polyhedra coupled with a common hinge. Furthermore, the BSUs can be folded and strung up from extending crease patterns laterally on a single flat sheet of paper. Here, we demonstrate

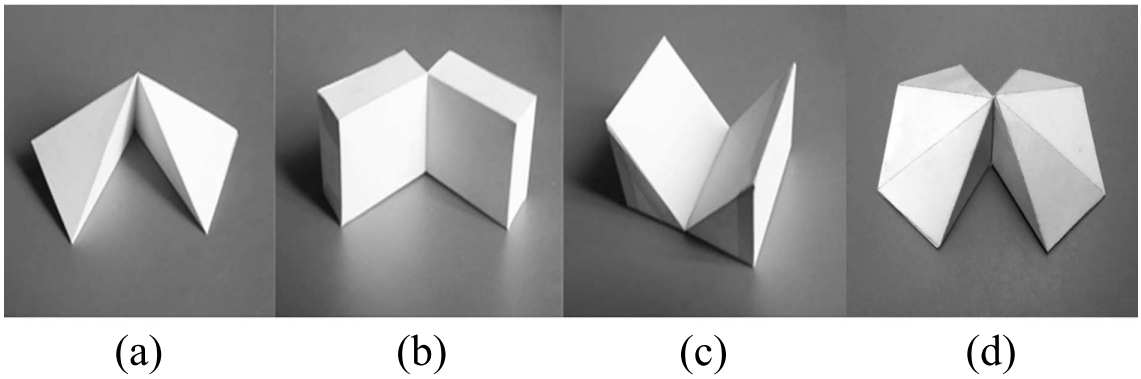

Figure 2.1. Four representative (a: tetrahedral; b: cuboidal; c: prismatic; d: pyramidal) BSUs folded from a single sheet.

four representative BSU's: tetrahedral, cuboidal, prismatic and pyramidal (shown in Fig. 2.1) stemming from the folding-cutting-joining processes on 2D sheets.

The BSU folding approach provides advantages such that: 1) The hinges are inherently embedded as the creases on the 2D pattern. Hence, no assemblages of separate joints are needed to construct the mechanism. 2) The internal space inside each BSU can be utilized for added functions, such as enclosing electronic and battery components for actuation. 3) Affording opportunities for planning anisotropic material properties on a unfolding pattern while the reconfigurability in mechanisms reorients the material and structure and thereby changes functionalities.

2.3 2D Crease-Cut-Attachment Pattern Synthesis

In our work, non-deformable paper sheets are used to construct the basic structural units. We model the creases as revolute joints (hinges), the uncreased facets as polyhedral surfaces and closed-form surfaces as component links. Line-cuts are necessitated for silhouetting the unfolded pattern of each polyhedral linkage and the attachments on each unfolded BSU pattern are considered as the post-processing to close physical volumetric unit as a rigid body.

2.3.1 Tetrahedral BSU patterns

Four triangular facets and six edges comprise a tetrahedral unit. In order to form a closed tetrahedron, each set of unfolded triangle patches needs to maintain (a) the edge-length consistency: any side length of each triangle must agree with the one to be joined from the other three triangles, respectively (i.e., in Fig. 2.2 (a): a=a', b=b', c=c'), and (b) the vertex-angle consistency: the sum of angles spanned by adjacent edges emanating from the vertex must be less than 2π, i.e., $\alpha + \beta + \gamma < 2\pi$. This arises from the fact that if the sum is equal to 2π, a tetrahedron converts to a plane; and if greater than 2π, a tetrahedron is not formable.

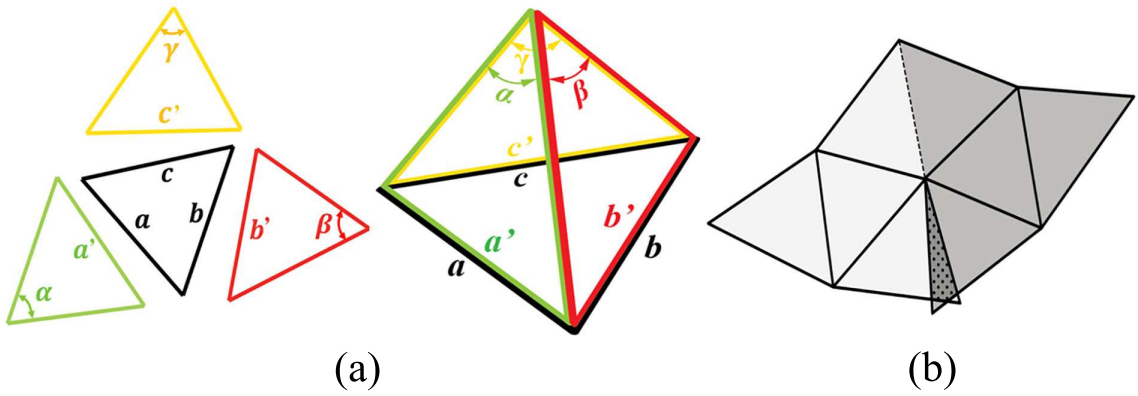

Figure 2.2. (a) 2D - 3D formation of a single tetrahedral unit (a, b, c denote the edges of each triangular facet; α, β, γ denote the adjacent vertex angles of a tetrahedron). (b) Self-overlapping on a unfolded tetrahedral BSU pattern.

Coupled mirror-image tetrahedra with a common hinge are labeled as a tetrahedral BSU. In general, while flattening each BSU, single paper consumption requires none of any two neighboring facets overlaps upon each other (dotted areas in Fig. 2.2 (b)). By unfolding a single polyhedral unit, we allow only 2 hinge edges on the pattern such that one hinge connects to the previous unit and the other connects to the next unit. Therefore, we predesign the hinge edges in a parallel manner and the unfolding net of each current unit is in between the adjacent hinges. Given that BSUs with

reflectional symmetry are periodically chained together, we are guaranteed to avoid self-overlapping pairs of adjacent facets after opening polyhedral BSUs into a 2D plane.

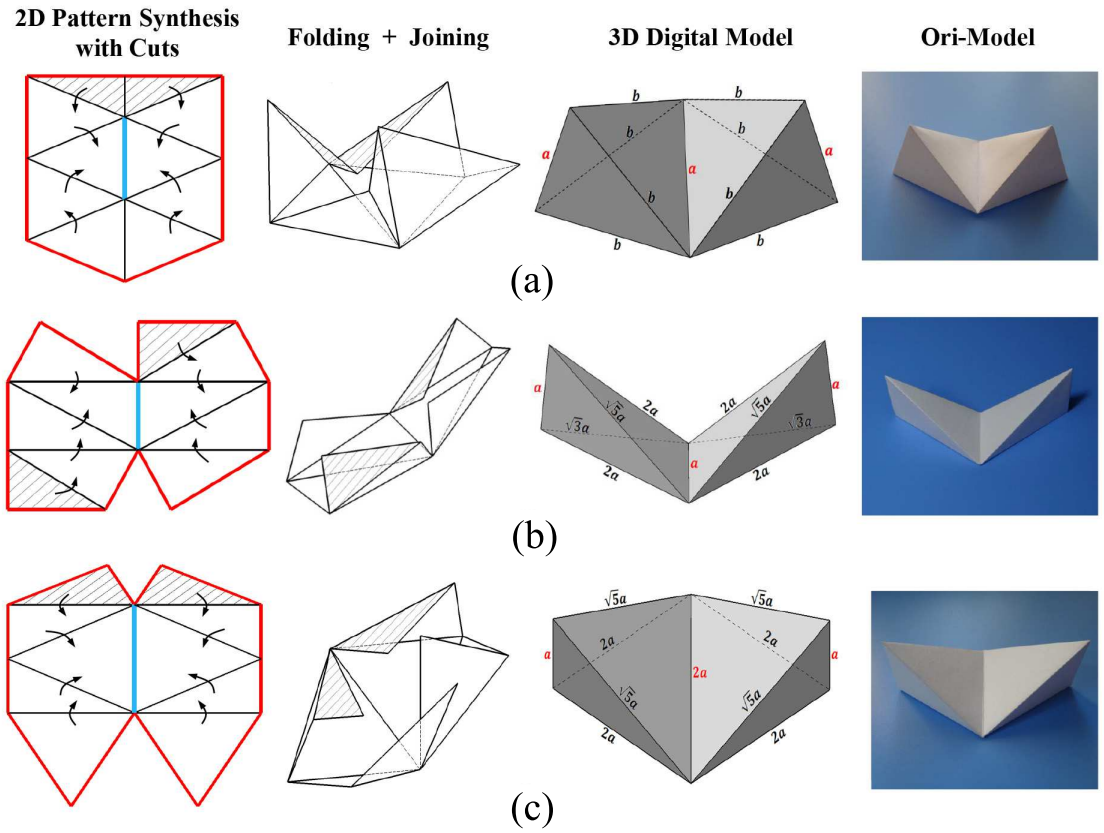

Figure 2.3. (a) Isosceles tetrahedral BSU; (b) Skew tetrahedral BSU; (c) Isos-equal tetrahedral BSU (*red*: overall cuts; *black*: folds; *blue*: the fold that functions as a common hinge; *shaded area*: attachments).

Fig. 2.3 shows 3 representative tetrahedral BSUs where each sides' geometry are: all isosceles triangles (shown as a: isosceles tetrahedron); all right-angle triangles of which edges are in the ratio of $1:\sqrt{3}:2:\sqrt{5}:2:1$ (b: skew tetrahedron); and the one having isosceles, equilateral and right-angle triangles with edge ratios of $1:2:\sqrt{5}:2:\sqrt{5}:2$ (c: isos-equal tetrahedron). Their corresponding 2D crease patterns are shown in Fig. 2.3.

A closed loop of serially connected BSUs (necessarily identical to each other) is defined as a *BSU ring*. In this kinematic chain, any two neighboring polyhedra can be viewed as a BSU. Geometrically speaking, in a tetrahedral BSU ring, 2 adjacent hinge axes are skew perpendicular and 2 alternate ones intersect at a common point. More complex tetrahedral mechanisms with multiple degrees of freedom can be achieved using serial, parallel and hybrid assemblies of BSU rings in a hierarchical manner.

2.3.2 Cuboidal BSU patterns

A number of engineering design practices [56, 57] have been recently revisiting the simple, combinatorial and space-efficient structure: the cuboid. Each cuboidal unit (including the cubic one) contains 12 edges and 6 surfaces while its flattened pattern opens up to 14 edges along the path surrounding the area. In accordance with 11 different planar nets of a cube [9], we start with various 2D patterns for constructing a single cuboidal unit (cuboidal edges are in the ratio of 3: 2: 1) and embed them with the attaching facets for gluing. When considering a cross-like shape as a parent pattern, we obtain 6 different layouts by arranging orientations of the top middle rectangles in grey (we call the base, shown in Fig. 2.4 (1-6)). Each layout yields 11 unique child patterns (see Fig. 2.4 (a-k) for the parent 5) referring to the same base's orientation. Note that the parent patterns are the patterns with the same net while altering the shape of each base rectangle. The child patterns are the ones with the same base rectangle while altering the nets. We eventually generate a total of 66 2D crease patterns in general to fold a cuboid with 12 patterns forming identical pairs.

The displacement and orientation arrangement of each attaching facet are based on the premise that we minimize the overall paper consumption (envelope size of each pattern) as well as the number of attaching facets. For instance the pattern (a) in Fig. 2.4, the two same colored edges (non-adjacent sets in red(a,a'), blue(b,b'), green(c,c'), and adjacent ones in yellow) coincide with each other after folding the net

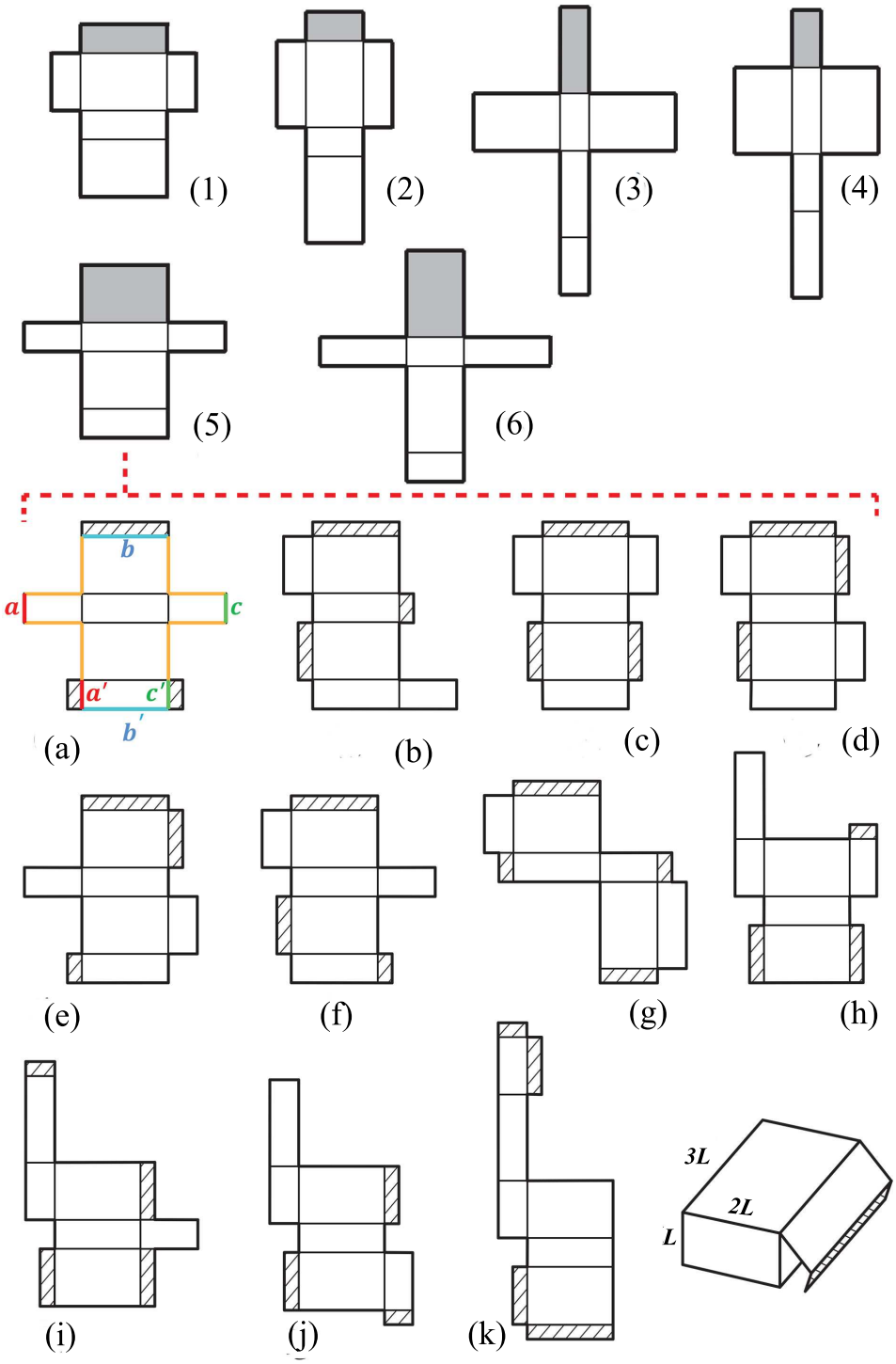

Figure 2.4. 54 unique 2D crease patterns with attaching facets for a cuboidal unit (6 parent patterns with a corresponding child pattern are shown).

up to a closed cuboid. We arrange and extend 3 attaching facets out of non-adjacent sets so that the cuboid can be enclosed efficiently without any curled-up corner.

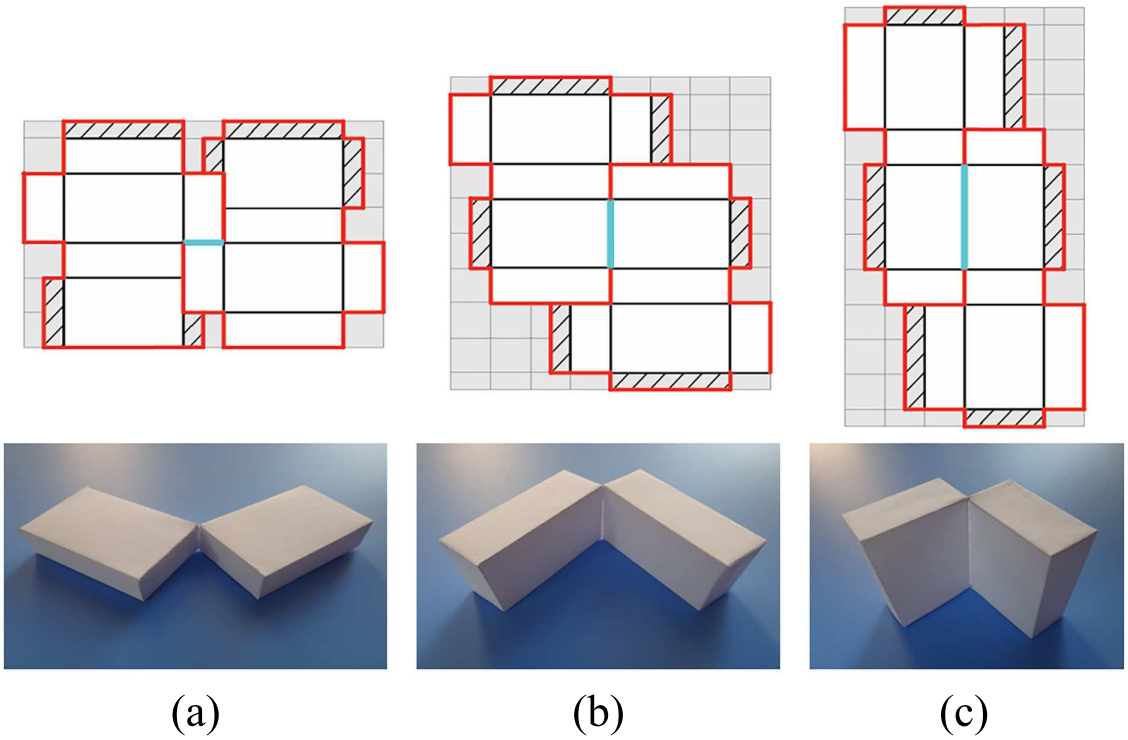

Figure 2.5. Net patterns of cuboidal BSU using 3 different edges as hinges (*red*: overall cuts; *black*: folds; *blue*: the common hinge).

Similar to the tetrahedral BSU formation, the net pattern for a cuboidal BSU can be eased out of a single piece of paper when (1) the hinge to be chosen out of three non-adjacent sets on one cuboidal unit pattern matches the one on the coupled pattern; (2) no self-overlapping occurs after combining two individual nets together; and (3) two built-up cuboidal units are symmetric about the common hinge axis. We synthesize 3 net patterns by picking an edge along the length, width and height individually as the common hinge. We use the most compact envelop area by brute-force searching to chose candidates from a total of 54^2 combinatorial possibilities for attaching-facet arrangement. Fig. 2.5 also shows the hands-on prototype corresponding to each cuboidal net pattern. Note again that a cuboidal BSU ring is a

closed-loop chain with coupled cuboidal BSUs and in which the adjacent hinge axes are skew perpendicular to each other.

2.3.3 Prismatic and pyramidal BSU patterns

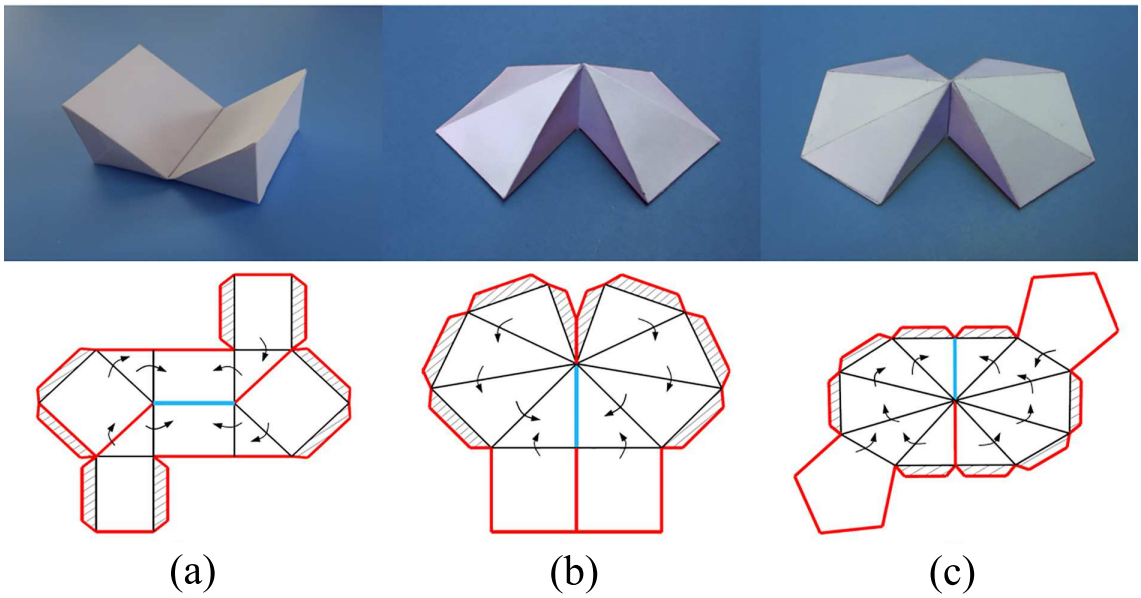

Figure 2.6. (a) Triangular prismatic BSU; (b) Rectangular pyramidal BSU; (c) Pentagonal pyramidal BSU.

Another two representative modules in the family encompass prismatic and pyramidal BSUs. Consider the (a) triangular prismatic, (b) rectangular and (c) pentagonal pyramidal BSUs in Fig. 2.6, each BSU consists of two mirror-image units with n-sided polygonal bases. In each unit, either a side edge or a base edge with skew perpendicularity can be selected as the common hinge edge. Observe that in these unfolded nets, the attaching areas are extended from a single side of each prism face and faces surrounding the apex in pyramidal BSUs.

2.4 Design for Self-Overlapping Avoidance

By unfolding a single polyhedral unit, we allow only 2 hinge edges on the pattern such that one hinge connects to the previous unit and the other connects to the next unit. Therefore, we predesign the hinge edges in a parallel manner and the unfolding net of each current unit is in between the adjacent hinges. Given that BSUs with reflectional symmetry are periodically chained together, we are guaranteed to avoid self-overlapping pairs of adjacent facets after opening polyhedral BSUs into a 2D plane.

2.5 Concluding Remarks

In this chapter, we present a novel folding framework, called "Kinetogami", with multi-hierarchical and foldable units including tetrahedral, cuboidal, prismatic, and pyramidal BSUs. Our primary focus is to create the polyhedral mechanisms using a single sheet of material. We further discuss our design principles to ensure that when flattening each BSU component, no adjacent facets are self-overlapping with each other. Hence, the individual components can be fabricated in 2D while folding and reconfiguring in 3D.

3. EULERIAN CYCLE, FABRICATION PRINCIPLES AND CONSTRUCTION RULES

The bulk of the research effort for the past two decades has been in the fields of Origami design of two dimensional (2D), or planar, fabrication where all the features created are essentially flat. This chapter discusses the layout planning and arrangement of aforementioned crease-cut-attachment pattern of single BSU patterns. Section 3.1 lays the groundwork of the fabrication and folding scheme. We present a generalized algorithm of finding an Eulerian cycle to connect BSUs and threading the cycle to achieve Kinetogami-derived polyhedral mechanisms. Section 3.2 further discusses an ameliorated folding process to optimize the size of flattened patterns within a compact rectangular envelope. Following this, we demonstrate 2 case studies of construction using the skew tetrahedral BSU and the cubic BSU. Section 3.3 concludes this chapter and discusses possible future work.

3.1 Introduction to Fundamental Layout Planning and Folding Scheme

We develop consistent fabrication principles that can be applied to a flat sheet while exploring reconfigurable properties. Our folding approach is deployed on a single compact sheet to achieve Kinetogamic polyhedral mechanisms. We introduce the cuts into the crease pattern to provide skeletal structures therefore multiple folding states are enabled by configuring. Generalized reasoning and fabrication procedures are demonstrated in the case studies of constructing (1) a hexagram-like mechanism using skew tetrahedral BSU, and (2) a deployable ring using cubic BSU.

3.1.1 Finding an Eulerian cycle

In our multi-primitive folding scheme, all folded polyhedral mechanisms originate from a single linear BSU string. At this point, we first achieve the generalization of producing an Eulerian cycle that travels each BSU (linkages) exactly once for any kinetogami-derived polyhedral mechanism.

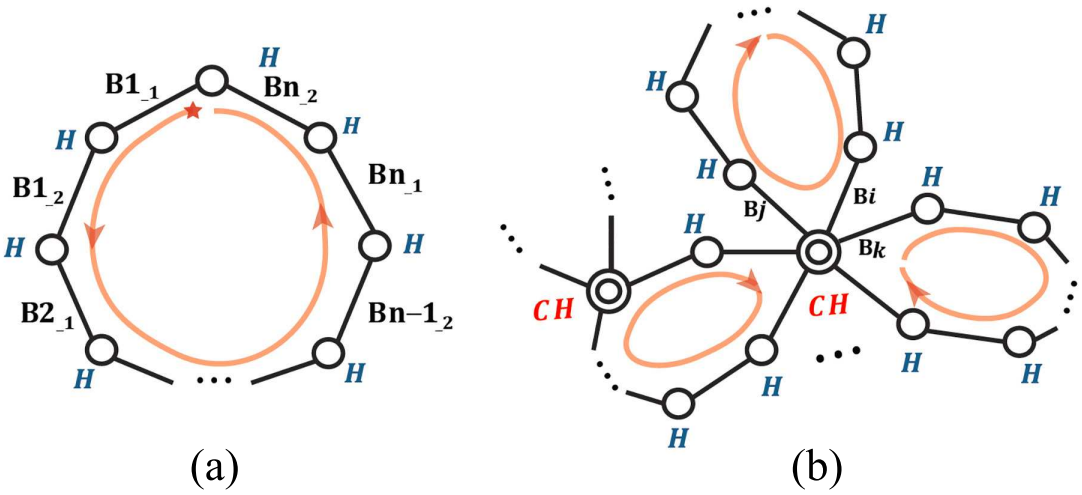

Figure 3.1. (a) Elementary-single-loop with n basic-structural-units $B_1, B_2, \cdots, B_n$. (b) Multi-loop that contains single and compound hinge joints.

Cyclic hinged dissection has received multiple studies on finding a traceable path to form any polypolyhedra shape [54, 55]. When considering the kinematic linkages, we start identifying the configuration space of the closed loop(s) polyhedral linkages. Milgram [58] discussed that closed loop revolute mechanisms have at least one planar configuration, a configuration that lies entirely in a single plane $R^2 \subset R^3$. Hence, the topological relationship of unfolded configuration of closed loop(s) polyhedral mechanisms can be described using a planar connectivity graph G. In the graph, polyhedral links are denoted by edges $(-)$ and hinge joints (H) are denoted by *ordinary nodes* $(\circ)$. Each ordinary node connects 2 links (edges) and it allows 1 rotational degree-of-freedom. When $k(k > 2)$ linkages are joined together while sharing a single hinge joint, this compound hinge joint (CH) is denoted by a *complex node* $(\circledcirc)$ and it allows

$k-1$ revolute mobility. Each single basic-structural-units B_i is composed of two adjacent links Bi_1 and Bi_2 coupled together. If n basic-structural-units $B_1, B_2, \cdots, B_n$ are chained in a single closed loop shown in Fig. 3.1 (a), it is defined as an *elementary-single-loop*. By picking arbitrary node(s) on each of m elementary-single-loops and joining them again to form compound hinges further give us a *multi-loop in the order of* m. The multi-loop construction guarantees non-intersecting edges given that each graph is a planar graph. Finally, we define that at any complex node, the two adjacent BSUs in the same elementary-single-loop are noted as a *pair BSUs*, such as B_i and B_j in Fig. 3.1 (b), and the adjacent ones in the different elementary-single-loops are considered as a *dual BSUs*, such as B_i and B_k. Thus, at each complex node, on one side of any BSU must be its *pair* and the other side must be its *dual*.

The problem herein is described as follows: given a connectivity graph of multi-loop in the order of m, where each elementary-single-loop consists of many basic structural units, to produce an Eulerian cycle which visits each BSU linkage exactly once. In order to tackle the problem, two operations are demonstrated as follows:

Operation1 *op1(CH_i)*: split each complex node (by the aforementioned multi-loop definition, complex node is the compound hinge that couples k BSUs, k is even and $k \geq 4$) into $k/2$ divisions where the dual BSUs are connected together. The set of all newly-created ordinary nodes at each complex node position are defined as a *complex set(CH_i)*. Hence, multiple cycles connecting nodes and edges will be generated.

Operation2 *op2(CH_i)*: In an arbitrary *complex set(CH_i)*, replace each BSUs connection to its dual back with a connection to its pair.

Based on these two operations, our method to find an Eulerian cycle is summarized in Algorithm 1. The following is the detailed proof of the algorithm:

Proof: Recall that in each connectivity graph G, each ordinary node connects only two edges. Since the connectivity graph is a planar graph, we have the following two explicit results: 1) For Operation1, each newly created vertex where dual BSUs

Table 3.1. Finding an Eulerian cycle inside any structure derived by Kinetogami.

Algorithm 1: Find an Eulerian cycle that visits each BSU only once
Input: Given a connectivity graph G;
Step:
1. Find all the *complex nodes* in G
2. **for** each *complex node* (CH_i) **do**
op1(CH_i)
end for
3. **for** each *complex set*(CH_i) which is from different cycles **do**
op2(CH_i)
end for

are jointed at in a *complex set*(CH_i) connects only two edges and it becomes an ordinary node. The process retains the planar properties. 2) For Operation 2, each newly created vertex after pair BSUs are coupled back also connects only two edges. These vertices become an ordinary node and it also retains the planar properties.

After Step 2 completes (for each *complex node*(CH_i), we do the Operation1), given that each node in the obtained graph G connects two edges, the obtained graph G only comprises of one or multiple cycles connecting nodes and edges. In each cycle, every node connects only two edges. Because the connectivity graph is a planar graph and the Operation1 retains the planar properties, these cycles do not intersect with each other. Then, we proceed to Step 3.

Note that each newly created node after Operation 2 still connects two edges. Therefore, after step 3, all the ordinary nodes in the obtained final graph G still have only two edges connected on each side. That is, G is composed of one or multiple cycles. However, since the original connectivity graph contains only one connected component, Step 3 ensures that it results in only one single non-intersecting cycle. This is due to the fact that if there exist multiple cycles, then we can return back

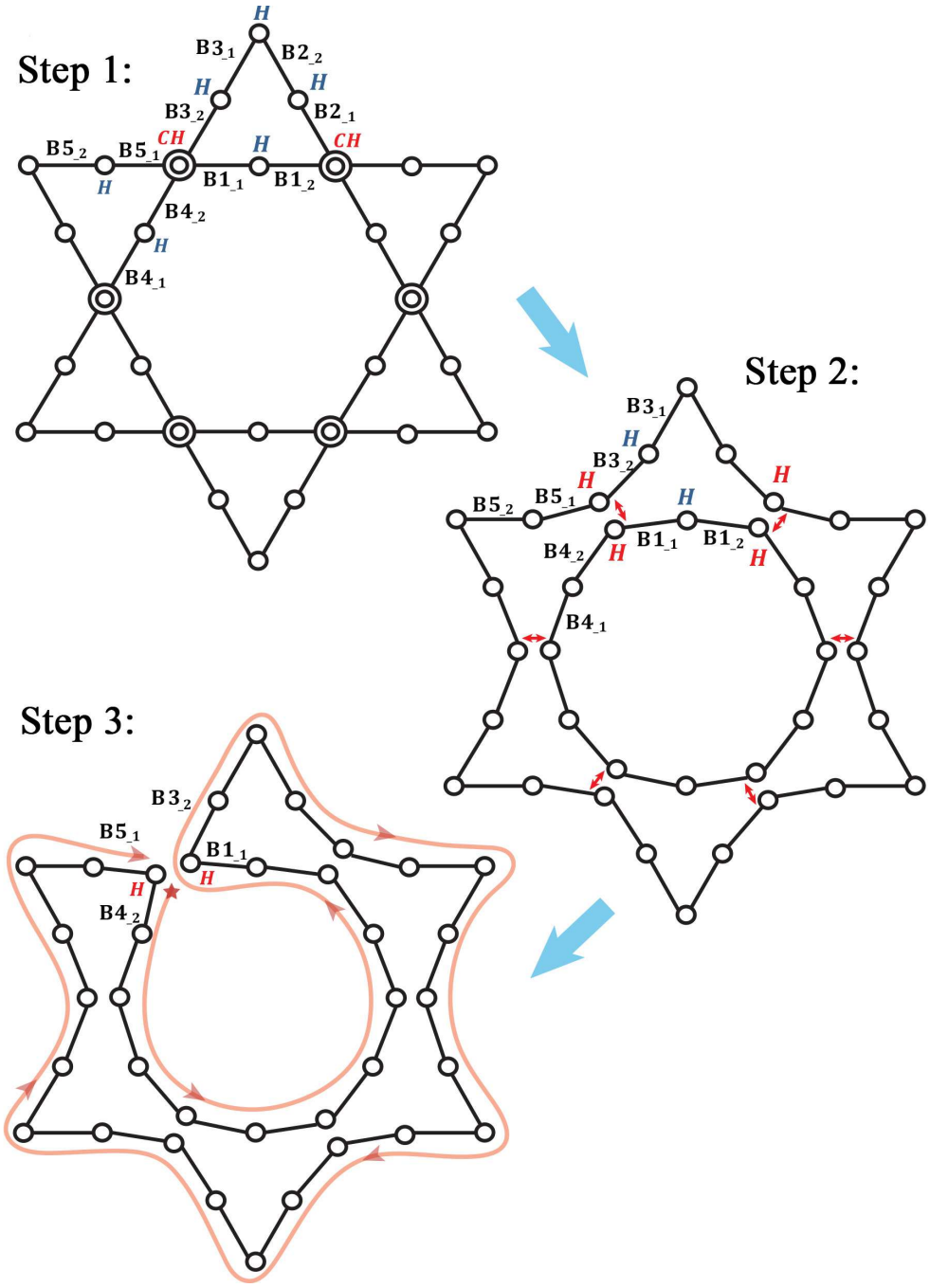

Figure 3.2. Eulerian cycle generation for a hexagram-like mechanism.

to Operation 2 to merge them. Thus, the resulting final graph G by this algorithm is a single Eulerian cycle without self-intersection. Fig. 3.2 shows a hexagram-like mechanism, wherein 6 identical equilateral loops connects with each other from head

to tail and each loop contains 3 BSUs. The mechanism has a total of six complex nodes CHs, where four BSUs, such as B_1, B_3, B_4 and B_5, are hinged together at each CH. Step 2 isolates 2 dual BSU pairs (B_1, B_4 as a dual and B_3, B_5 as another) and generates 2 new cycles where each ordinary node connects only two edges. Finally, replacing each BSU's connection back to its pair (B_1 hinges to B_3, and B_4 hinges to B_5) results in an Eulerian cycle for the mechanism.

As for the time complexity of this algorithm, it is $O(m+n)$, where m is the number of the nodes and n is the number of edges in G. Therefore, once, again, any resulting connectivity graph can become a single closed cycle and the Eulerian path is found with a long non-intersecting BSU string.

3.1.2 Case studies on folding a BSU string to final construct

After finding the Eulerian cycle, We demonstrate the subsequent folding processes using 2 case studies of constructing (1) a hexagram-like mechanism using skew tetrahedral BSU, and (2) a deployable ring using cubic BSU. For both of these case studies, the construction rules are generalized through the following sequences:

i) Duplicate the single crease pattern of skew tetrahedral BSU (see the grey area in Fig. 3.3 (a)) and cubic BSU given in Fig. 3.4 (b) so that one can linearly extend them along a strip of sheet, then fold each pattern up and obtain a long BSU string shown in Fig. 3.3 (b);

ii) Deploy the polyhedral mechanism into a planar configuration: the hexagram-like mechanism into its configuration with six 3stBSUs laying down in Fig. 3.3 (c), and the serial cubic ring configuration itself. Then we select the adjacent hinges based on skew perpendicularity

- Tetrahedral BSU has the least hinge selection options in the fact that each tetrahedron is composed of only 2 skew edges. Recall that we geometrically demonstrate 3 representative BSUs with skew perpendicular hinges and their

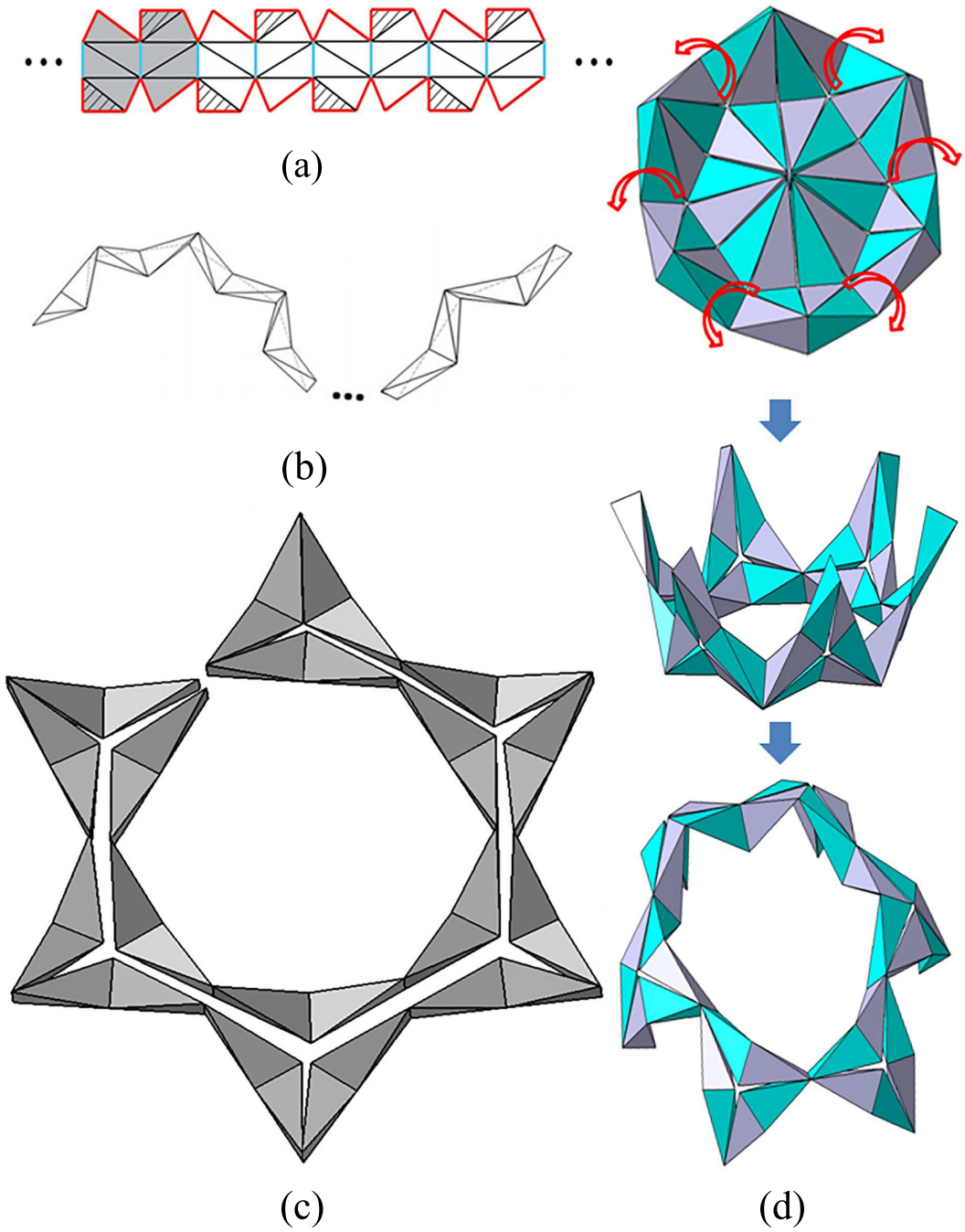

Figure 3.3. Fabrication and construction rules for building a hexagram-like mechanism. (a) linearly duplicating the single unfolded skew tetrahedral BSU pattern along a strip of sheet. (b) folding each BSU pattern up into a BSU string. (c) threading the BSU string throughout an Eulerian cycle for the overall mechanism. (d) reconfiguring the mechanism among two different configurations.

corresponding creases on 2D are synthesized to be linearly arrayed (see the blue lines in Fig. 3.3 (a)).

- Unlike tetrahedral BSU patterns, 2 sets of 4 edges on each current cubic BSU pattern (see Fig. 3.4 (a)) can be chosen for the hinge coupling the previous BSU pattern, denoted as $I_{1,2,3,4}$, and the hinge which is coupling the next one, denoted as $O_{1,2,3,4}$. Folding a single cubic BSU pattern gives rise to 3 different spatial hinge-hinge relations defined as follows: (1) *coplanar parallel*: 2 edges functioning as hinges on each cubic unit are within the same surface plane while parallel to each other, such as I_1 and O_1 or I_1 and O_2; (2) *diagonal parallel*: 2 hinges are parallel to each other but sitting along the diagonal direction in a cube, such as I_2 and O_3; (3) *skew perpendicular*: 2 hinges on each

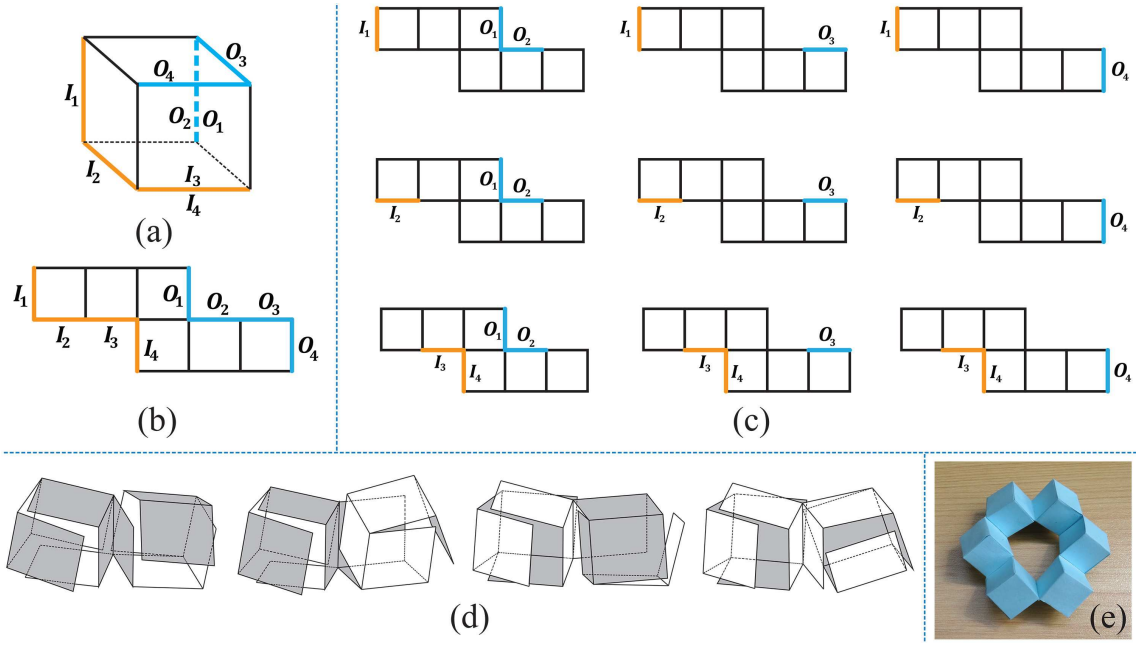

Figure 3.4. Fabrication and hinge selection for cubic derivatives. (a) a single folded cube with 6 facets. (b) unfolded cubic pattern and possible hinge-hinge selection on pattern (*orange*: the hinge that couples the previous BSU; *blue*: the hinge that couples the next BSU). (c) 9 variations of different hinge-hinge combination. (d) 4 variations of different mountain-valley folding at the common hinge. (e) a folded ring with 3 cubic BSUs.

cubic unit are neither parallel nor intersecting, but perpendicular to each other, such as I_2 and O_4. 3.2 provides a summary of hinge-hinge spatial geometric relations covering all possible combinations of I_i and O_j, where $i, j = 1, 2, 3, 4$. To ensure a specific deployable kinematic performance, we choose the hinge-hinge combination that results in the skew perpendicularity of adjacent hinge axes. The whole configuration space is enlarged as well by 4 types of different sequential mountain and valley folding at the common hinge of one cubic BSU (Fig. 3.4 (d)).

Table 3.2. Spatial hinge-hinge relation of a single cubic BSU.

Combination	O_1 / O_2	O_3	O_4
I_1	coplanar parallel	skew perpendicular	skew perpendicular
I_2	skew perpendicular	diagonal parallel	skew perpendicular
I_3 / I_4	skew perpendicular	skew perpendicular	coplanar parallel

iii) Find an Eulerian cycle starting from one BSU to travel and visit each polyhedral BSU exactly once inside the unfolded configuration. We herein demonstrate again the cycle for the hexagram-like mechanism using aforementioned Algorithm 1(shown in Fig. 3.2 and Fig. 3.3 (c)).

iv) Thread the long folded BSU strings along the path, attach all the disconnected compound joint together, and close all the loops into the final constructs.

3.2 Ameliorated Process for Compact Layout Planning

As discussed, each depolyable polyhedral mechanism derived from 4 BSUs reconfigures into a long BSU string and eventually yields a lengthy strip of paper. Hence,

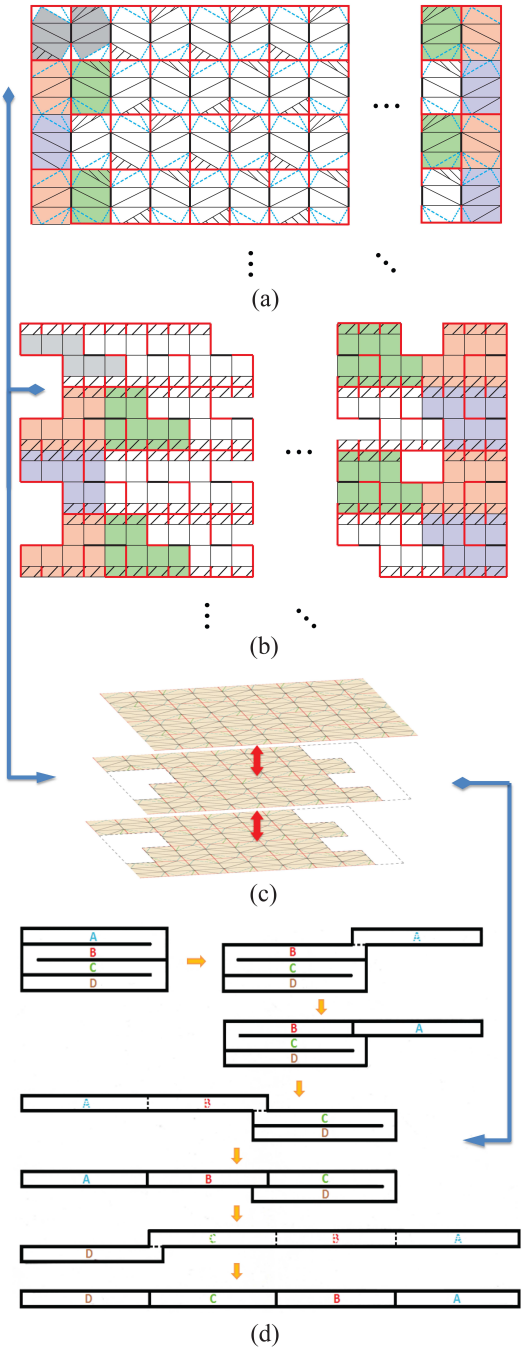

Figure 3.5. Ameliorated processes for a compact 2D pattern layout. (a)-(b) overall pattern planning and arrangement for the skew tetrahedral BSU and cubic BSU (the symmetric green-red-purple areas are the turning areas that fold 3 times). (c) attaching 3 sheets together (top layer remains turning areas, while the rest two layers without the turning areas). (d) sequences of unfolding the rectangular pattern into a linear strip.

we start modifying and re-initiating the 2D layout design on an ideal rectangular-size paper rather than an interminable strip. The fabricating strategies are completed involving another 3 preparation steps:

i) As illustrated in Fig. 3.5 (a) and (b), expanding the BSU crease pattern laterally and vertically on a sheet, apply cuts-creases arrangements to each row and zigzag turns between rows. The overall cuts-crease pattern is represented in colors and the operations will proceed in sequence: to cut along *red* lines, fold *black* lines for construct polyhedral links, fold *blue* dashed lines for enclosing additional surfaces, and attach *shaded regions* for adhesion).

ii) Attach 3 sheets together where the top layer remains the original pattern with green-red-purple turning areas while the rest two layers without the turning areas. (See Fig. 3.5 (c)).

iii) After cutting, stack down each row gradually by folding the green areas backward and then red areas downward shown in Fig. 3.5 (a, b) and eventually lining up a long strip (sequences shown in Fig. 3.5 (d)), then folding BSUs into a long string.

In Step ii, the purpose of the 3-sheets adhesion is to balance the thickness of each polyhedral surface because the turning areas are stacked upon each other three times in the third step as per the row above. We maintain the rectangular paper intact by allowing only line cutting so that: 1) no paper material is wasted (occurs if hollowing out), and 2) the assembly facets are attached inside the tetrahedra and the surface thickness can be increased to enhance structural characteristics such as stiffness and load carrying capacities.

3.3 Design for Intersection-Free Folding Motion

Once the Eulerian cycle is generated for a connectivity graph, we cut the cycle at an arbitrary node so that the closed path can always be opened into a straightened string without self-intersection. When considering the volumetric polyhedral

linkages instead of edges of negligible thickness, the appropriate synthesis of the predictor of reconfigurability allow us to ensure every continuous folding motion free of intersection. Recall in Section 4 that 1) if staying below the rigid state threshold of the vertex angle, the string of tetrahedral BSUs has been proven to be ringed; 2) while enabling the number of BSUs greater than 2, the strings of cubic, prismatic and pyramidal BSU have also been proven to be ringed. That is to say, the intersection between adjacent BSUs occurs if and only if the rigid-state-threshold is designed to be exceeded and units are still chained together in a closed loop. Otherwise, each neighboring BSUs in the Eulerian cycle are sufficient to fit into any local turning or straightening scenario. According to the formation principles we have discussed for the connectivity graph in Section 3.1.1, each constructed polyhedral mechanism is composed of single or multiple loops that topologically allows only ordinary nodes and complex nodes, and geometrically requires adjacent joint axes with skew perpendicularity. Hence, given a specific topological configuration in the connectivity graph, by finding the elementary single-loop with the least edges and constraining the vertex angle from going beyond the rigid-state-threshold, we are guaranteed that the physical BSU string can be folded from a straightened configuration and ringed into loop(s) without intersecting any other BSUs.

3.4 Representation of Combinatorial & Hierarchical Building Architecture

This next two Sections present the fundamentals of how to construct polyhedral mechanisms using tetrahedral, cuboidal, prismatic and pyramidal BSUs. From a single serial loop, to the parallel and hybrid multi-loop assemblies, the derived mechanisms deliver the self-deploying and reconfigurable characteristics. This Section describes the combinatorial and hierarchical building architecture using the skew tetrahedral BSU. In the next Section, we present our prototypical results using differ-

ent BSUs. The experimental results show the proof of concept of our aforementioned fabrication and folding theories.

Dating back to 1929, Paul Schatz [59] first invented the single closed chain with an even number of symmetric tetrahedra. Schattschneider and Walker later decorated the tetrahedra chains and called it Kaleidocycle [60]. A ring hinged with 3 tetrahedral BSUs can be simplified into 6 rigid rods, the deployable mechanism is named threefold symmetric Bricard linkage with 1 DOF [61]. How to flatten and fold up the parallel mechanisms that contains multiple loops, however, is still a challenge for engineers to synthesize and even to perceive.

In the formation chapter 2, the representatives for each primitive BSU were geometrically chosen based on a main feature that the two adjacent hinge axes in each unit are skew perpendicular to each other. Next, we sequentially connect mirror-image BSUs into closed loop(s) so that each loop fulfils the plane-symmetric and trihedral linkage conditions [62, 63], and accordingly, results in a deployable kinematic property. We demonstrate herein the hierarchical architecture of reconfigurable polyhedral mechanisms derived from BSUs. Starting from a single BSU, higher level locomotion is enabled by using serial, parallel and hybrid assemblies. Each derived structure and mechanism can be considered as a new BSU to repetitively or cumulatively achieve more complicated ones, while at each generation the construct is capable of self-reconfiguring among multiple configurations and folding states.

3.5 Prototypical Results

For an explicit demonstration, skew tetrahedral BSU (we call stBSU, see Fig. 2.3 (b)) as a basis turns out to be combinatorial and topological in both structural and kinematic perspectives. The shown white and blue units are mutually symmetric in a BSU. By connecting three skew tetrahedral BSUs in a serial closed loop (we call 3stBSU), we form a equilateral-triangle-like structure (see "Single closed loop" in Fig. 3.6). Hinging six 3stBSUs serially further gives a closed-surface hexagon-like

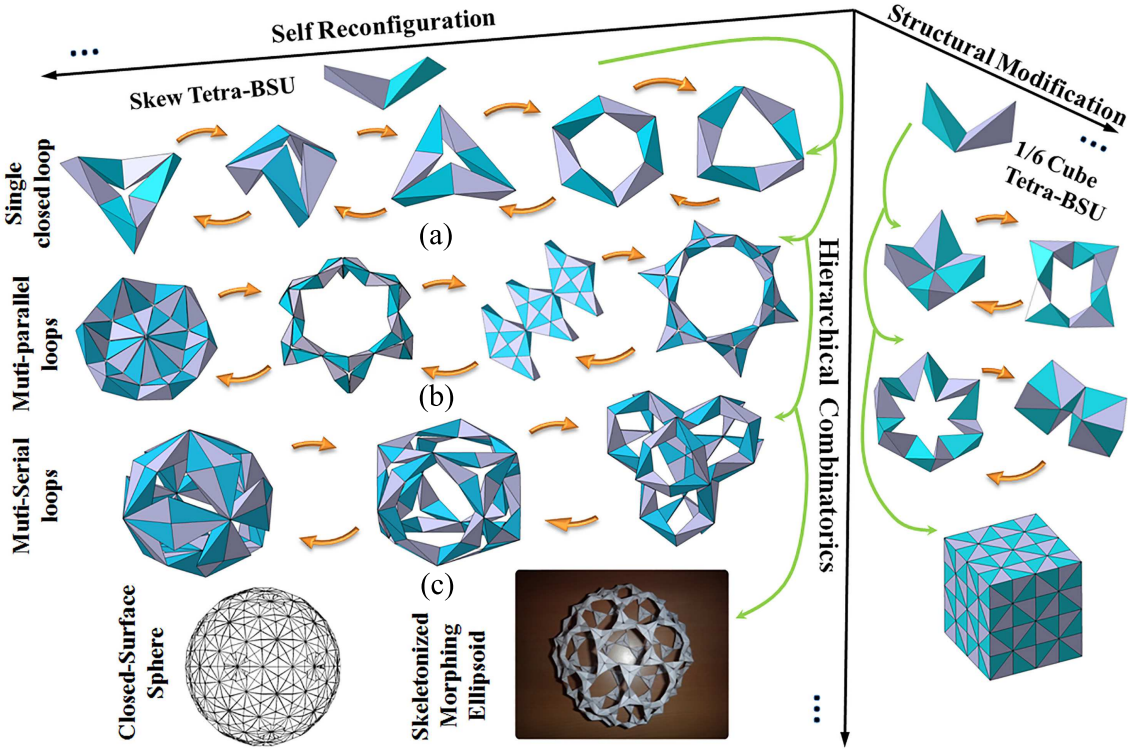

Figure 3.6. Kinematical combinatorics of tetrahedral BSUs. (a) a single-closed-loop containing 3 skew tetrahedral BSUs. (b) a multi-serial-loop containing 6 single-closed-loop. (c) a multi-parallel-loop containing 8 single-closed-loop.

structure shown in "Multi-Serial-Loops" of Fig. 3.6 and the paper model in Fig. 3.7 (b). The 3stBSU can be reconfigured to a zigzag mechanism and the hexagram-like mechanism with unfilled central space (see "Multi-Serial-Loops" in Fig. 3.6 and the paper model in Fig. 3.7(f)). By initializing one configuration of each reconfigurable BSU and building them up cumulatively, it gives rise to versatile rigid structures and movable mechanisms, i.e., the closed-surface sphere in Fig. 3.6 with overall 540 tetrahedral BSUs with paper model shown in Fig. 3.7 (c), and the skeletonized morphing ellipsoid with overall 216 stBSUs (See the paper model in Fig. 3.7 (h)). Given a total of 180 stBSUs, we also achieved a closed-surface ellipsoid in Fig. 3.7 (d) with varying compliance in different Sections. Eventually, modifying the size of BSUs enables different solid structures with overall 192 tetrahedral BSUs to be transformed as well (see the derivatives in "Structural Modification" Section of Fig. 3.6). Gao et al. [64] presented a hexapod locomotive robot by stringing up 3 skew tetrahedral BSUs as each limb and connecting 6 3stBSUs serially. Three potential gaits patterns are also simulated for the robot: squatting/rising, squirming and slithering.

The analogical closed-loop(s) mechanism construction and self-deployable kinematic characteristics are also investigated using cubic BSUs. Many algorithmic and programmable approaches have considered how to fold a linear chain of cubes and achieve any polycube shape [52] [53]. The work demonstrated here is different because our approach lays out hinge orientation on 2D, folds cubic BSU strings into closed loop(s) to construct kinematic mechanisms. Starting from a single cubic BSU, one can join n identical BSUs in a closed loop while alternating successive hinge orientations with a degree of perpendicularity. By satisfying the plane-symmetric and trihedral linkage conditions [63], it gives construction of serial cubic mechanisms that reveal the same self-deployable properties (Case n=3 are show in Fig. 3.7 (i,j) and case n=4 are show in Fig. 3.7 (k,l)). In Fig. 3.7(m), the mechanism consisting of 3 cuboidal BSUs (cuboidal edges are in the ratio of $3:2:1$) is able to deploy (see Fig. 3.7 (n)) into the triangle-like configuration in Fig. 3.7(o). The same self-deployable performance is exploited using the prismatic and pyramidal BSU rings shown in Fig. 3.7

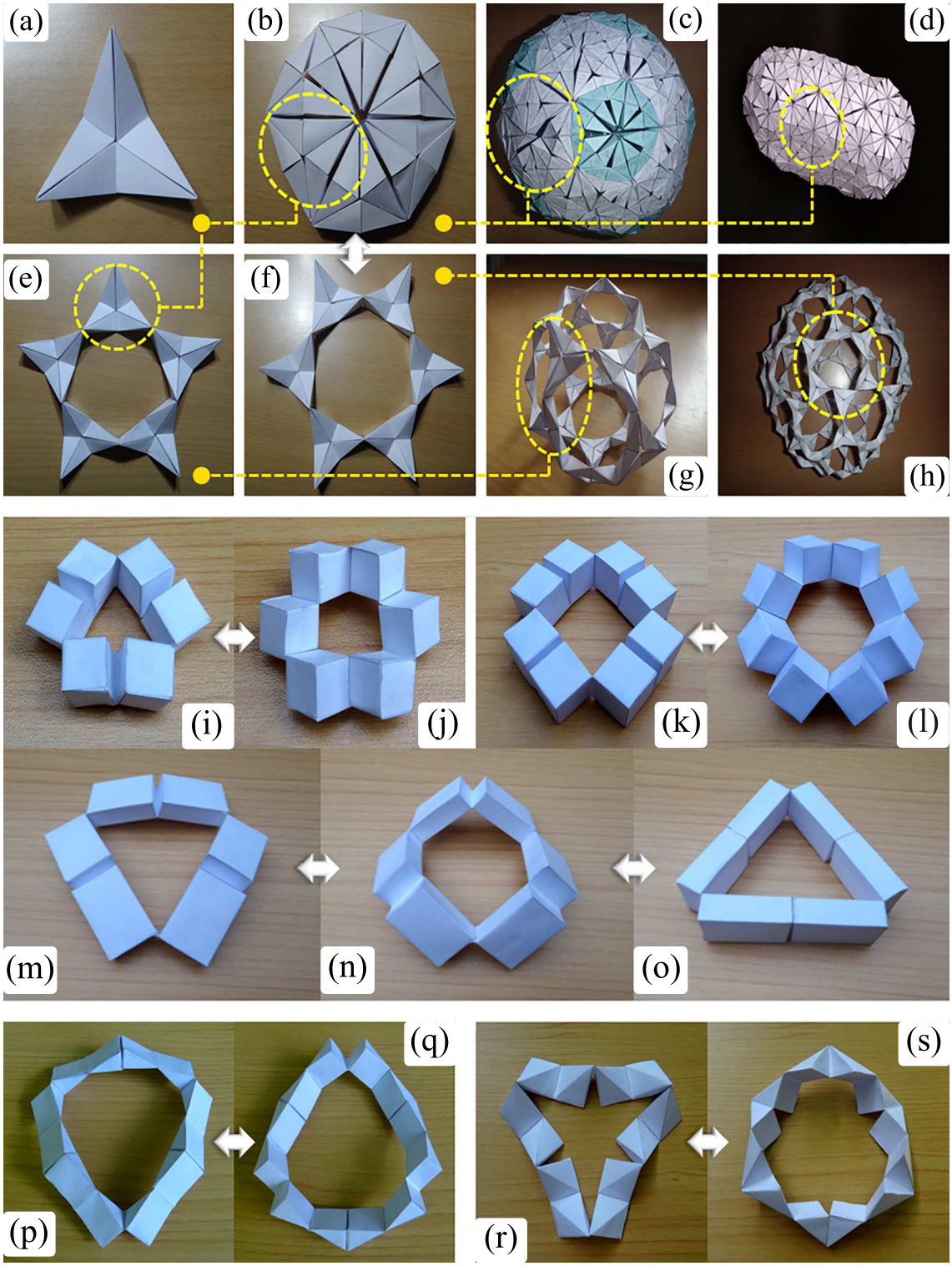

Figure 3.7. Prototypical Kinetogamic derivatives from 4 BSUs: (a)-(h) constructs using tetrahedral BSUs. (i)-(o) constructs using cubic / cuboidal BSUs. (p)-(q) constructs using prismatic BSUs.(r)-(s) constructs using pyramidal BSUs.

(p,q) and Fig. 3.7 (r,s). Therefore, we show the proof of concept of our prototypical experiments and we then detail the kinematic analysis of each polyhedral mechanism in our subsequent work.

3.6 Concluding Remarks

In this chapter, we mainly discuss how to cyclically arrange the aforementioned crease-cut-attachment pattern of each BSU and design the layout planning on a single sheet of material. In particular, we first linearly extend a single BSU unfolded pattern along a long strip of sheet and sequentially fold each pattern up into a string. Then the string is threaded throughout an Eulerian cycle, wherein a generalized algorithm of finding the cycle and its proof are given in Section 3.1.1. Finally, we attach all the compound joints together while closing each individual loop of the final construct. After achieving the fundamental objectives of fabrication, folding and flattening, we further present an improved zigzag folding process to optimize the overall pattern size within a compact rectangular envelope. By following this approach, the substrate thickness is increased and structural characteristics such as stiffness and load carrying capacities are thereby enhanced on the surface. Two case studies using the skew tetrahedral BSU and the cubic BSU are demonstrated along with the discussions. In the last Section, we discuss our folding strategies on how to ensure that no intersection of BSUs occurs during the continuous folding motion.

The Kinetogami folding scheme encompasses foldable and reconfigurable modules that can be combinatorially and hierarchically connected. In this chapter, we also discuss the construction strategies and prototypical results of building BSUs into different polyhedral structures and mechanisms. Each derived structure and mechanism can be considered as a new basis to repetitively or cumulatively achieve more complicated ones, while at each generation the construct is capable of reconfiguring among multiple configurations and folding states. It will be interesting to investigate the po-

tential functionality of these mechanism and assign appropriate lightweight material at surfaces and hinges.

4. GEOMETRIC AND KINEMATIC INTERPRETATION OF RECONFIGURATION USING TETRAHEDRAL BSU

The advantages of reconfiguration in "Kinetogami" are twofold and highly coupled. It is based on both the ease of fabricating in 2-D followed by folding to 3-D, and the highly efficient reconfiguration between mechanisms and structures, that provides the affordances for changing behaviors, such as load carrying capacities or locomotion capacities. Locking the global or the local zones provides both mobility and rigidity of 3D mechanisms in scalable engineering systems. Folding mechanisms are used initially with cutting and gluing to form the baseline topology of the device, and unfolding and ungluing can be used during operation of the device to change the baseline topology.

In this chapter Section 5.1, specially using isosceles tetrahedral BSU, we first develop the mathematical representation that maps mechanism's self-deploying capability into the 2D crease pattern design. Following this, via investigating a measurable geometric parameters in the early synthesis stage, one can predict if a ring with even number of BSUs can perform the continuous rotation. Section 5.2.1 introduces the $\Phi - T$ transformation system to generate single-loop closure equation. Furthermore, the system coefficient matrices and topological graph are derived for a hexagram-like mechanism. The mobility of single- and multi-closed-loop mechanism are also studied in Section 5.2.2 and Section 5.2.3.

4.1 The Geometric Synthesis of Reconfigurability

It is a difficult task to describe and predict the possible variation of configuration states (Ω) during the folding operation on flat sheets. Continuous, restricted and prohibitive rotations were observed within Kaleidocycle structures. We therefore

propose a *predictor of reconfigurability* by concentrating on spatial perception and engineering-domain knowledge. The reconfigurability here is defined as the ability of a BSU ring to perform the "full body" rotation. Thus, one can design a desired motion of morphing structures and reconfigurable mechanisms using measurable design parameters.

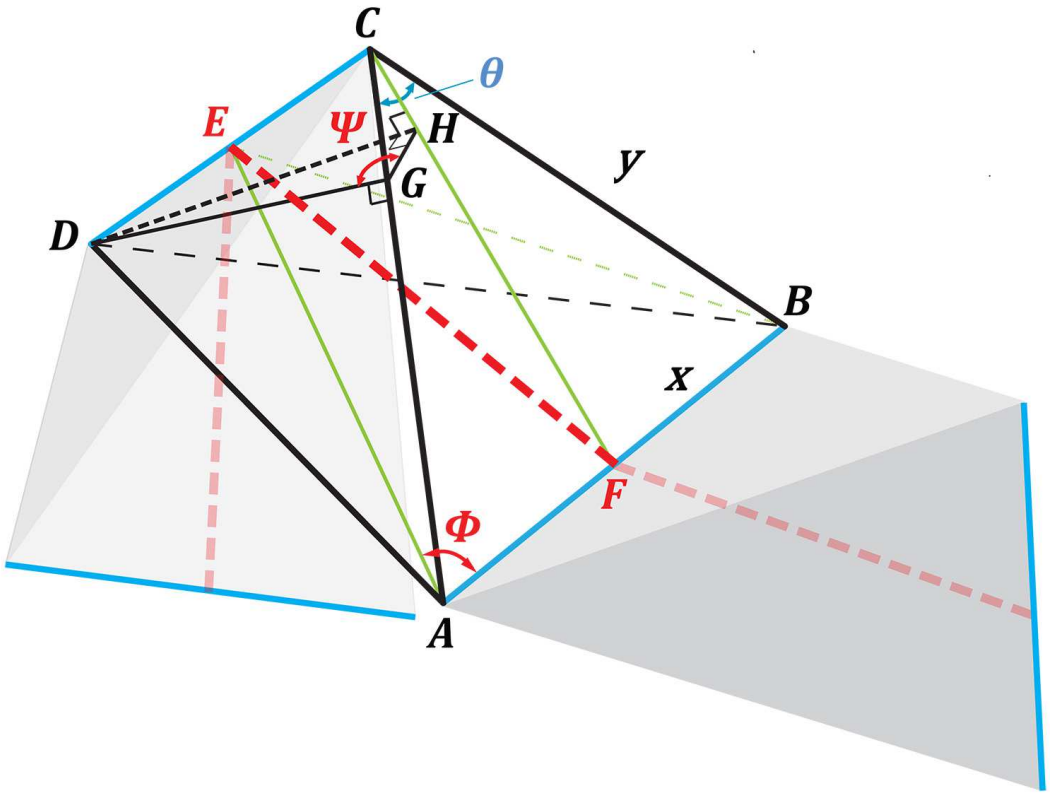

Figure 4.1. Geometric parameters for determining variation of configuration states.

The synthesis rules are processes developed by evaluating the vertex angle of each side of an isosceles tetrahedral BSU. For a tetrahedral BSU ring, each tetrahedral unit is interpreted as a common normal of its two skew perpendicular joint axes, called a "rotating rod" represented as the dashed red line segment EF in Fig. 4.1).

This *predictor of reconfigurability*, θ, is an intrinsic and measurable characteristic parameterized in the flat pattern with 4 identical isosceles triangles, as shown in Fig. 2.3 (a). It can be defined if a single closed BSU ring is able to rotate continuously,

with a limited range or become a rigid structural body by the following reasoning: Let the half base length ($\frac{AB}{2}$ or $\frac{CD}{2}$) be x, and equal side length (AC, AD, BC, BD) be y, therefore $\theta = 2\arcsin(x/y)$. Identification of θ arises by solving equations in two particular cases shown below, while increasing the vertex angle θ from zero:

- if the angle $\Phi = \angle(AB, ACD)$ remains larger than the threshold value $360°/2n$ (see Equation (4.1)), where n is the number of isosceles tetrahedral BSUs in the ring, then the single ring is capable of performing a full body rotation. This arises because the mechanism can pass through its singular configurations when all the tetrahedra gather towards the center. The threshold value for Φ is represented as:

$$\Phi_{Threshold} = \arccos\frac{x}{\sqrt{y^2 - x^2}} = \frac{360}{2n}. \tag{4.1}$$

item Afterward the ring performs a to-and-fro motion (no "full body" rotation) until the dihedral angle $\Psi = \angle(ABC, ACD)$ rises to $360°/2n$. A rigid-body state is achieved right at the threshold value being satisfied (see Equation (4.2)). It's because when the ring is folded, all internal tetrahedral surfaces meet and interfere with each other. The threshold value for Ψ can be represented as:

$$\Psi_{Threshold} = \arcsin\frac{y\sqrt{y^2 - 2x^2}}{y^2 - x^2} = \frac{360}{2n}. \tag{4.2}$$

These two equations lead to two threshold values for the predictor. For instance, the boundaries of the vertex angle in a chain of 3 isosceles tetrahedral BSUs are 53.13° and 70.53° for identifying and predicting a fully reconfigurable, limited reconfigurable or rigid body states (See Fig. 4.2 (a)). Extremal reachable values of θ allow us to define the range of 3 reconfigurable states, which are summarized as below in Equations (4.3), (4.4) & (4.5), and lead to the corresponding plot in Fig. 4.3.

Rigid Body State:

$$\theta = 2\arcsin\sqrt{\cot\frac{180}{n}\tan\frac{90}{n}}. \tag{4.3}$$

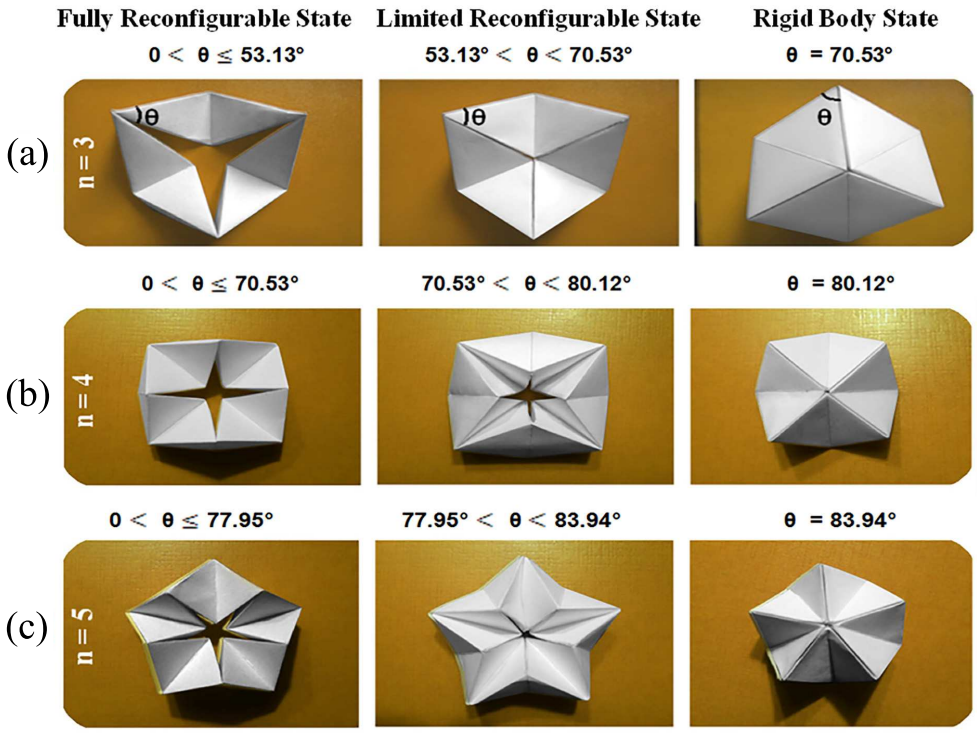

Figure 4.2. Prototypical demonstration of fully, limited reconfigurable and rigid-body state: single ring (a) with 3 isosceles tetrahedral BSUs. (b) with 4 isosceles tetrahedral BSUs. (c) with 5 isosceles tetrahedral BSUs.

Limited Reconfigurable State:

$$2\arcsin\frac{1}{\sqrt{\tan^2\frac{180}{n}+2}} < \theta < 2\arcsin\sqrt{\cot\frac{180}{n}\tan\frac{90}{n}}. \tag{4.4}$$

Fully Reconfigurable State:

$$0 < \theta \leq 2\arcsin\frac{1}{\sqrt{\tan^2\frac{180}{n}+2}}. \tag{4.5}$$

The plot shows a monotonically increasing region of the general reconfigurable state. Naturally, the final specification of the predictor θ depends on the choices of n. With the increase in the number of isosceles tetrahedral BSUs, one can expect a slow-growing space of fully-reconfigurable-states, and the rigid-body-state threshold for θ approaches (but never reaching) 90 degrees. In general, the isosceles tetrahedral BSU

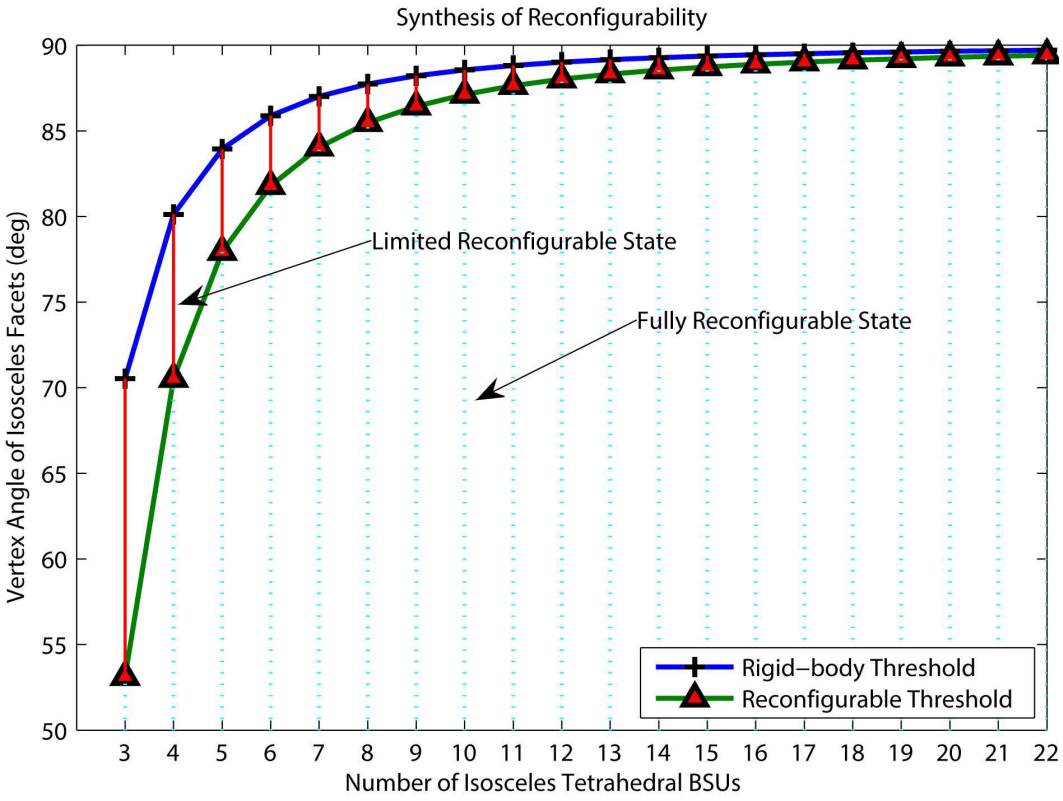

Figure 4.3. Thresholds of fully, limited reconfigurable and rigid-body state.

string can not be ringed if one continues to increase θ after reaching the rigid-body-state threshold. Note that the corresponding dihedral angle Ψ inside our presented cubic, prismatic and pyramidal units are fixed to be $\pi/2$, thus Equation (4.2) indicates that a closed loop suffices to be formed given that the number of BSUs in the ring n is greater than 2.

4.2 Mobility Analysis and Discussions

4.2.1 Interpretation using $\Phi - T$ transformation system

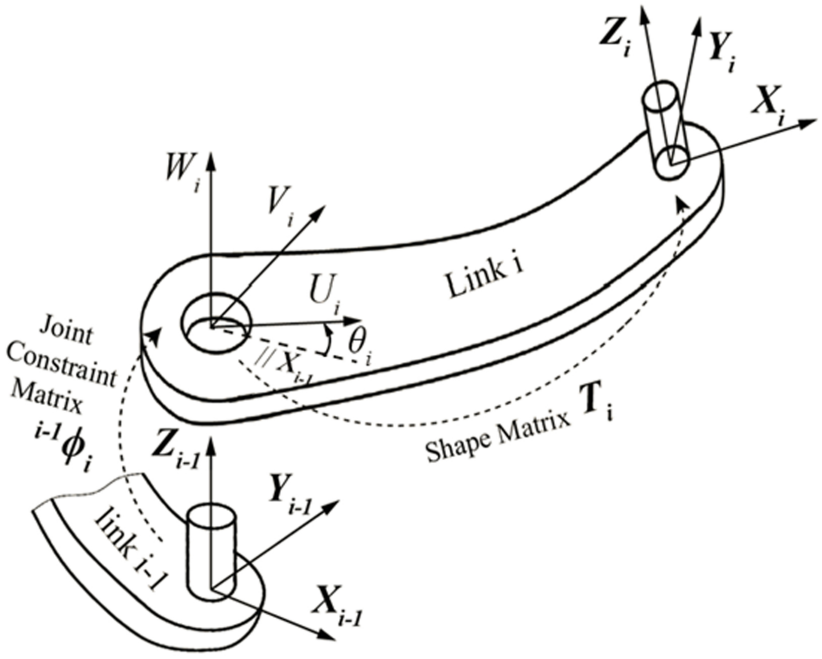

Figure 4.4. The joint constraint matrix and shape matrix definition in $\Phi - T$ transformation system.

Sheth and Uicker [65] presented a standard geometric terminology, called $\Phi - T$ matrices for the kinematic analysis of spatial closed-loop mechanisms. Consider the successive links where two Cartesian coordinate frames are attached on the mating joint element (see Fig. 4.4), the first frame denoted X_{i-1}, Y_{i-1}, Z_{i-1} is fixed to link

$i-1$ with Z_{i-1} along the i th joint axis, while the second frame U_i, V_i, W_i fixed to link i has W_i lying along the i th joint axis and U_i usually along the i th link's length orientation. The relationship between the XYZ_{i-1} and XYZ_i frames can be formulated using a distinct variable transformation part: the joint constraint matrix ${}^{i-1}\Phi_i$ (the i th joint variable θ_i is the rotation angle about joint axis Z_{i-1} from X_{i-1} to U_i), and a constant transformation part: the shape matrix T_i (relates XYZ_i to UVW_i). The loop closure equation can be written as:

$$\left[{}^{0}\Phi_1\right] \cdot \left[T_1\right] \cdots \left[{}^{n-1}\Phi_n\right] \cdot \left[T_n\right] = \sum_{i=1}^{n} \left[{}^{i-1}\Phi_i\right] \cdot \left[T_i\right] = I \tag{4.6}$$

where ${}^{i-1}\Phi_i$ is the joint constraint matrix and T_i is the shape matrix.

To represent the kinematics of each single closed-loop limb using the $\Phi - T$ transformation system, we consider each skew tetrahedral unit as a rigid link (see yellow line segments in Fig. 4.5). Each link is skew perpendicular to its 2 adjacent hinge axes highlighted in blue in Fig. 4.5. Hence, the transformation matrices for each of the six joints can be written as:

$${}^{i-1}\Phi_i = \begin{bmatrix} \mathrm{C}\theta_i & -\mathrm{S}\theta_i & 0 & 0 \\ \mathrm{S}\theta_i & \mathrm{C}\theta_i & 0 & 0 \\ 0 & 0 & 1 & 0 \\ 0 & 0 & 0 & 1 \end{bmatrix}, where \quad i = 1, 2, \ldots, 6. \tag{4.7}$$

and the transformation matrices for each link can be written as:

$$T_{1,3,5} = \begin{bmatrix} 0 & 1 & 0 & \mathrm{L} \\ 0 & 0 & 1 & 0 \\ 1 & 0 & 0 & 0 \\ 0 & 0 & 0 & 1 \end{bmatrix}, \; T_{2,4,6} = \begin{bmatrix} 1 & 0 & 0 & \mathrm{L} \\ 0 & 0 & -1 & 0 \\ 0 & 1 & 0 & 0 \\ 0 & 0 & 0 & 1 \end{bmatrix} \tag{4.8}$$

The six shape parameters L are equal in length and the 6 joint variables θ_i fulfill the following conditions during the motion:

$$\theta_1 = \theta_3 = \theta_5 = A, \quad \theta_2 = \theta_4 = \theta_6 = B \tag{4.9}$$

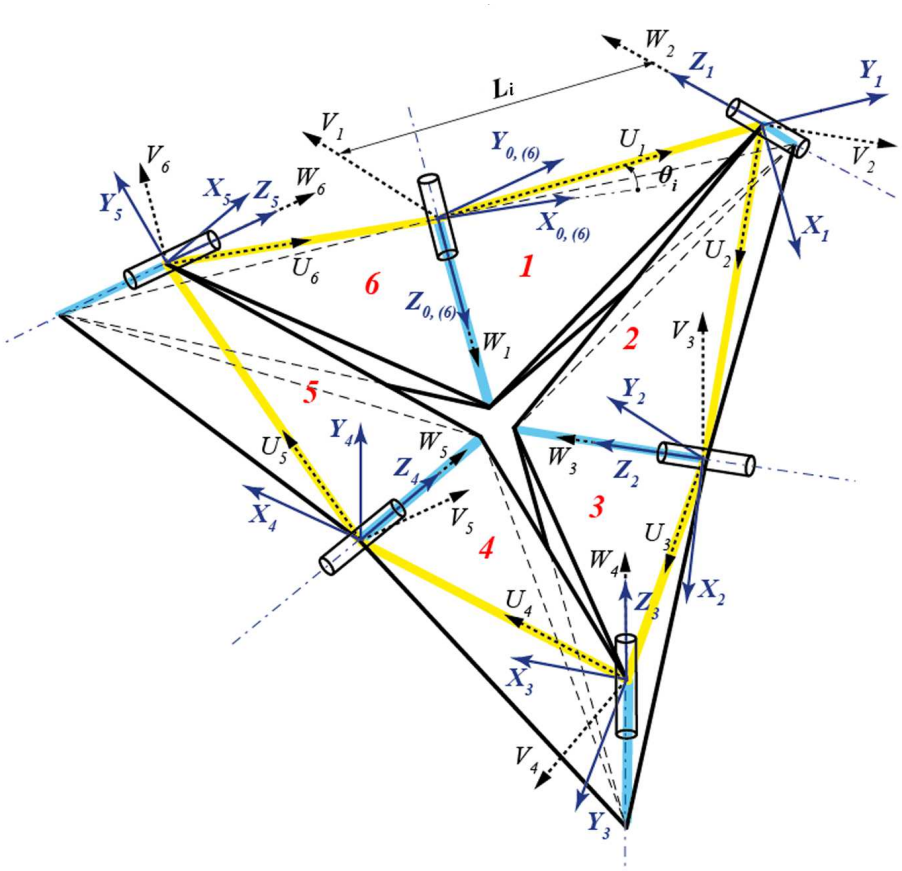

Figure 4.5. $\Phi - T$ transformation matrices for a skew tetrahedral ring.

By substituting the 4×4 transformation matrices into Equation (4.6), one can generate the geometric relationship between the 2 joint variables A and B in each individual limb:

$$B = \sin^{-1}\left(\frac{\cos(A)}{-\cos(A) - 1}\right), \ where \ -\frac{2}{3}\pi \leq A \leq \frac{2}{3}\pi. \tag{4.10}$$

4.2.2 Single-loop analysis

In this Section, we discuss the mobility analysis strategy using the system coefficient matrix [65] for the aforementioned hexagram-like mechanism. Earlier efforts on the mobility determination of rigid-body mechanisms goes back to Chebyshev [66], Grübler [67], and Hunt [68], etc. These fundamental approaches are based on sub-

tracting the overall constraints from the degree of freedoms of all links, but neglecting certain special geometric conditions such as perpendicularity and parallelism which the mechanical system possesses. In every $\Phi - T$ transformation system, the number of independent inputs q is equal to the degree of freedom, m. By using the chain rule, the time derivative of ith joint's variable θ_i can be derived as:

$$\dot{\theta}_i = \sum_{j=1}^{m} \frac{\partial \theta_i}{\partial q_j} \dot{q}_j = \sum_{j=1}^{m} \theta'_{ij} \dot{q}_j \tag{4.11}$$

where θ'_{ij} denotes $\frac{\partial \theta_i}{\partial q_j}$ and $\dot{q}_j$ is the time derivative of jth independent input. By differentiating the loop closure equation with respect to q_j, i.e., with respect to any of potential inputs, and substituting the following equation (Q_i is the derivative operation matrix):

$$\frac{\partial \Phi_i}{\partial q_j} = Q_i \, \Phi_i \, \theta'_{ij} \tag{4.12}$$

the derivative of loop closure equation is derived as follows:

$$\begin{aligned} &[{}^0A_1 \, Q_1 \, {}^1A_2 \cdots {}^nA_1 \, {}^1A_0]\theta'_{1j} \, \dot{q}_j + \\ &[{}^0A_1 \, {}^1A_2 \, Q_2 \, {}^2A_3 \cdots {}^nA_1 \, {}^1A_0]\theta'_{2j} \, \dot{q}_j + \cdots + \\ &[{}^0A_1 \, {}^1A_2 \cdots Q_n \, {}^nA_1 \, {}^1A_0]\theta'_{nj} \, \dot{q}_j = 0 \end{aligned} \tag{4.13}$$

We define that $D_i = {}^0A_i \, Q_i \, {}^0A_i^{-1} = {}^0A_i \, Q_i \, {}^iA_0$, so that Equation (4.13) can be rearranged as:

$$D_1\theta'_{1j} \, \dot{q}_j + D_2\theta'_{2j} \, \dot{q}_j + \cdots + D_n\theta'_{nj} \, \dot{q}_j = 0 \tag{4.14}$$

Since the joint constraint matrix is orthogonal and Q is anti-symmetric, the D matrix has only 6 independent elements. The compact form of Equation (4.13) can be derived out as:

$$\begin{bmatrix} D_1(2,1) & \cdots & D_n(2,1) \\ D_1(3,1) & \cdots & D_n(3,1) \\ D_1(4,1) & \cdots & D_n(4,1) \\ D_1(2,3) & \cdots & D_n(2,3) \\ D_1(2,4) & \cdots & D_n(2,4) \\ D_1(3,4) & \cdots & D_n(3,4) \end{bmatrix} \begin{Bmatrix} \theta'_{1j} \\ \theta'_{2j} \\ \cdot \\ \cdot \\ \cdot \\ \theta'_{nj} \end{Bmatrix} = N \begin{Bmatrix} \theta'_{1j} \\ \theta'_{2j} \\ \cdot \\ \cdot \\ \cdot \\ \theta'_{nj} \end{Bmatrix} = \mathbf{0} \tag{4.15}$$

in which N is called the system coefficient matrix of a mechanical system and the degree-of-freedom of the system can be obtained as:

$$m = n - rank(N) \tag{4.16}$$

By implementing the system coefficient matrix for an individual limb, we attain its representation in a reduced row echelon form shown as below:

$$N = \begin{bmatrix} 1 & 0 & 0 & 0 & 0 & \frac{\sin B(\cos A+1)}{\sin A(\cos B+1)} \\ 0 & 1 & 0 & 0 & 0 & -1 \\ 0 & 0 & 1 & 0 & 0 & \frac{-\sin B(\cos A+1)(\cos A+\cos B+\cos A\ \cos B-1)}{\sin A(\cos B+1)} \\ 0 & 0 & 0 & 1 & 0 & \cos A+\cos B+\cos A\ \cos B-1 \\ 0 & 0 & 0 & 0 & 1 & \frac{\sin B(\cos A+1)}{\sin A(\cos B+1)} \\ 0 & 0 & 0 & 0 & 0 & 0 \end{bmatrix} \tag{4.17}$$

The mobility of each individual limb accordingly is $m = 6 - 5 = 1$.

4.2.3 Multi-loop topological representation and analysis

As for the system coefficient matrix N of a multi-closed-loop mechanical system, each column corresponds to an individual joint variable and each 6 rows represent an independent loop. The number of independent loops λ in a mechanism is determined using the Euler formula:

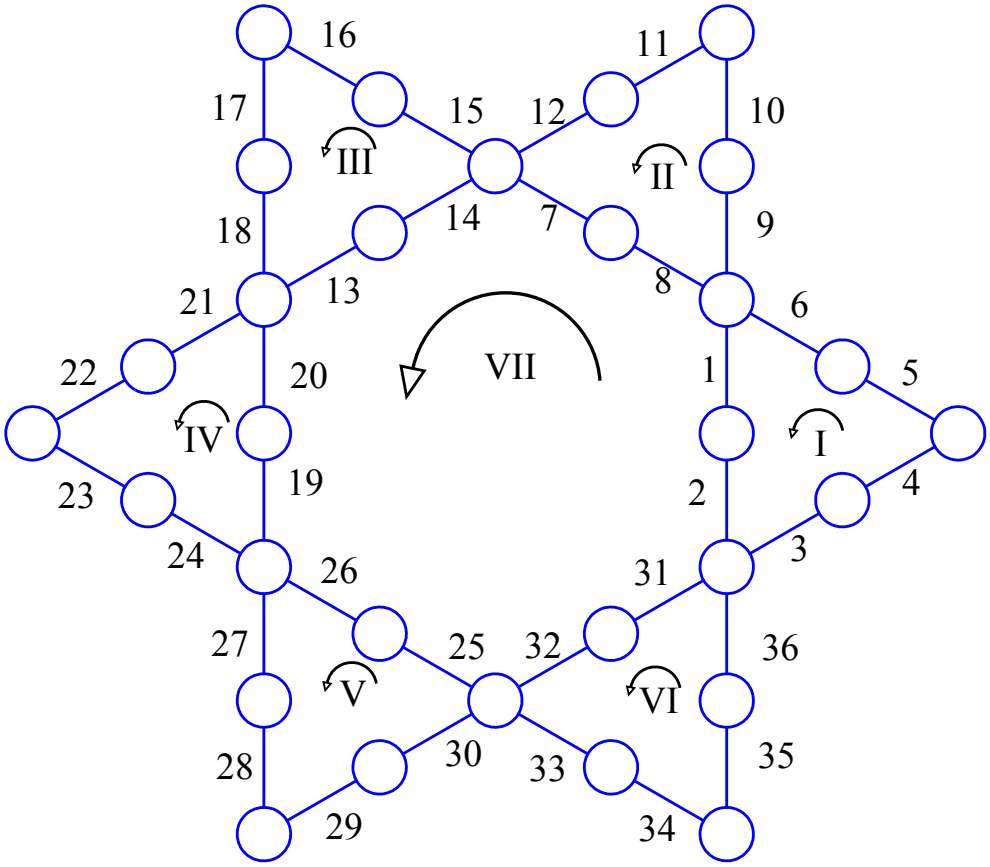

Figure 4.6. Topology graph of the hexagram-like mechanism (42 revolute joints and 36 tetrahedral links).

$$\lambda = n - l + 1 \tag{4.18}$$

where n is the number of joints and l is the number of the links. For this hexagram-like mechanism, λ is 7 given that $n = 42, l = 36$. We further assemble 7 independent loops into an overall 42 by 42 system coefficient matrix. 7 independent loops are listed as below and illustrated in a topology graph shown in Fig. 4.6, where tetrahedral links are denoted by edges $(-)$ and hinge joints are denoted by circles $(\circ)$.

- Loop I: links $1 - 2 - 3 - 4 - 5 - 6$
- Loop II: links $7 - 8 - 9 - 10 - 11 - 12$

- Loop III: links $13-14-15-16-17-18$
- Loop IV: links $19-20-21-22-23-24$
- Loop V: links $25-26-27-28-29-30$
- Loop VI: links $31-32-33-34-35-36$
- Loop VII: links $2-1-8-7-14-13-20-19-26-25-32-31$

The numerical results of the rank analysis indicates that the mobility of the mechanism $m = 42-35 = 7$ for any general configuration, while the instantaneous mobility could vary in special geometric conditions and different singular configurations.

4.3 Concluding Remarks

In this chapter, our first objective was to study how geometric properties on the crease pattern affect the kinematic performance of a folded tetrahedral BSU ring. To this end, we proposed the *predictor of reconfigurability*, a measurable design parameter on 2D for determining whether the ring can perform full rotation or become a rigid structure. We mathematically derived two critical threshold values for the proposed angle parameter and classified regions of the general reconfigurable states. Next, taking the hexagram-like mechanism as an example, we used the $\Phi - T$ transformation system and obtain the loop closure equation for a single tetrahedral ring. Further analysis of mobility boundary was also conducted for both single- and multi-loop construction scenarios. With upcoming applications in designing foldable structures, the understanding of possible variation of kinematic configurations and the corresponding geometric features on the flat is a challenging goal to achieve. We believe that this chapter offers an appropriate geometric and kinematic interpretation to overcome this challenge in the context of our Kinetogami folding scheme.

5. MECHANICAL APPLICATIONS DERIVED FROM KINETOGAMI

In this Chapter, we initiate the re-fabrication of the crease pattern in Section 6.1 using additive manufacturing technology. As a demonstration artifact, a multi-material sheet is 3D printed with elastomeric flexure hinges connecting the rigid plastic facets. We further envision that many alternative material constructions and functional electrical networks can be achieved in a single build. The main goal of Section 5.2 is to demonstrate a locomotive robotic application inspired by Kinetogami. To this end, we present "HexaMorph", a novel starfish-like hexapod robot designed for modularity, foldability and reconfigurability. The proposed hexapod robot is fabricated using single sheets of cardboard. The electronic and battery components for actuation are allowed to be preassembled on the flattened crease-cut pattern and enclosed inside when the tetrahedral BSU are folded. The design and folding paradigm provides a novel approach for building reconfigurable robots using a range of lightweight foldable sheets.

5.1 Material Selection for Substrate and Hinge

The design theories and fabrication concepts of Kinetogami have been proved on the paper substrate. Besides paper, a wide variety of non-wovens open up the possibilities for exploring the substrate selection and surface properties (wettability, creasability (wrinkle-resistance), adhesive properties, and stiffness) for a variety of future applications. Considering Kinetogami's application in an engineering context, we further explores an alternative substrate which contains anisotropic material properties such as stiffness in planes and high flexural characteristics about hinges.

5.1.1 Applying multi-material additive manufacturing

As the rapid prototyping technique via building 3D objects layer upon layer, additive manufacturing, namely, 3D printing, has extensively impact the traditional manufacturing tools, assembly processes and supply chains and thereby new materials and products emerge. It is envisioned that 3D printing will provide a powerful tool to analyze the synergetic role of material properties of the constituents materials, combined with geometry, hierarchy and size scales on the different characteristics [38,69]. Heterogeneous material printed substrate with various mechanical properties, such as stiffness and overall energy dissipation capacity, have been proposed recently (OpenFab [70] and Digital anisotropy [71]).

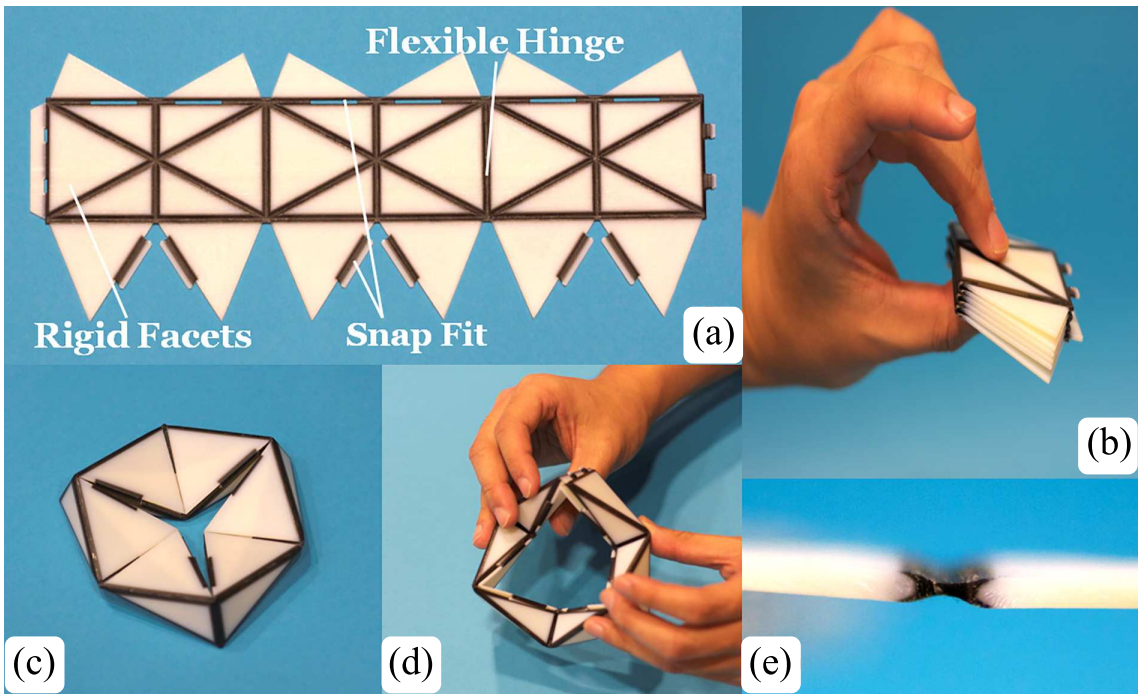

Figure 5.1. (a) 3D Printed multi-material sheet. (b) compactly flat-folded configuration. (c) folded into 6 tetrahedral BSUs in a ring. (d) morphed among configurations. (e) flexure hinge.

On the other hand, flexure joints [72] have been frequently applied in engineering such as self-folding morphing mechanisms [6, 73–75] and robotic origami [76, 77].

Fig. 5.1 (a) shows the printed multi-material sheets where flexural hinges merge with rigid polypropylene facets as produced particularly by Objet Connex 350™. The net build size is $320mm \times 108mm \times 1.5mm$ and it can be folded fully into a $52mm \times 108mm \times 9mm$ package (See Fig. 5.1 (b)) without cracking and springing. Deploying the crease pattern and refolding it along with the predesigned snap-fits give one a rotating tetrahedral BSU ring in Fig. 5.1 (c) and (d). Compared to flat contact between the plates and the hinge, the interconnecting cross section shown in Fig. 5.1 (e) resolves fatigue cracking and provides more flexibility in the elastomeric joints.

5.1.2 Vision of integration of substrate-hinge-electrical network

Substrate solutions. In this thesis, we further envision that the integration of basic substrate, hinge and functional electrical networks for actuation and motion control, will be accomplished by simultaneous fabrication of mechanical and electrical components within a quasi-2D substrate. Substrates (2.5 D) can be manufactured using ink jet printing or cut from sheet materials using laser cutting. Directly printing conductors on our substrate constructions is possible using existing techniques with adaptations. Conductors will be directly printed on the substrate by screen printing, ink-jet printing, or selective wetting of pre-patterned surfaces (patterned by composition or texture via lithography, sputtering, and/or vapor deposition).

Hinge solutions. The main challenge associated with printed electrical networks (power circuits and sensors) includes that compliance/stretchability at the joints in order to enable folding and compound folds. Beside the flexure joints co-printed with the rigid facets using additive manufacturing techniques, various material combinations of fibrous substrates, fabrics and elastomers are envisioned to build the substrate and flexure joints. Such combinations are classified into 1) naturally bonding materials (such as silicone-based glass fibers and elastomers), 2) mechanically bonding materials (fabrics and elastomers), and 3) adhesively bonded materials (using chem-

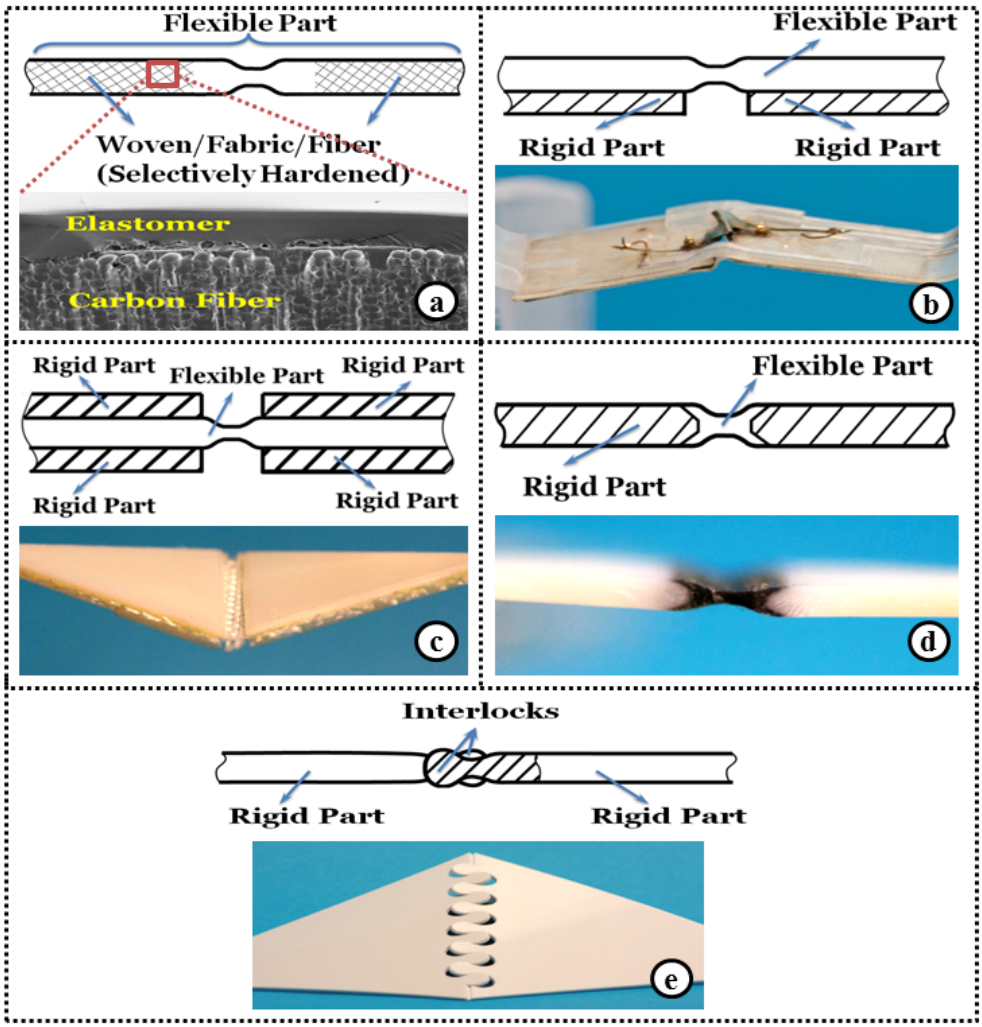

Figure 5.2. Different substrate-hinge fabrication: (a) carbon fiber composites. (b) tile/elastomer assembly. (c) tile/fabric assembly. (d) multi-material 3D printed. (e) interlock assembly. (Figures (a) and (b) provided by Professor Rebecca Kramer).

ical or textural modification to surfaces). Fig. 5.2 shows different existing substrate fabrications and embedded hinging processes. In Fig. 5.2 (a), the carbon fiber composite material forms the basic flexible substrate, wherein both sides of the material are selectively hardened. Fig. 5.2 (b) shows a two-tile (fiberglass) system that is folded with a planar shape memory alloy actuator [77]. Fig. 5.2 (c) illustrates an alternative system where the central fabric layer functions as the flexural joint and rigid plates

attach on both sides. Multi-material printing technology allows us to integrate rigid facets with interconnecting flexible joints show in Fig. 5.2 (d). Finally, Fig. 5.2 (e) shows the folding can also be achieved by geometrically designing the interlocking patterns on the flat. Besides, existing materials may undergo bulk modifications to enable compatibility. For example, mixing glass micro/nano-particles into 3D printer resin will be directed towards enabling bonding between silicone-enhanced 3D-printed parts and silicone-based elastomer.

Electrical network solutions. For this proposed system, ideal actuators need be planar, reversible, and embedded within the substrate/electronics base layer. Low-risk options need to be explored include patterned and annealed 2D shape memory alloy sheet or spring actuators for linear and rotary actuation [76] and pneumatic actuation [78]. Reversible folding using local and global triggers such heat, light, and solvents [79]. Heat-responsive shape memory polymer can be integrated with small heaters to perform bending functions. Larger systems, on the other hand, need to be designed to include practical actuators relative the scale, such as micro-motors.

5.2 HexaMorph: A Reconfigurable and Foldable Hexapod Robot Inspired by Kinetogami

5.2.1 Comparison of HexaMorph and existing modular robotic systems

Recent literature shows that engineers and scientists have used principles of folding for the robotic designs using programmable material [76] and displaying self-assembly capacities [5] and locomotive gaits [80]. The robot with foldable skeletons can be eased out of flat sheets of material so that it is lightweight and inexpensive, enabling batch fabrication and economies of scale. On the other hand, the advances in self-reconfigurable robots have drawn attention for assisting production manipulation [81] and planetary exploration [82]. A high degree of redundancy, modularity and complexity in functionality are encapsulated in many self-morphing robotic systems, for instance, M-TRAN [83], ATRON [84] and Miche [56].

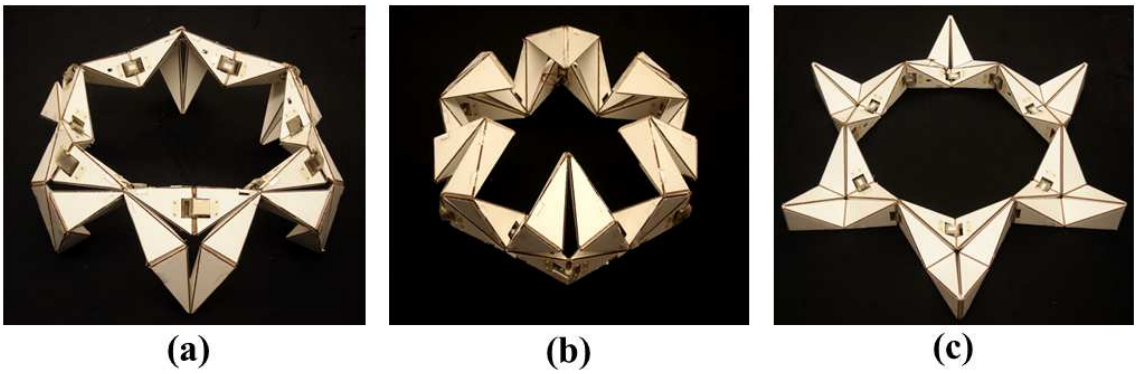

Figure 5.3. A foldable and reconfigurable starfish-like robot, "HexaMorph". (a) standing configuration. (b) "huddled" towards the center. (c) fully-deployed configuration.

In this Section, we present a Kinetogami-inspired robotic application on the aforementioned hexagram-like mechanism, called "HexaMorph" shown in Fig. 5.3. It resembles the *Leptasterias hexactis*, known as a six-rayed starfish in the family of Asteroidea. In contrast with the conventional mechanical prototyping with rigid rods, joints and electric components, the construct of the robot has advantages over the existing self-reconfigurable robots for the following reasons:

i) In geometry, unlike most modular robotic systems with tree or open-chain architecture, there is no central body-platform in HexaMorph and each limb is interconnected within a closed-loop form. This special structure enables the robot to continuously flip inside out, exhibiting the self-deploying and space-filling characteristics.

ii) The robot transforms its body among different configurations via actuating servos at different positions, rather than successively detaching and reconnecting modules from one another.

iii) For manufacturability, our design methodology enables fabrication and assembly in 2D, folding and reconfiguring in 3D.

5.2.2 Substrate and electronics design

3mm-thick corrugated cardboards are used as the substrate surfaces for the robot. Each limb in its compact volume is $15in \times 13in \times 4in$. The robot's net weigh is 0.765 kg with only the cardboard tetrahedral modules, and overall 2.72 kg including all the functional components. After creating the folds, cuts and snap-fits on 2D aforementioned stBSU pattern, we lay down and preassemble the electronic components on the flat.

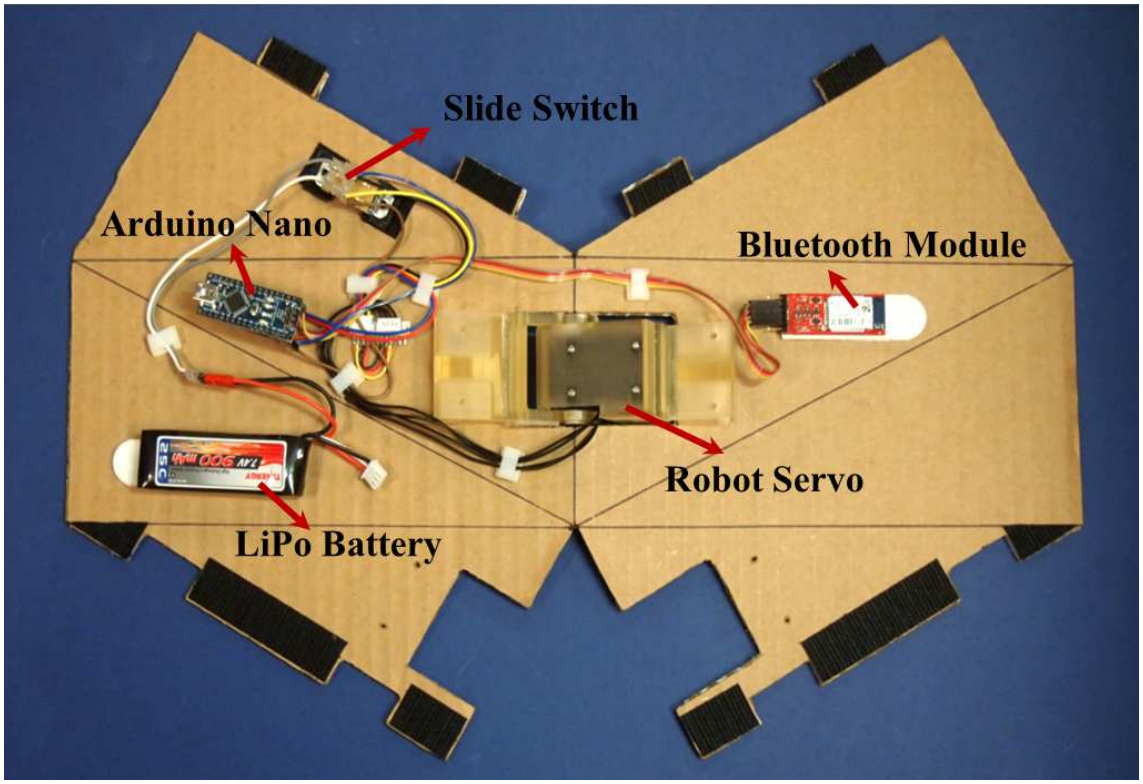

Figure 5.4. Electronics layout on a single skew tetrahedral BSU pattern.

Fig. 5.4 shows the electronics layout on a single skew tetrahedral BSU pattern. Our electronics design for HexaMorph comprises four major components: the PC for motion planning and running GUI, 1 Arduino Nano for motion control, 1 Bluetooth module for wireless communication between PC and Arduino, and 12 robot servos for actuation and position sensing.

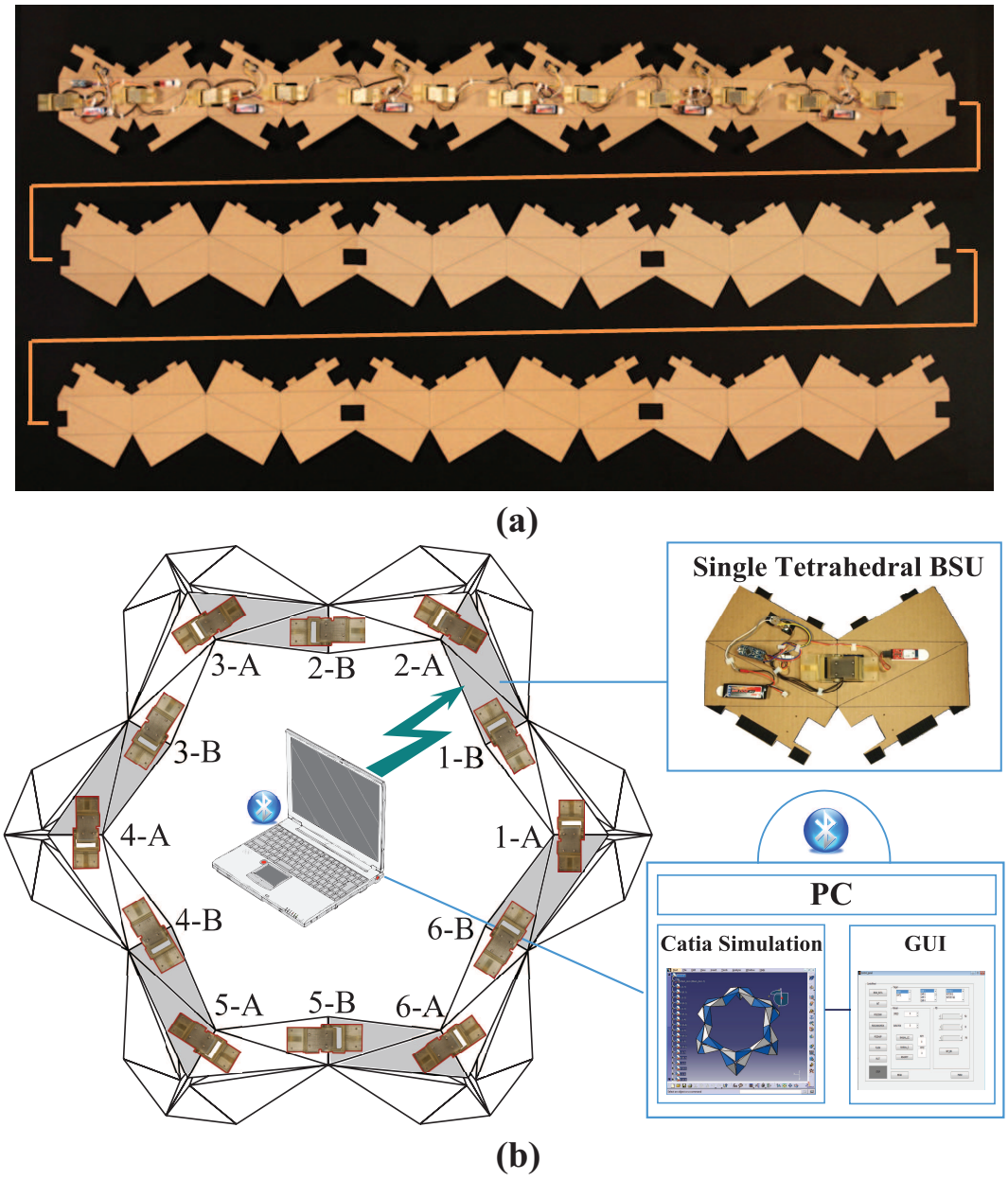

Figure 5.5. (a) Overall 2D pattern with all the electronic components. (b) system pipeline and wireless control strategy.

Fig. 5.5 (a) further shows an overall flattened strip containing 18 periodic stBSU patterns and electronic components on the pattern. The first row shown in Fig. 5.5 (a) indicates the 2D pattern of the stBSU string that travels the inner loop VII shown

in Fig. 3.2. Folding the patterns in the second and third rows together constructs the rest of stBSU string in the Eulerian cycle.

We place 12 HerkuleX DRS-0101 robot servos at each hinge joint inside the inner loop, shown in Fig. 5.5 (b). Six servos labeled "A" are inside each limb and the remaining six labeled "B" sit between 2 adjacent limbs. The resulting redundant actuation is needed to assist the robot passing through the singular configurations and balancing the torque due to the symmetry in structure. To assist in planning the associated complex joint motions, CATIA simulation is used to design the reconfiguration and generate joint angles. The Arduino Nano processes all the motion sequences sent from the PC and distributes into 12 servos. When considering the modularity of each single loop, 2 adjacent servos coupled inside each tetrahedral BSU are powered with 1 Tenergy Li-Po battery (7.4v, 900mAh). Twelve daisy-chained robot servos together process different motion planning synchronously. Therefore, by closing each BSU and each individual loop up, we complete the fabrication and assembly for the hexapod robot.

5.2.3 Reconfiguration design and motion control

Biologically-inspired robotics [85] and biorobotics design [86] involve endeavors of adopting the understanding of animal behaviors and embedding resemblant flexibility in robots. In this section, we propose 2 reconfiguration patterns for the hexapod tetrahedral robot: self-deploying and locomotive squirming.

Self-deploying: Nature employs efficient, elegant patterns and strategies of deploying, for instance, the petals of morning glory flower unfold from the bud and curl up back. As discussed in Section 2, both the individual single-closed-loop limbs and the multi-closed-loop robot are capable of self-deploying continuously from inside out since the mechanisms satisfy plane symmetric and trihedral linkage conditions. Twelve servos are synchronously operated to employ this motion. Starting from a standing posture shown in Fig. 5.6 (a), the hexapod robot deploys its initial configu-

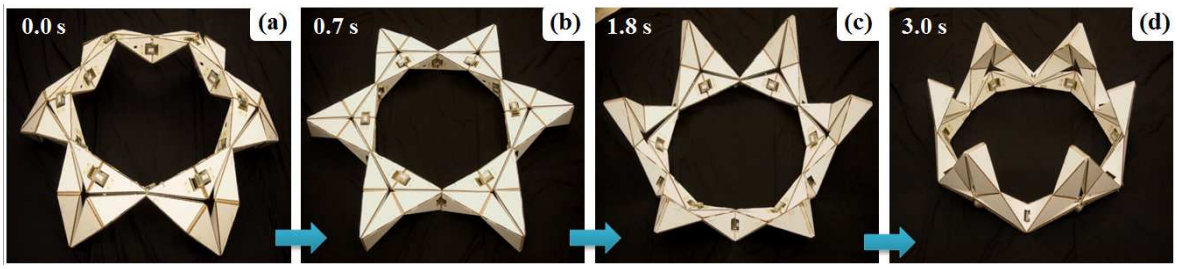

Figure 5.6. Sequences of self-deploying motion. (a)-(b) moves from initial standing configuration to the fully-deployed configuration. (c)-(d) closes up to a smaller envelope volume.

ration internally through the fully-deployed configuration on the ground (see Fig. 5.6 (b)), then towards the final "bristled" configuration (see Fig. 5.6(d)). This particular type of reconfiguration allows the robot to transform from a functioning stance containing stretched limbs to a storage or packaging stance with compact envelope volume. The deploying motion takes 3 seconds and can be operated on the flooring of multiple materials such as tile, wood, bamboo and plastic.

Squirming: The second reconfiguration designed for the robot is locomotive. We decompose the hexapods into one forelimb, four middle limbs and one hindlimb towards any orientation around the body. A squirming sequence comprised of 2 steps is shown in Fig. 5.7. After fully deploying its "huddled" body on the ground (see Fig. 5.7 (a-c)), the special geometry reduces its mobility to 3 and six servos between 2 adjacent limbs start driving the robot to squirm forward and balance the toque. The robot first moves the forelimb forward while anchoring the hindlimb, shown in Fig. 5.7 (d). The whole skeleton is stretched along the squirming direction. The robot then pulls the hindlimb to slide forward while anchoring the forelimb (see Fig. 5.7 (e)), so that the skeleton contracts back to the original configuration. The overall motion proceeds like a squirming inchworm.

A one-way friction solution was applied to ensure that the moving and anchoring can happen simultaneously along the same direction. We use One-way Glide^{TM}where

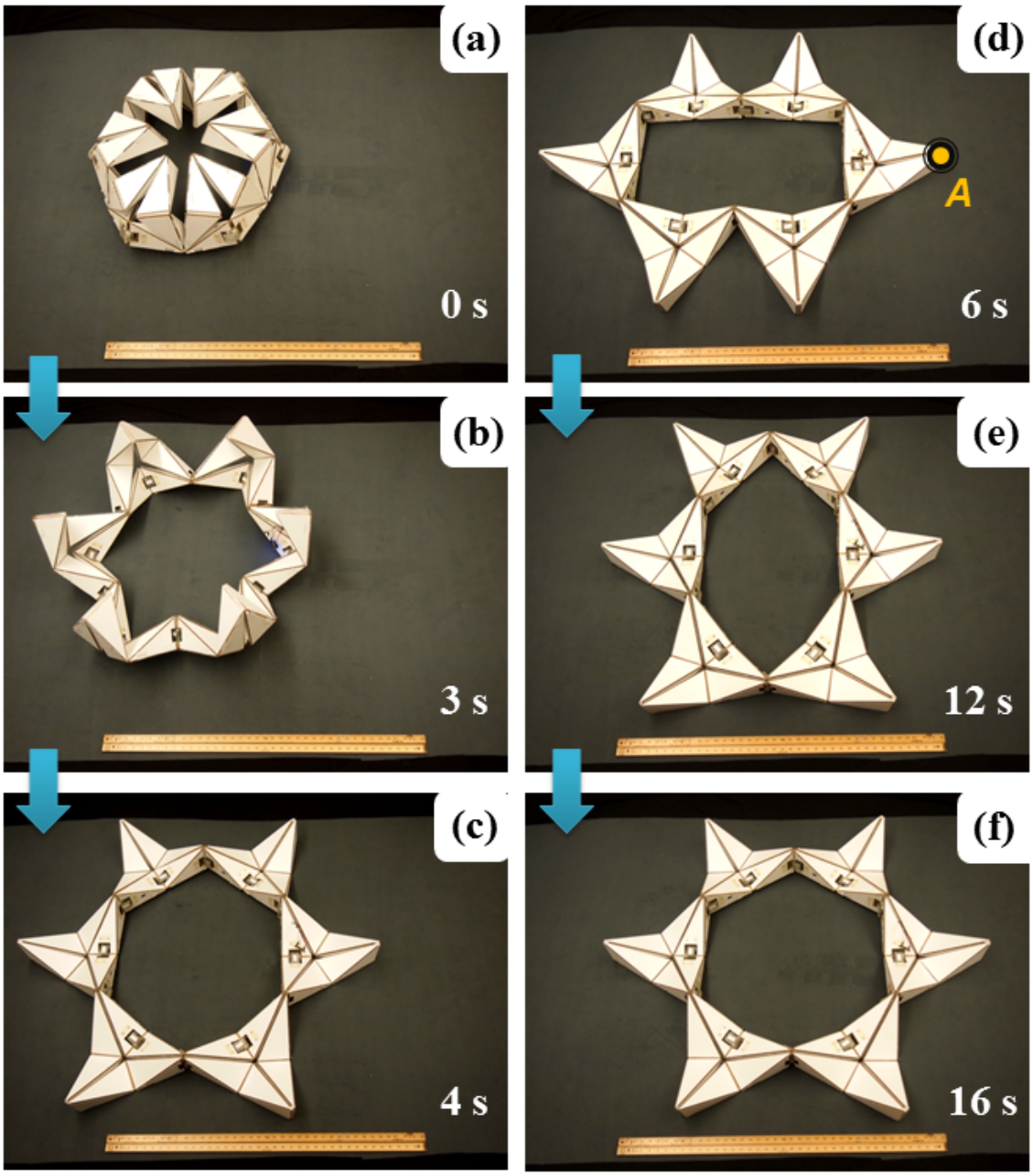

Figure 5.7. Sequences of locomotive squirming motion. (a-c) opens its body till all limbs are stretched. (c-d) drives one limb while anchoring another one in order to squirm.

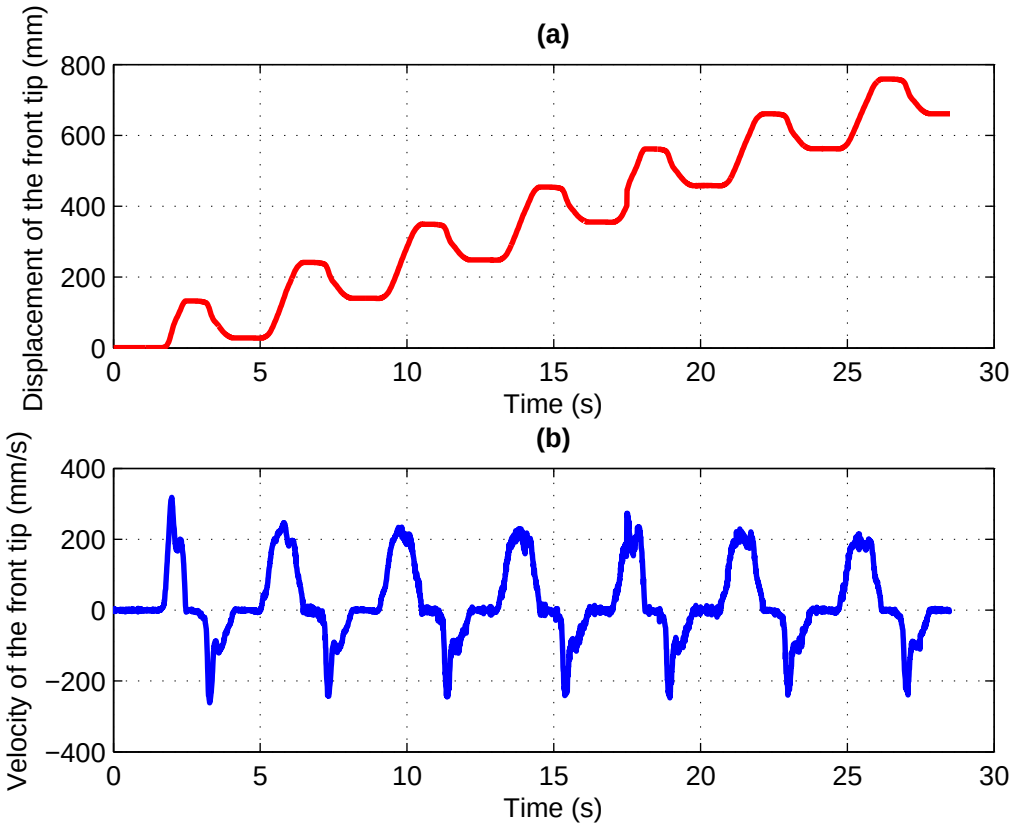

Figure 5.8. (a) The displacement of the robot front tip "A". (b) the velocity of the robot front tip "A".

the tilted inner fibers allows the surface to slide in one direction only and resist sliding back. Fig. 5.8 (a,b) shows the displacement and velocity of the front tip of the robot (illustrated as point "A") over time. The displacement during each advance stroke is measured to be 200mm followed by 40 % backward-slip motion due to the friction. The maximum velocity of the robot is 240mm/s. Whenever the robot reaches the initial regular hexagram-like configuration, it is capable of converting the squirming direction by rearranging the functions of each limbs.

5.2.4 Simulation results of other locomotive gaits

Besides the self-deploying and locomotive squirming motion, we propose herein 3 other potential modes of motion, or gait patterns using the simulation results: squatting/rising, inchworming and slithering. The kinematic simulation is developed using CATIA^{TM}DMU package. In the following paragraphs we specify the motion planning for each gait:

Squatting and Rising: A well-known tripod periodic pattern [87, 88] is implemented in order to generate an alternating squatting-and-rising motion for the robot. We assign the identical limited range of flipping to the periodic limbs and then shift to the other three. The robot thereby performs a continuous rising and squatting motion while maintaining the contact on ground. The weight of the robot is simply shifted alternately from one tripod to the other. Choreographed motion tracking is shown in Fig. 5.9 (a, b, c) below.

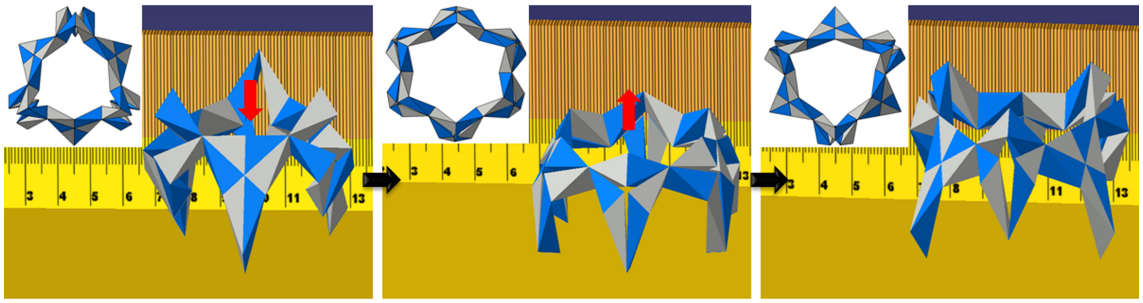

Figure 5.9. Squatting and rising gait proposed for HexaMorph. (a) three alternative limbs flip while the other three stretch. (b) six limbs reach the same configuration to lower the robot height. (c) previous flipped and stretched limbs alternate with each other and lift the robot height.

Inchworming: The energy consumption of biped or multiped walking motion is high and it requires complicated motion planning and actuation sequences. Inchworming, or shuffling, on the other hand, gives rise to many potential mechanical advantages of locomotion generation. We decompose the robot skeleton into two

forelimbs, two middle limbs and two hindlimbs towards any orientation around the body. The proposed inchworming gait comprises 2 steps shown in Fig. 5.10, wherein the red arrows represent the direction that limbs are about to move: (1) moving two hindlimbs forward while anchoring the forelimbs, so that the robot skeleton contracts along the sliding (shuffling) direction (Fig. 5.10 (a)). (2) pulling two forelimbs to slide forward while anchoring the hindlimbs, therefore the robot stretches its body backwardly (Fig. 5.10 (b)). The overall tetrapod motion proceeds like a body-lifted inchworm and the middle limbs are lifted above the ground all the time. Whenever the robot reaches a configuration (Fig. 5.10 (c)) in between two stretched positions, it is capable of converting the moving direction by rearranging the function of each limb (Fig. 5.10 (d)), similar to the squirming motion presented in the last section. Note that the one-way friction stripes are attached to the front and hind limbs to ensure the moving and anchoring occurs at the same time. This one-way friction strategy can be modified when decreasing the material weight of the robot.

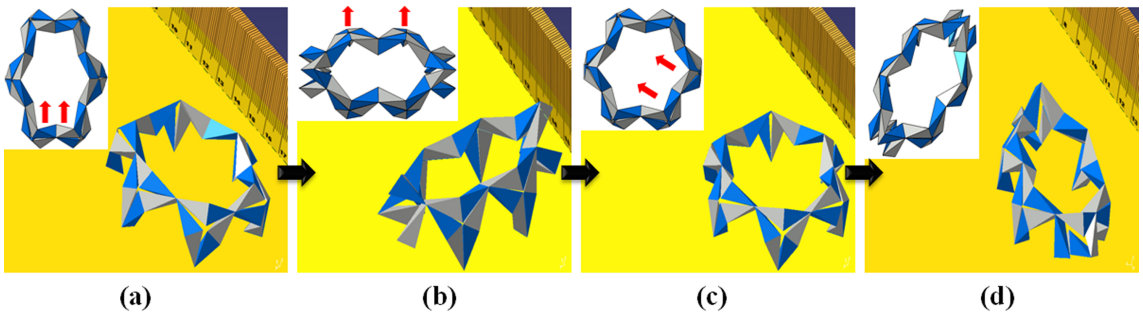

Figure 5.10. Inchworming gait proposed for HexaMorph. (a) driving hindlimbs forward while anchoring the forelimbs (robot body contracted). (b) moving forelimbs forward while anchoring the hindlimbs (robot body stretched). (c)-(d) converting the motion direction by rearranging the function of each limb.

Slithering: To demonstrate the reconfigurable and gait-changing capabilities of HexaMorph for accomplishing tasks under different environments, we present another locomotion: slithering like a snake. A zigzag pattern of the robot is designed as its initial configuration. By creating an alternating linear motion (red arrows in Fig. 5.11)

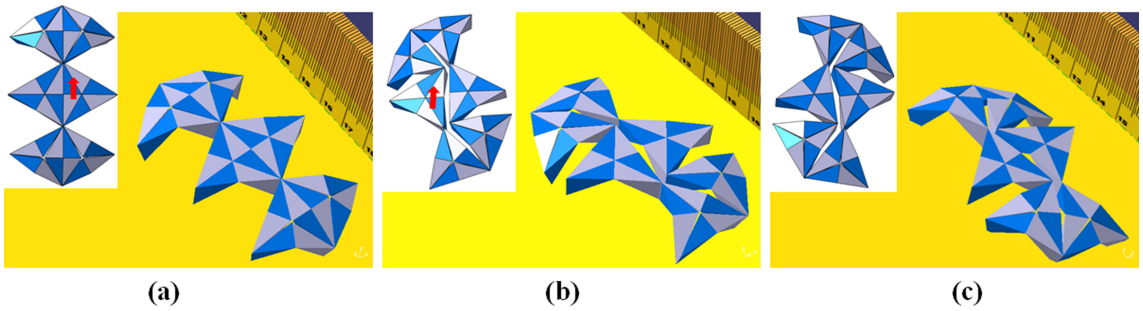

Figure 5.11. Slithering gait proposed for HexaMorph. (a) driving the right middle limb to linearly slide forward. (b) alternating the left middle limb to slide forward.

between two middle limbs, the body of the robot follows a twisted wiggling movement that mimics the snake-turning.

We further envision that HexaMorph is capable of adjusting its body frequently in an adaptive manner to provide a wide range of gaits: laying down on the ground then deploying itself up, adjusting its height through rising and squatting, squirming multi-directionally in a wide open place and finally slithering through a narrow space.

5.3 Concluding Remarks

The main objective of this chapter is to discuss the different material selection for the substrate and hinges, and the mechanical applications derived from Kinetogami. The multi-material printing technology allows us to integrate rigid facets with interconnecting flexible joints as an alternative material construction that can be folded. In the first section, we also present our vision of an integrative manufacturing paradigm that embeds the sheet-based multi-material construction with the folding and actuation functionality.

In the second section, we present HexaMorph, a novel hexapod robot design inspired by Kinetogami. The capability of our folding scheme enables a variety of mechanical and robotic designs by simply assembling substrate pattern and functional components on 2D, and folding and reconfiguration in 3D. We discuss the electrical

design and actuation strategies for the robot, and propose two unique reconfiguration motions: self-deploying and locomotive squirming on the physical prototype.

Our future work will further explore lightweight materials with improved mechanical properties at substrates and hinges, and improve the one-way friction strategy to provide stronger resisting force and avoid backward slippage. In addition, a thorough understanding of singularity of the robot is needed for an optimal selection of the number of inputs. Due to HexaMorph's capability of performing reconfiguration, we will implement the proposed simulated gaits and investigate the reconfiguration planning for the potential applications of deployment, search, and reconnaissance.

To this end, we complete the design and fabrication pipeline of Kinetogami. To further understand the embedded form-and-function prototyping, we found our Kinetogami work is limited because we are only considering the shape of polyhedral primitives themselves made by cutting and folding. In the next phase, we introduce 3D printing in our Kinetogami framework to enhance the shape complexity using cuboidal BSUs.

6. REVOMAKER: ENABLING FUNCTIONALLY-EMBEDDED PROTOTYPING USING MULTI-DIRECTIONAL 3D PRINTING

In recent years, 3D printing has gained significant attention from the maker community, academia, and industry. This is in part due to its flexibility in creating complex geometric shapes, in using multiple materials, and partly due to the emergence of DIY printers that enable low-cost prototyping to support iterative design. Current unidirectional extrusion systems require printing sacrificial material to support printed features such as overhangs. Further, integrating functions such as sensing and actuation into these parts requires additional steps and processes to create "functional enclosures", since design functionality cannot be easily embedded into prototype printing. All of these factors result in relatively high design iteration times.

In order to create complex geometries such as overhangs and undercuts, current additive manufacturing systems need to provide means to support the printed features of subsequent layers. In the material extrusion process, this is typically done by printing fine scaffold structures from the build material (See Fig. 6.1 (a)). Such sacrificial support structures require additional material and consume a large portion of the printing time. Post-processing operations, thereby, are necessitated for separating the printed objects with built-in support. The methods and ease of removal of support structure varies by extrusion methods and build materials, including lye bathing for the soluble support, and mechanical cutting and peeling away for the non-soluble support.

In addition, current plastics-based 3D printing is more suitable for fabricating the decorative models, design concept prototypes and customized products. Traditional design tools and fabrication methods implicitly prevent designers from encapsulating full functionalities in the early design concept prototyping stage. Therefore, designers are forced to design individual parts using 3D printing, assemble them similar

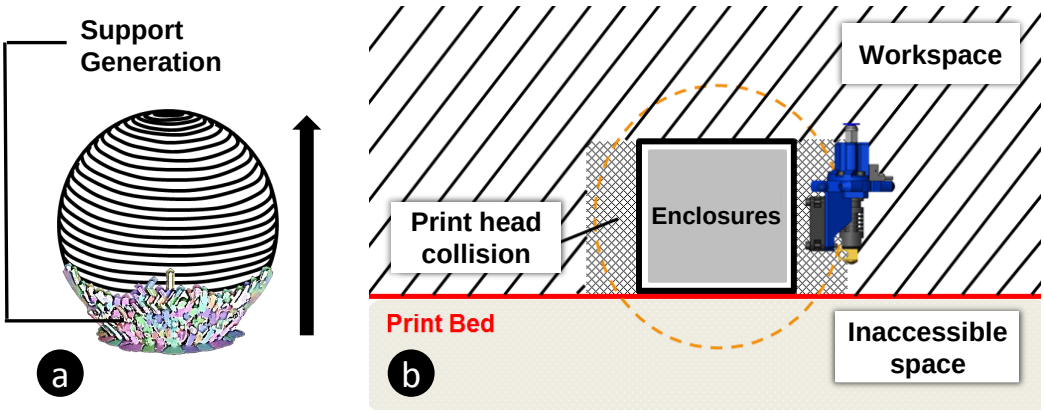

Figure 6.1. For instance, in order to print a sphere, traditional material extrusion process (a) generates sacrificial material to support printed overhanging features, and (b) has limited printing space if one intends to print around an enclosure.

to conventional manufacturing, and iteratively create additional functionalities. Currently, by leveraging the ability to directly embed components during printed parts, many researchers have explored combining additive manufacturing and Direct Write (DW) technologies. Specific applications include signal routing [89], 3D antennae [90], conformal electronics [91], discrete electronics [92], strain gauge sensors [93], force sensors [94], magnetic sensors [95], and batteries [96, 97]. While embedding of a diverse collection of foreign elements, circuits, and sensors has been demonstrated for multiple AM processes, there remains significant need for computer-aided design tools to support modeling of these heterogeneous assemblies and their multi-functionality.

In this section, we present an alternative 3D printing process that can combine functional design along with the shape creation by embedding components during 3D printing. With traditional printing, placing such enclosures on the print bed will not allow layer-wise fabrication since the printhead intersects with the enclosure and any geometry beneath is infeasible to print (See Fig. 6.1 (b)).

In this Chapter, we demonstrate a multi-directional 3D printing process that is capable of inherently reducing build and support consumption, and producing a new

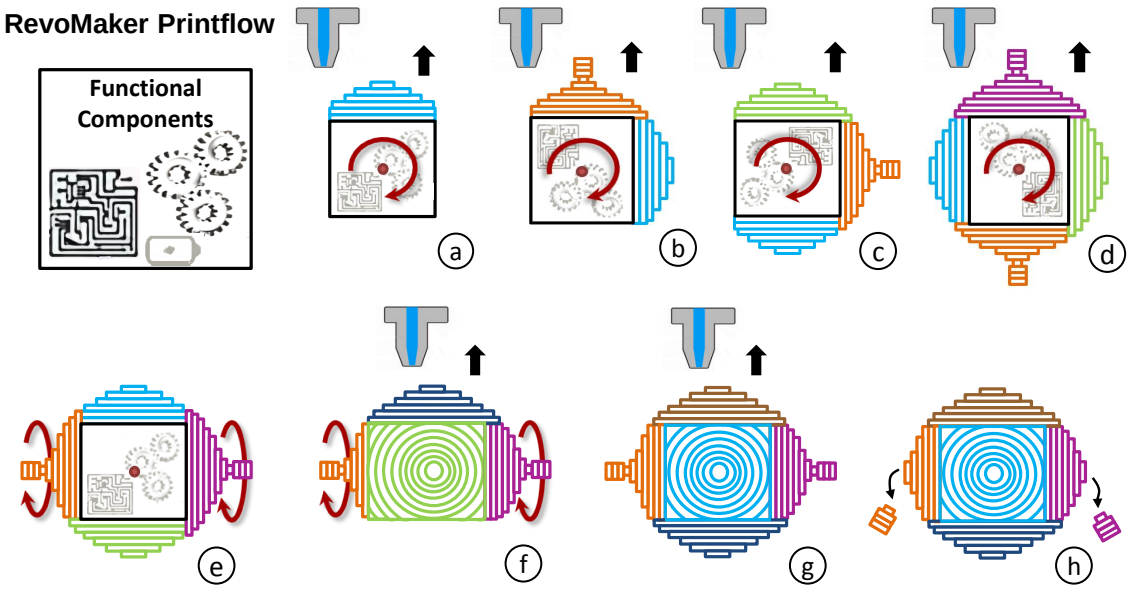

Figure 6.2. (a)-(d) revolving a cuboidal base about the out-of-plane central axis and printing four partitioned geometries around the base. A pair of handles are added to the opposite facets, allowing the cuboid to be gripped for the next run of rotation. (e)-(g), revolving the cuboid about the in-plane central axis and printing the rest two partitioned geometries. (h), snapping off two extra handles when the print is completed.

genre of custom products with higher levels of functionality. The key idea is to enclose functional components inside a laser-cut cuboidal enclosure, which is also a printing base inscribed within a desired shape. By revolving the cuboid shown in Fig. 6.2, we print partitioned geometries on and around each facet. In RevoMaker, the cuboidal base (a) encapsulate advanced functionality the user does not need to have detailed knowledge of, (b) saves time and print material for 3D printing by using laser cutting, (c) doubles up as a platform for 3D printing, and (d) also structurally adheres to the 3D printed material. Our system affords a high manufacturing precision by (a) seamlessly printing exterior skin geometries in a single build (no gap between partitions), (b) enabling directly side-surface functionalities that also interact with housed modules in a compact volume, and (c) ensuring a strong bond within overlapping partitions since the print material fuses with itself. Thus we enlarge the design space of

3D printing to go beyond simple parts using the volume within the 3D printed shape itself to embed functionality. Different use cases that demonstrate the feasibility are discussed later in this paper.

In general, our design goals for RevoMaker are:

- Less use of build material
- Significant reduction of support consumption
- Reduced need of post-processing operation
- Embedding of functional components

The work of RevoMaker consists of two parts: 1) the optimization algorithmic design to reduce build and support material consumption, and 2) the mechanical implementation and machine design. The first part presented in Sections 6.2.1 $\sim$ 6.2.3 was achieved in collaboration with my colleague, Yunbo Zhang. Currently our approach is more suitable for the object shapes that approximate the cuboid, and requires combining laser cutting process and manual user involvement.

6.1 Related Work

6.1.1 Hollowing and optimizing support generation

Previous research studies have been dedicated to reduce both the printing volume and support generation. A natural way to reduce printing volume is to hollow the model based on physical-geometric optimization [98]. Another research intended to improve the structural integrity by generating *honeycomb-cells* inside model [99]. However, none of these existing methods generate an interior space that is well-structured and fully used for functional enclosures. On the other hand, methods were proposed to reduce support materials by optimizing the model orientation for printing [100, 101], and optimizing support scaffolding structures that consume less material

[102–105]. Due to the unidirectional printing process, the reduction of support in general is quite limited and can hardly be post-processing free.

6.1.2 Multi-axis manufacturing

In the areas of additive manufacturing and process design, Song [106] and Pan et al. [107] developed a 6-DoF Steward mechanism to continuously print conformal feature, such as textures or patterns, on curved and irregular surfaces. This CNC-based accumulative process enables continuous fabrication with different size, shape resolution requirements. Traditional multi-axis fabrication solutions might also reduce the need for support by tilting the nozzle or object.

Recently, by combing the geometric accuracy of 5-axis CNC milling and the layer principles of additive Solid-Freeform-Fabrication (SFF)technique, researchers have developed a superior manufacturing process, called *Shape Deposition Manufacturing* (SDM) [108]. The method allows the manufacturing of fully-functional parts with conformal embedded electronics and with multi-material properties. The multi-material structure is generated by depositing subsequent compacts of different materials. However, such expensive and complex multi-axis systems have higher overheads such as:

- the demanding control strategies for motion synchronization
- the complexity of path-processing planning and mechanical calibration
- the difficulty of adhering print material onto largely slanted or bottom surface due to the effect of gravity

In our approach, by adding 1 DOF to a cuboid and using printer's own X-, Y- and Z-step precision, we (a) add much greater functionality and capability to the resulting low-cost process and product and (b) utilize gravity to allow the print material to firmly adhere to horizontal surface.

6.1.3 Fast fabrication of 3D objects

By introducing intermediate low-fidelity fabrication into traditional slow but hi-fidelity printing process, Mueller et al. and Beyer et al. proposed a variety of alternative fabrication methods, such as printing wireframe mesh of a object [109], substituting sub-volumes of a model with standard Lego building blocks [110] and laser-cut parts [111]. These different approaches effectively reduced the printing time while preserving the shape of a model. Besides, Hansen et al. [112] achieved a parallel printing process via microvascular multi-nozzle Arrays.

6.1.4 Printing with functional effect

A fundamental advantage of the layer-by-layer fabrication approach found in 3D printing is the ability to access the entire volume of the workpiece throughout the build process [113]. This allows for the direct fabrication of functional products and assemblies within the additive manufacturing machine. Prevost et al. [114] proposed an approach to generate models which can stand alone by deforming the initial inputs. Umetani and Schmidt [115] optimized the orientation of a model for 3D printing to increase mechanical strength and structural soundness. Other interesting works involve printing kinematic mechanisms [116, 117], working prototypes [118], articulated models [119, 120], prosthetics [121–123].

6.2 How RevoMaker Works

In placing the cuboidal base within a desired shape, a key challenge is related to how to pose the objective function so the number of possibilities of cuboidal orientations and printing sequences are balanced to reduce the support generation as well as the use of print material. Furthermore, when printing one facet after the other, the print nozzle should not intersect with the material already printed, and merge the new partitioned shape well with the old. In this Section, we first discuss how we

formalize these objectives across many geometric shapes, and then followed by our mechanical implementation of RevoMaker.

6.2.1 Objective function

Given an input triangular mesh model $M = (\mathcal{V}, \mathcal{E}, \mathcal{F})$, we introduce Cuboidization, an algorithm that generates an interior cuboid C, where all six facets C_f^i ($i \in (1, 2, ...6)$) of the cuboid partition M into six outward regions $M_p^i s$. Recent research effort such as orthogonal slicing [124] and approximate pyramidal decomposition [125] introduce different partitioning strategies on the overall shape of an object to improve fabrication accuracy and for minimal number of pyramidal parts. In contrast, the main goals of Cuboidization are two folds: (1) create the cuboid with as large volume as possible to save print materials and (2) six outward regions M_p^i add up to as little overhangs as possible to save support material. Considering the time consumption and effort on post-processing, in our work, the reduction of support material generation takes priority over augmenting the cuboid volume. Hence, we define the objective function as follows:

$$\arg\max_{C} F_{vol}(C) \quad s.t. \sum_{i=1}^{6} F_{overhang}(M_p^i) = 0, \tag{6.1}$$

where F_{vol} measures the volume of C and $F_{overhang}$ evaluates the overhanging feature of M_p^i. Leveraging F_{vol} and $F_{overhang}$ is not a trivial task since $F_{overhang}$ depends on C but it can be only evaluated after the region partition is done. Therefore, it is not feasible to analytically solve Equation (6.1) using nonlinear optimization approaches.

In our work, an overhang-aware multi-loop optimization framework shown in Algorithm 1 is proposed to resolve this problem. The outer loop uses a *Particle Filtering* based sampling algorithm to generate a set of principal axes for the cuboid (also called *cuboidal orientation*), see Section "Initial orientation sampling". Inside the inner loop, by inputting three orthogonal vectors **u**, **v** and **w** as the principal axes for the cuboid, we generate and compute the size of the largest cuboid inscribed (Section "Cuboid generation"). After obtaining the cuboids over all orientations, we compare their

Table 6.1. Algorithm of cuboid generation.

Algorithm 2: Multi-loop Cuboidization

Input: M is input model, l is the maximum level of Particle Filtering;

Output: C is the cuboid that partitions M, and S is the printing sequence;

Function $(C, S) = FindCuboidization(M,\ l)$

$currentLevel \leftarrow 0$;

$currentCuboidSet \leftarrow \varnothing$;

$newOrientationSet \leftarrow InitialOrientationSampling()$;

while $currentLevel < l$ **do**

foreach *orientation* $\mathbf{O}_i \in newOrientationSet$ **do**

C $\leftarrow GenerateCuboid(M, \mathbf{O}_i)$;

$(C.V, C.A_{overhang}, C.S) = EvaluateCuboid(M, C)$;

$currentCuboidSet$ += C;

$newOrientationSet = OrientationResamping()$;

$currentLevel \leftarrow currentLevel$ +1;

return *BestRanked(currentCuboidSet)*;

Function $(V, A_{overhang}, S) = EvaluateCuboid(M,\ C)$

$V \leftarrow CalculateVolume(C)$;

$A_{overhang} \leftarrow +\infty$;

foreach $S_{temp} \in$ *All Printing Sequence for* C **do**

$A_{temp} \leftarrow CalculateOverhangingArea(M, C, S_{temp}$;

if $A_{temp} < A_{overhang}$ **then**

$A_{overhang} \leftarrow A_{temp}$;

$S \leftarrow S_{temp}$;

return $V, A_{overhang}, S$;

volume, overhanging features, and retain B top-ranked candidates with least support consumption for user to select the final print. How different printing sequence would

affect the resultant partitioning as well as support avoidance is discussed in the Section "Optimization of printing sequence". Currently, our Cuboidization algorithm is more suitable for processing shapes with topological genus of 0, and preferably those that approximate the cuboid. Models with high genus (rings, knots, etc.), long and curved protruding features, or massive small curvy features, limit our approach to provide less support structures, see Fig. 6.3.

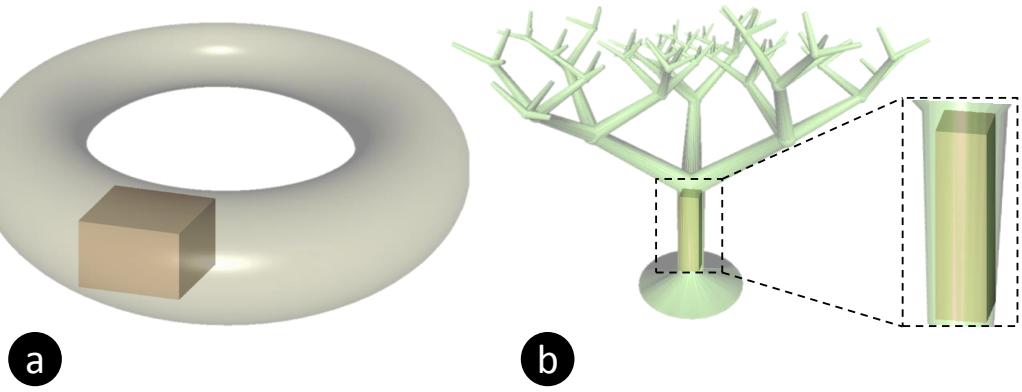

Figure 6.3. (a) Inapplicable cases where overhanging features can not be largely reduced. For instance, (a) a 3D shape with high topological genus such as a ring of genus one, or (b) with long and branched protruding features such as a tree.

6.2.2 Overhang-aware Cuboidization framework

Initial orientation sampling. In order to find an optimized interior cuboid for each model, we first consider sampling a set of cuboidal orientation using a particle filtering based approach. As each orientation matrix $\mathbf{O}_i$ consists of three unit orthogonal vectors $\mathbf{u}_i$, $\mathbf{v}_i$ and $\mathbf{w}_i$ as column vectors, the sampling is performed for the three components one after another. Without loss of generality, $\mathbf{w}_i$ is determined initially. We uniformly sample K points on a Gauss sphere, and each of the samplings is assigned to $\mathbf{w}_i$ (see Fig. 6.4(a)). For each $\mathbf{w}_i$, the second uniform sampling is performed on a unit circle laying on the normal plane of $\mathbf{w}_i$ in order to obtain L samples of $\mathbf{u}_i$

and $\mathbf{v}_i$ (shown in Fig. 6.4 (b)). Note that, as opposite direction results in the same $\mathbf{O}_i$, we consider herein only the semisphere and semicircle, where the polar point for semisphere and end point of semicircle are arbitrarily positioned. For each model, there are $K \times L$ orientations in total to be evaluated and filtered.

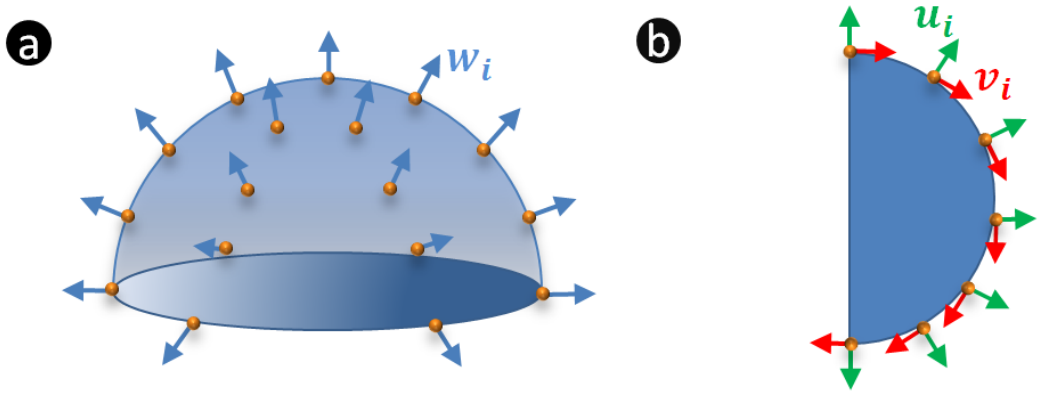

Figure 6.4. (a) sampling the unit vector $\mathbf{w}_i$ (b) sampling the unit vectors $\mathbf{u}_i$ and $\mathbf{v}_i$.

Cuboid generation. Given a determinate orientation, the second part of algorithm generates a cuboid with as large volume as possible inside M. We use a heuristics based methods [126] to balance the resultant quality as well as computation efficiency. The generation details are discussed as follows: followed by the orientation $\mathbf{O}_i$, a small enough cuboid C_i is initialized at the center of a largest inscribed sphere within M. The six facets of C_i then move along their corresponding normal directions to incrementally expand the size of the cuboid. At each augmentation step, the corner collision is detected. The iteration stops when no facet can be moved further. All possible cuboids inscribed inside M along orientation $\mathbf{O}_i$ are recorded and indexed by volume, and the one with the maximum volume will be returned as the resultant candidate .

Evaluation of overhangs. With the partitioned model, an overhanging evaluation function is defined as follows:

$$\sum_{j=1}^{6} \sum_{f_k \in \mathcal{F}_{M_p^j}} F_{area}(f_k), \tag{6.2}$$

$$F_{area}(f_k) = \begin{cases} 0 & if\ \mathbf{n}_{f_k} \cdot \mathbf{n}_{M_p^j} < \delta \\ area\ of\ f_k & otherwise \end{cases} \tag{6.3}$$

$F_{area}(f_k)$ measures the overhanging area on each facet f_k depending on whether the dot product of its normal $\mathbf{n}_{f_k}$ and the normal of C_f^j is less than the threshold. All results in this paper use δ to be $-\cos 45°$, unless otherwise stated.

Filtering and re-sampling. According to the evaluation results, we select N orientations with least sum of overhanging areas. To avoid selecting too many similar cuboids, we discard those orientations with less variation and only the ones with larger than 70% variations are kept. The following equation is used to evaluate the variation of two orientations $\mathbf{O}_i$ and $\mathbf{O}_j$:

$$\begin{aligned} F_{var} = &|\mathbf{u}_i \cdot \mathbf{u}_j| + |\mathbf{u}_i \cdot \mathbf{v}_j| + |\mathbf{u}_i \cdot \mathbf{w}_j| \\ &+ |\mathbf{v}_i \cdot \mathbf{u}_j| + |\mathbf{v}_i \cdot \mathbf{v}_j| + |\mathbf{v}_i \cdot \mathbf{w}_j| \\ &+ |\mathbf{w}_i \cdot \mathbf{u}_j| + |\mathbf{w}_i \cdot \mathbf{v}_j| + |\mathbf{w}_i \cdot \mathbf{w}_j| \end{aligned} \tag{6.4}$$

At each selected orientation, we uniformly resample over its neighborhood region with a radius ϵ on the Guass sphere, and generate the new set of cuboids. The empirical values of K for initial sampling and resampling are set as 25 and 10. We use $L = 10$ for both samplings and $N = 5$ for the resampling process. Thus, for each model we evaluate 1250 orientations after two sampling processes in total and final B top-ranked candidates with least support material generation are retained for user to select by leveraging the physical dimension and shape of functional components.

6.2.3 Optimization of printing sequence

While evaluating the overhanging feature over six partitioned geometries, it is crucial to determine the optimal printing sequence simultaneously. In order to achieve

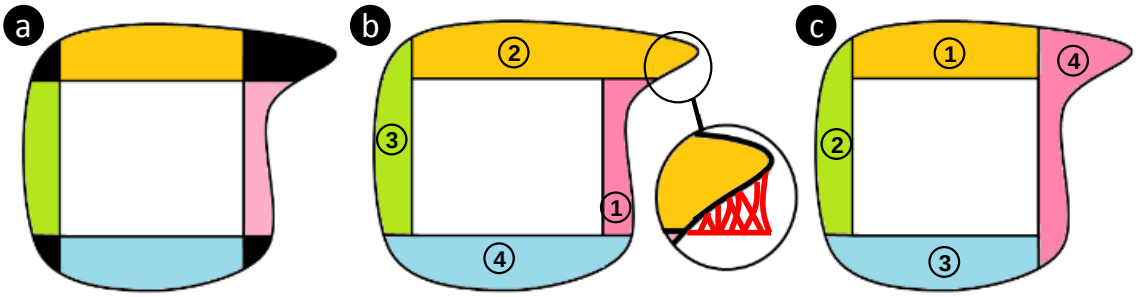

Figure 6.5. (a) partitioning based on above-facet regions and corner regions (b) printing sequence 1 generates support material (c) printing sequence 2 generates no support material.

the minimal number of serialized rotation and accordingly minimal effort of handling, we define our strategy of printing such that: (1) four adjacent partitioned geometries about a central axis of the cuboid are printed by intermittently rotating the axis by 90 degrees, and (2) the rest of the two opposite partitions are printed afterwards by rotating every 180 degrees about a second central axis which is orthogonal to the previous one. This reduces the number of degrees of freedom to two and the intermediate number of handling to one. Through initial partitioning, the model can be inherently segmented into the print regions right above each cuboidal facet (the pink, yellow, green and blue regions shown in Fig. 6.5 (a)). As for the corner regions shown in black in Fig. 6.5 (a), we assign each of them into its neighboring above-region(s). Here the printing strategy is that once the first facet is determined, each corner region is always assigned to the later-to-print above-region that follows a single rotational direction (for instance counterclockwise shown in Fig. 6.5 (b)). In doing so, it also generates extended underlying surface to support the corner geometries after each rotation. Note that different selection of the initial facet to be printed on results in different support generation scenarios. As shown in Fig. 6.5, the sequence (b) generates support in the right upper corner while in (c) it is totally support-free. For each cuboid with determinate size and orientation, we search over 30 different combinations of printing sequence around six cuboidal facets and choose the one with

less or no support generation. These combinations vary based on which facet is the first to be printed on, the rotational direction and the selection of two facets that stay as the last-to-print ones.

6.2.4 Mechanical implementation behind RevoMaker

Ultimaker 2 3D printer. Fig.6.6 (a) shows an assembled view of the mechanical and electrical apparatus that are extended onto Ultimaker2. All of the models shown in this paper were printed on this modified 3D printer, i.e., an open-source fused-filament extrusion system with $230mm \times 225mm \times 205mm$ build volume and up to 20 microns print accuracy. The filament material used for printing is the $3mm$-diameter Polylactic acid (PLA).

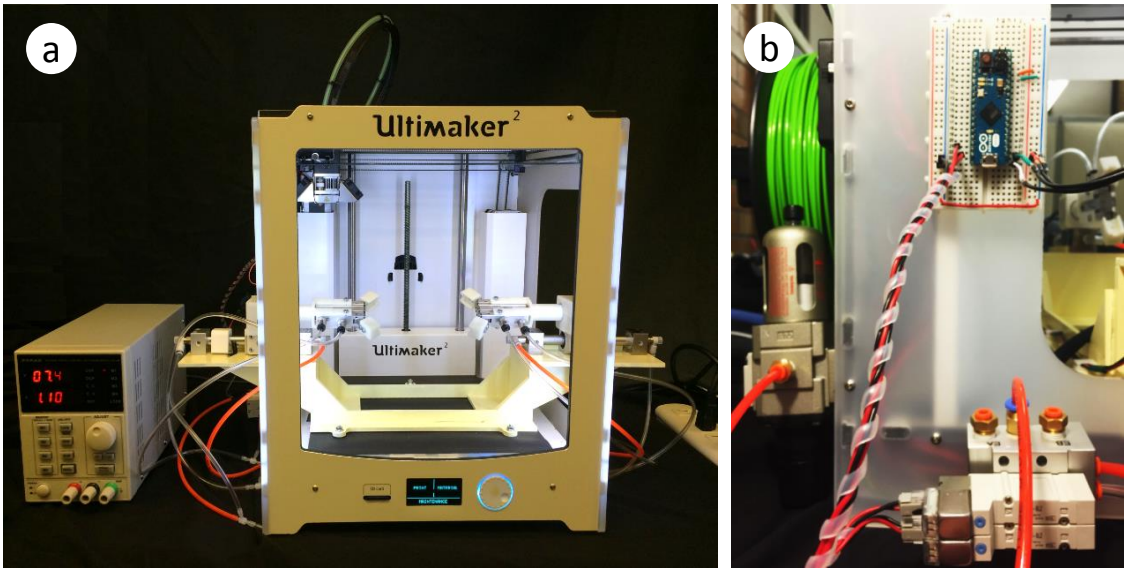

Figure 6.6. We extend a standard low-cost FDM printer, UltiMaker2, with mechanical, electrical and pneumatic devices.

Laser cutting of cuboidal base. Unlike the standard bed material used in FDM printers where extruded plastic needs to be easily peeled off from the print bed, we select a $3mm$-thick *Plexiglas*® DP-95 acrylic sheet as the build surface material for each facet of the cuboidal base. This cell-cast material is available with low heat

capacity and matte finish on both sides to ensure a very firm first-layer PLA bonding with little pre-heating process.

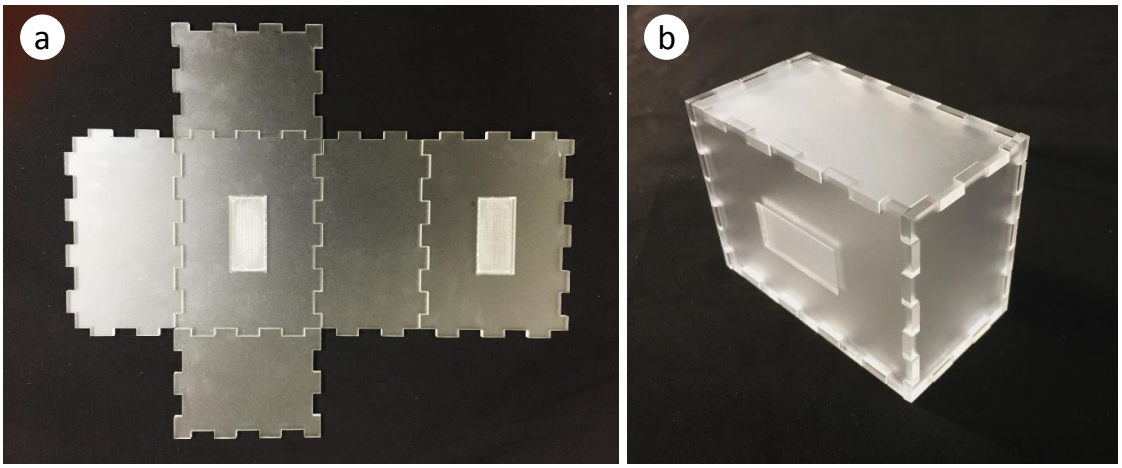

Figure 6.7. (a) a flattened cuboidal net pattern using laser-cut facets and slots; (b) a folded cuboid.

Six rectangular facets and twelve edges comprise a cuboidal base. We synthesize the interlocking teeth pattern along each edge so that six facets can be rapidly press-fit together seamlessly (see Fig.6.7). In order to level and secure the cuboid during printing, two $32mm \times 15mm$ rectangular slots are also engraved on a pair of opposite cuboidal facets (also called side-facets) using laser cutting. Our experimental results show that for each model it takes on the average 5 to 10 minutes to laser cut the facets and approximately 1 minute to assemble the cuboid.

Embedding of functional modules. The internal space inside each cuboid base is utilized for embedding functionalities. This standardized cuboidal space can house a wide variety of mechanical, electronic, sensory and actuation components, including but not restricted to processor chips, sensors, springs, gears and motors. By providing channels in the printed material, external devices such as lights and wind-up keys can then interconnect with the housed components inside to enhance visual, motion and movement functionalities, through the slots and holes already added on each of six cuboidal facets. Our process is relatively simple when compared to the traditional

processes where multiple high-fidelity printed parts must be assembled in 3D while enclosing motors and sensors. We lay down and pre-assemble functional modules on the "flat" unfolded cuboid. We then close the cuboid by folding, and "coat" the external skin shapes over it using our 3D printing process.

Fixation, revolving and gripping. Three degrees-of-freedom movements are needed for realizing the multi-directional printing: (1) translation along X to fixate and release the cuboidal base, (2) rotation about X to revolve the cuboid facets around, (3) and angular motion to deliver strong gripping to the handles. We attach an acrylic stand with 2 cantilevered support plates to our build platform. A pair of linear air cylinders sits on the support plates to fixate or release the cuboid from both sides. These magnetically coupled linear cylinders (CY3R-10-65) are powered pneumatically and controlled by a solenoid valve (see Fig.6.6 (b)). To enable the revolute motion, two HerkuleX DRS-0201 robot servos rest on the air cylinders and two connected air fingers (MHY2-10D) provide angular gripping motion. In RevoMaker, we first hand delivers the cuboidal base to the center of the printer. These 180-degree angular fingers are initially closed and fit into side slots to secure the cuboid by squeezing. After one partitioned geometry is printed on top of the build surface, the servos synchronously revolve the base by 90 degrees. Therefore, four facets surrounding the revolute axis can be printed in the first run of revolving (see Fig.6.8 (b)-(e)). Note that during printing, two opposite facets among the four are chosen to add two collinearly-aligned handles outside the geometries. The purpose of adding these handles is for the grippers to secure the model in the second run of revolving while avoiding directly contact the printed surface.

After we releasing the grippers, we rotate the part such that the grippers close over the handles from both sides. Once the remaining two partitioned geometries are printed, we snap off two handles for completing the print. Throughout the whole fabrication process, we calibrate the surface location of the cuboid twice before printing the first and the fifth facets. The corner coordinates of the rectangular facets and slots are recorded as the reference coordinates for the print head to start printing.

6.3 Prototypical Results and Use Cases from RevoMaker

6.3.1 Sculptural objects

According to the Cuboidization results on a number of genus 0 models with different overhanging features on different locations, including man-made art objects and organic forms, our optimization framework generates cuboids that allow zero support material to the printed geometries. Five sculptural models including a small Hexacronic Icositetrahedron, spherical ball, Max Planck, French bulldog, Mickey Mouse, bulldog were fabricated with empty cuboids first to verify our optimization framework with reduction of print and support material. Fig.6.9 (a) shows the partitioned result of a small Hexacronic Icositetrahedron where 6 "mountain"s are extruded and connected from 6 cuboidal facets, respectively. After laser cutting the cuboid and printing around each facets (see Fig.6.9 (b)-(g)), we achieve the final print with 6

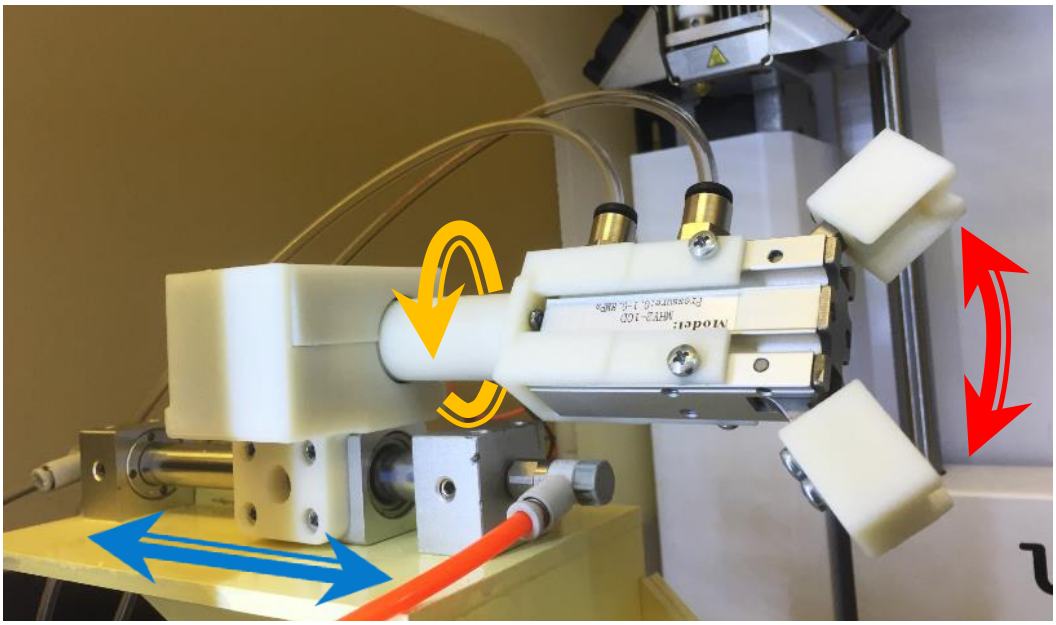

Figure 6.8. Each gripper from both sides has 3 degrees-of-freedom: (1) translation to fixate and release the cuboidal base, (2) rotation to revolve the cuboid facets around, and angular motion to apply gripping force to the handles.

Table 6.2. Comparison of time and total material reduction using RevoMaker and Ultimaker 2.

Models	RevoMaker		Ultimaker 2				time reduction	total material reduction
	time (hh:mm)	build volume (cm^3)	time (hh:mm)		build volume (cm^3)			
			t_{min}	t_{max}	V_{min} ($V_{support}$)	V_{max} ($V_{support}$)	compared to t_{min}	compared to V_{min}
Sphere	**4:03**	**61.7**	4:58	4:58	77.9 (0.3)	77.9 (0.3)	18.4%	20.8%
Max Planck	**6:11**	**114.6**	8:13	9:16	142.6 (7.4)	163.8 (28.6)	23.5%	19.6%
Bulldog	**7:36**	**133.8**	10:52	12:43	177.3 (26.7)	215.9 (65.3)	20.8%	24.5%
Mickey	**6:15**	**112.2**	8:22	15:01	138.4 (6.4)	257.2 (125.2)	25.3%	18.9%
Star	**9:06**	**165.5**	11:25	13:32	200.6 (12.6)	231.9 (43.9)	20.3%	17.5%
PC Mouse	**2:55**	**48.4**	4:38	6:44	76.7 (10.9)	111.3 (45.6)	37.0%	36.8%
Bulbasaur	**5:24**	**93.7**	6:37	7:17	109.7 (1.7)	121.6 (13.6)	18.39%	14.6%

*By placing model in different orientations, t_{min} and t_{max} are the minimum and maximum time duration using Ultimaker 2; V_{min} and V_{max} are the minimum and maximum consumption of material (build + support), $V_{support}$ is only the consumption of support material. Using RevoMaker, the time statistics of Cuboidization for each selected model (top down), included in the total time, are 30s, 2min 33s, 6min 45s, 5min 03s, 1min 10s, 1min 02 s, 4 min 17s, respectively.

different color and a "UIST 2015" logo on it. Fig.6.10 shows the rest of the models with their support generation using Ultimaker 2, partitioned results and final prints, respectively. In order to validate the strength in our approach to save time, build material and support material, we compare the fast-printing results using both RevoMaker and Ultimaker 2 over seven selected models.

As shown in Table. 6.2, comparing to t_{min} and V_{min}, Revomaker achieves a 23.4% reduction of printing time, and 21.8% reduction of total material consumption on average. The main strength of our multi-directional printing process is that it provides significant reduction of support material generation. When carefully comparing two printing procedures. we observe that the regular unidirectional extrusion process initially generates skirts and rafts on the print bed to smooth the printing flow and to assist bed adhesion, then it prints 3∼4 solid adhering layers and followed by the hollowed structures inside. Our approach requires periodically printing 1 adhering layer 6 times for the six partitioned geometries. Together with the two added handles, it leads to a modest improvement in printing time and overall material consumption.

6.3.2 Use case 1: Custo "Mice", customizable mice

We customize a computer mouse for an ergonomical fit to the palm and tailored functionalities. Dating back to 1964, Dr. Douglas Engelbart invented the first computer pointing device with one button on top and two wheels on the underside. The mouse began to multiply rapidly with embedded mechanical, optical and electronic systems. However, creating a mouse design from scratch and prototyping enclosures can be a iterative and daunting task especially for novices. It requires 3D modeling, molding/tooling design and physical assembly to be integrated seamlessly to fit all individual components inside an exterior shell. More importantly, with traditional injection molding, it is difficult to mold reentrant features and side-surface functions such as buttons.

To demonstrate the whole fabrication process, Play Doh was initially used for one to create the shape of the mouse (see Fig.6.11 (a)). In doing so, the user is able to quickly verify a list of customizable human factors regarding the size range of hands, finger extension and palm comfort. In our custo"mice" the user also specify the middle-click to be operated by thumb on the side of the mouse. Then its shape was captured using a 3D scanner, shown in Fig.6.11 (b). The algorithm generates the size of the cuboidal base and provides slot-cuts for the button areas in the partitioned geometries, shown in Fig.6.11 (c,d). Matching slot-cuts on the cuboid provide a cantilever which deflects to actuate internal switch when the external button area is pressed. Fig.6.11 (e) shows that all added functional modules are pre-assembled on the flattened laser-cut facets and enclosed inside the cuboid when closed. These modules include 3 buttons for left-, middle-, and right-clicking; light-emitting diodes (LEDs) and photodiodes to detect movement relative to the underlying surface; printed circuit board (PCB) with electrical resistors, capacitors, integrated circuits (ICs) mounted on; and rechargeable battery. Lastly, the custom-made geometries are printed around the cuboid to complete the prototyping and ready for use directly after printing (see Fig.6.12).

6.3.3 Use case 2: wind-up Pokémon

To further expand the design space for functional products, we enclose passive-actuated wind-up motor with gears and springs inside the cuboidal base. One of the popular Pokémon character Bulbasaur is selected in this example due to its large amount of overhanging features, shown in Fig.6.13 (a). Similar to the previous procedures, we partition six geometries around an embedded cuboid (see Fig.6.13 (b)), and enclose the cuboid with laser-cut facets and kinematic components including the wind-up motor and batteries (see Fig.6.13 (c)). After taking it out from Revomaker, we insert another Pokémon character Pikachu's tail into the back hole of Bulbasaur, and a wind-up key into the side hole of Bulbasaur to waggle the tail. Besides, one

can insert a pair of LEDs into the eyes of Bulbasaur, and the eyes start blinking simultaneously after winding, shown in Fig.6.13 (e).

6.4 Concluding Remarks

In this chapter, we explored a multi-directional 3D printing process not only to reduce the consumption of print and support material, but also to enable a new breed of custom products with embedded functionalities. We propose the Cuboidization algorithm to generate a cuboidal enclosure, also as the printing base, with as large a volume as possible inside the model and featuring as few overhangs as possible. Therefore, we modify and enhance an existing 3D printer by adding a revolving DOF to a laser-cuttable and foldable cuboidal platform, to allow multi-directional 3D printing and functionally-embedded product design. We believe that the modularization of functionalities and integration of 3D shapes will open up a new genre of 3D printing and eventually alleviate design and assembly burdens.

Using Revomaker, the 3D printer we developed in implementing the above process, we printed a number of sculptural models and two functional products, i.e., a customizable computer mouse and wind-up toy. We thus demonstrated its capabilities in combining functional design along with the shape creation. By only marginally increasing the complexity of a current off-the-shelf machine, we add much greater functionality and capability to the resulting process and products. Therefore, a wide variety of custom functionalities can be directly fabricated together with the shape creation.

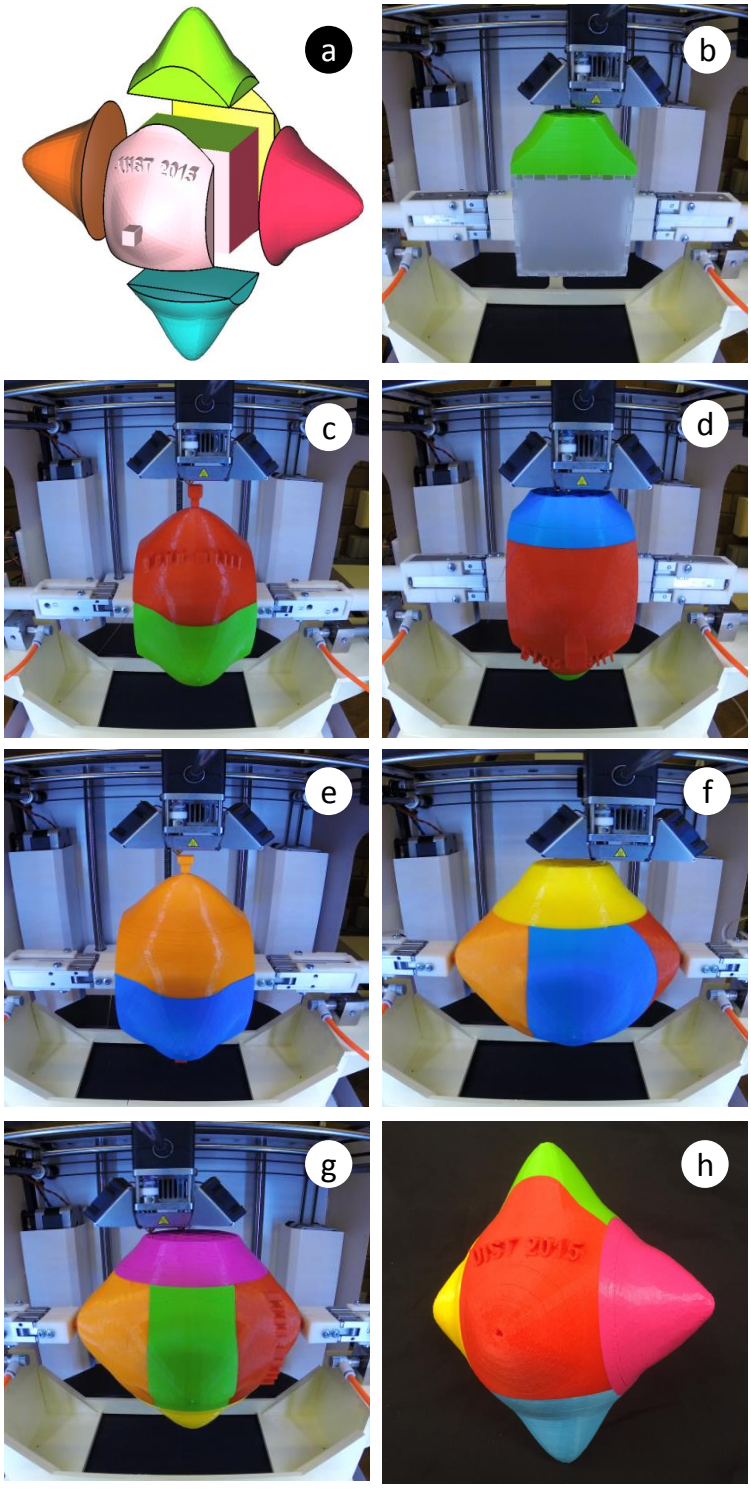

Figure 6.9. (a)Cuboidal generation and partitioned results of a small Hexacronic Icositetrahedron with the "UIST 2015" logo. (b)-(g) printing 6 partitioned geometries intermittently around a revolving cuboidal base using our method. (h) final print.

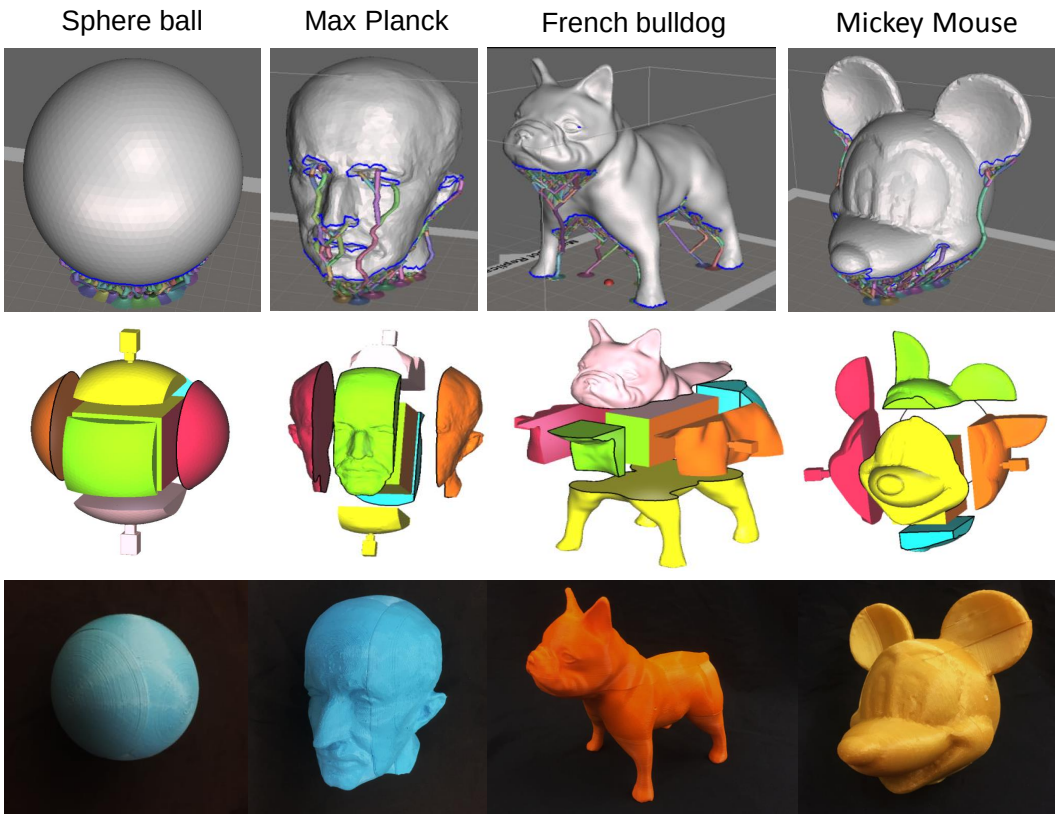

Figure 6.10. first row: visualization of support generation for a sphere ball, Max Planck, French bulldog and Mickey Mouse head using existing FDM printing process in Ultimaker2 (the model is oriented where less support structures are created. second row: partitioned results of each model. third row: prototypical results of each model.

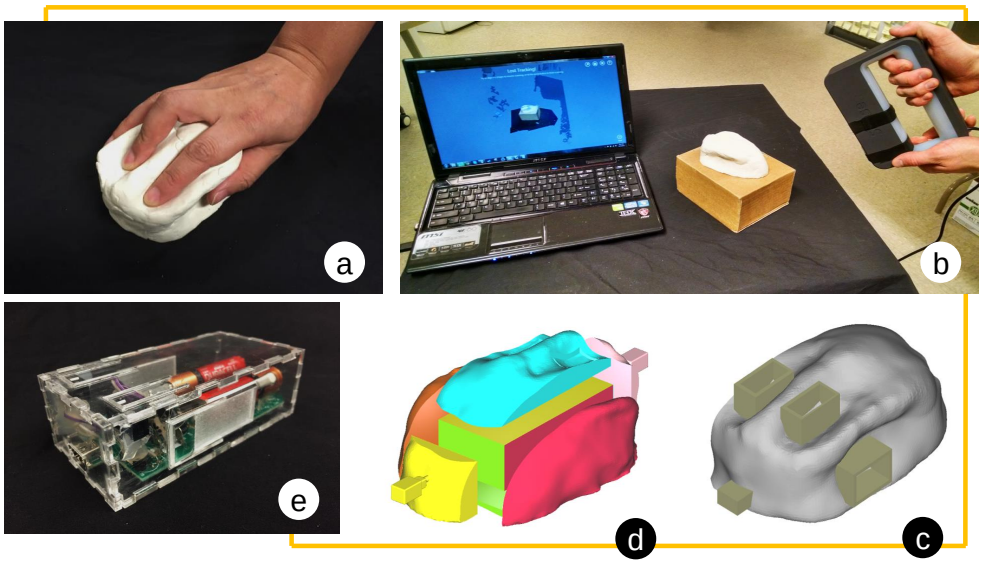

Figure 6.11. (a) user interaction to tailor the shape of his/her ergonomical-fitting mouse using Play Doh. (b) 3D scanning (c) hollowing the digital model with slot-cuts to separate out three button areas. (d) six partitioning geometries around an embedded cuboid. (e) enclose buttons, printed circuit board and optical components inside the laser-cut cuboid.

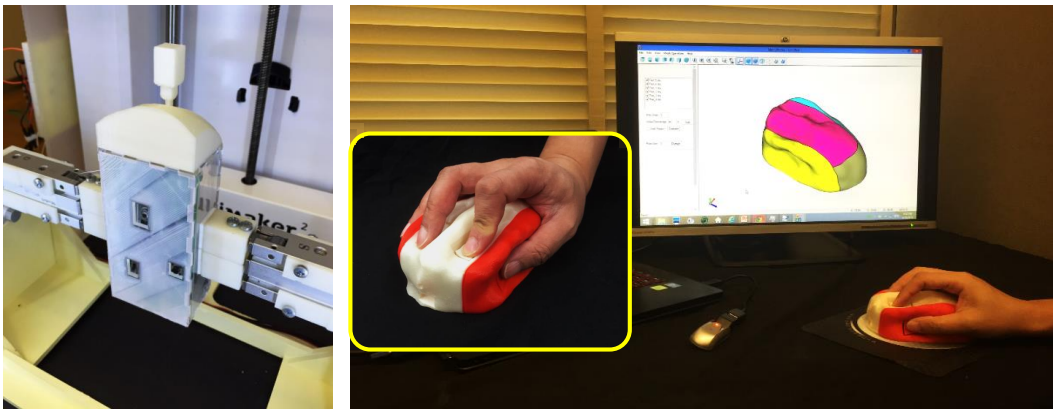

Figure 6.12. Revomaker prints the partitioned geometries around the cuboidal enclosure and delivers a functional and ergonomical computer mouse right after printing.

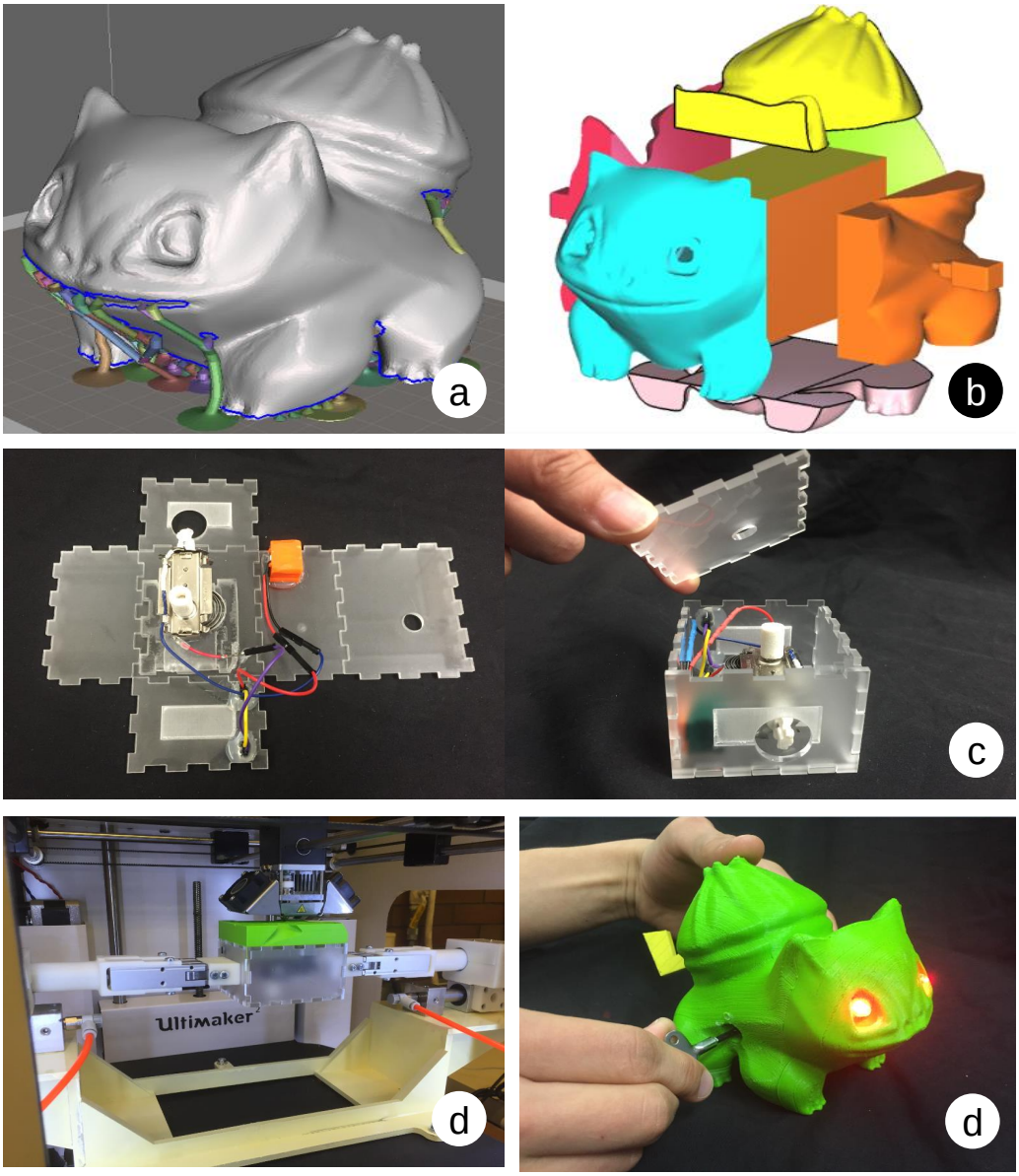

Figure 6.13. shows (a) support generation for Bulbasaur (b) six partitioning geometries around an embedded cuboid. (c) pre-assembling the wind-up motor and batteries onto flattened laser-cut facets and close the cuboid as a printing base. (d) printing the Bulbasaur shape around the cuboid. (e) winding the Bulbasaur up to trigger tail-waggling and eye-blinking.

7. SYSTEM LIMITATION, CONCLUSION AND FUTURE WORK

7.1 Conclusion

The abilities of Kinetogami enable foldable mechanistic designs by varying layouts and materials on 2D, and hence results in multiple embedded functionalities in 3D. RevoMaker further provides a seamless prototyping platform to integrate encased functional components with 3D shape creation. The main goal of this work, to render complex reconfigurable structures, mechanisms and functional products from planar sheets, has potential for both the practical world and the creative world. We have found the applications of our folding framework in the structural, robotic and custom product designs to be of great relevance. The interaction between 2D and 3D, with deliberate or apparent transformation, augmented by shape, pattern and motion, all contribute to a rich realm of possibilities for designers, engineers and even artists to work together. Active logos, interactive surfaces, reflective panels, customizable products, are all possibly integrated together with the Kinetogami folding scheme and RevoMaker multi-directional 3D printing in a dynamic flow of folding, transforming, prototyping, and putting to use.

Currently, Our Kinetogami folding framework and RevoMaker prototyping system still have the following limitations:

- In our Kinetogami work, polyhedral BSUs are investigated with special geometric properties and limited material selections. We are still facing the design challenges of using a wide range of geometric primitives and materials to establish a more general building architecture of polyhedral mechanisms.

- From the BSU family, our RevoMaker system focuses on a single cuboidal unit to demonstrate functionally-embedded additive manufacturing process. In addition, the Cuboidization algorithm is more suitable for processing the models

that approximate cuboids, and the encased components are no longer accessible once the 3D printing is completed.

- The systematic design strategies on how and where to embed functional components inside BSUs are not explored in our current Kinetogami and RevoMaker frameworks.

7.2 Future Work

Future work of this thesis can address the following:

(1) Investigation of various geometric exploration, material compatibility, folding strategies and integrative manufacturing processes to enhance Kinetogamic folding scheme using digital fabrication.

(2) Integration of Kinetogami and RevoMaker to achieve both the reconfiguration and shape complexity using BSUs.

(3) Exploration of modular-based function and form embedding and systematic development of prototypical products to demonstrate diverse product forms and functionality.

Initial thoughts in exploring each of these possible future directions will be explained in the following subsections:

7.2.1 Various foldable construction enabled by digital fabrication

With the trend and capability of digital fabrication, a booming *Do It Yourself* movement has been significantly shifting and integrating the role of a designer, assembler and manufacturer into an integrated one. The fabrication tools, such as 3d printer and laser cutter, are available in a desktop size and able to build the material objects from the digital designs. The overarching aim here is to understand requirements, capacities and challenges of the digital fabrication. From Kinetogami system, we envision a general class of polyhedral primitives to be established for

building multi-loop(s) structures / mechanisms with any pre-synthesized shapes. We also envision the functional materials with programmed configurations, which will require studies in material compatibility, stimuli-driven reactive materials, and novel integrative manufacturing processes. For example, many pre-programmed functional sheets will be printed and self-configured, and then fit together like 3D puzzle pieces to form a larger device, such as the spherical robot. Depending on the scale of the end device, various stages of design and assembly may be required.

Substrates (2.5 D) may be manufactured using ink jet printing or cut from sheet materials using laser cutting. Directly printing conductors on our substrate constructions is possible using existing techniques with adaptations. Conductors will be directly printed on the substrate by screen printing, ink-jet printing, or selective wetting of pre-patterned surfaces (patterned by composition or texture via lithography, sputtering, and/or vapor deposition). Similarly, pneumatic lines can directly be printed. The compliance/stretchability at the joints in order to enable folding and compound folds material requires studies of combinations of fibrous substrates, fabrics and elastomers. Such combinations include naturally bonding materials (such as silicone-based glass fibers and elastomers), mechanically bonding materials (fabrics and elastomers), and adhesively bonded materials (using chemical or textural modification to surfaces).

7.2.2 Integration of Kinetogami and RevoMaker

For the models where large protruding features cover around the geometry, it is difficult to resolve the support-free printing using a single polyhedral base. We envision the multi-polyhedral base generation for better approximation. In doing so, the overhanging features on a model can be further partitioned and eliminated while printing over more polyhedral facets. Furthermore, given an input model that requires degrees-of-freedom between different body sections, a single or multiple hinged BSU ring can be constructed initially and print head completes “coating” the geometries

afterwards around the whole assembly. This also allows the additional functions to be encapsulated independently inside multiple enclosures. For those functional products where the battery or other actuation components requires frequent replacing, our Revomaker printing process can be modified to leave one surface of the polyhedral base printed with surrounding gaps, so that it can be opened and closed.

7.2.3 Modular-based form and function embedded design

With the increasing prevalence in open source hardware and software, electronics platforms such as the Arduino and the Raspberry Pi, and the more recent emergence of organizations such as Local Motors, the push towards modularity in design is greater than ever. In addition, innovative companies such as Shapeways are already putting custom 3D printed designs into practice with their 3D Design to Order programme.

Ulrich [127] makes the argument for modularity from an organizational standpoint: modular designs for products require a similar modularization of organizations: its division into specialized groups with a narrow focus (p. 138). He argues that this allows for the development of organizational expertise with regards to specific functional elements. This is true from an educational point of view as well: modularity allows for the stratification of subject knowledge into different levels of abstraction. Different levels of modularity allow for movement between different levels of abstraction, which in turn allow designers to develop a deep understanding of the system being designed [128]. The library of hardware functional modules can include pluggable embedded electronics and interconnected mechanical modules. The surrounding printed material covering will act as the active "skin" that senses, receives input and incorporates with the hardware modules through deformable areas and internal channels inside the surfaces. Each functionally-embedded and 3D-printed object can be further modularized and integrated to achieve more advanced functionalities.

Embedded Electronics: Inexpensive embedded platforms such as the Arduino are intended for hobbyist/educational purposes and not for use in actual end products, which is clear from the design choices made by these platforms. For example, they have a relatively large form factor and are designed with the expectation that they will be powered from either a USB port or a wall socket, in a majority of the cases.

Interconnected Mechanical Modules: After a set of electronic modules are housed inside the standardized polyhedral space, designers can further interconnect mechanical building kits in or across bases to enhance the motion and movement functionalities. These kits will be designed involving linkages, joints (revolute, prismatic, and spherical), tighteners, gears, compliant units (springs, dampers) and flexible units. Specific sensory and measurement kits including visual modules (eg. camera units), position modules (eg. infrared sensors), motion modules (eg. accelerometers), temperature modules (eg. thermistors), optical modules and pressure modules can be further studied and embedded.

Active Skins: By providing channels, reentrant and protruding functional features such as push-buttons and snap-fits, external devices such as lights and wind-ups, and external bases will be designed to be able to communicate with the components housed inside, through the slots and holes already added on each of the enclosure facets. It is envisioned that the printed material which covers the polyhedral base could also act as an active "skin" which can sense and receive input through deformable areas "push buttons" built into the "skin" as for example on the computer mouse.

LIST OF REFERENCES

LIST OF REFERENCES

[1] B.G. Winder, S.P. Magleby, and L.L. Howell. Kinematic representations of pop-up paper mechanisms. *Journal of Mechanism and Robotics*, 1(2), 2009.

[2] C. Sung and D. Rus. Foldable joints for foldable robots. *Journal of Mechanism and Robotics*, 7(2), 2015.

[3] J.P. Whitney, P.S. Sreetharan, K.Y. Ma, and R.J. Wood. Pop-up book mems. *Journal of Micromechanics and Microengineering*, 21(11), 2011.

[4] T. Tachi and K. Miura. Rigid-foldable cylinders and cells. *Journal of the International Association for Shell and Spatial Structures(IASS)*, 53(4):217–226, 2012.

[5] S. Felton, M. Tolley, C. Onal, D. Rus, and R. Wood. Robot self-assembly by folding: A printed inchworm robot. In *In Robotics and Automation (ICRA), 2013 IEEE International Conference*, pages 277–282, 2013.

[6] S. Felton, M. Tolley, E. Demaine, D. Rus, and R. Wood. A method for building self-folding machines. *Science*, 345(6197):644–646, 2014.

[7] D.Y. Lee, J.S. Kim, J.J. Park, S.R. Kim, and K.J. Cho. Fabrication of origami wheel using pattern embedded fabric and its application to a deformable mobile robot. In *In Robotics and Automation (ICRA), 2014 IEEE International Conference*, pages 2565–2565, 2014.

[8] R. Niiyama, R. Rus, and S. Kim. Pouch motors: Printable/inflatable soft actuators for robotics. In *In Robotics and Automation (ICRA), 2014 IEEE International Conference*, pages 6332–6337, 2014.

[9] E.M. Arkin, M.A. Bender, E.D. Demaine, M.L. Demaine, J.S.B. Mitchell, S. Sethia, and S.S. Skiena. When can you fold a map? *Computational Geometry*, 29(1):23–46, 2004.

[10] E.D. Demaine, M.L. Demaine, and J.S.B. Mitchell. Folding flat silhouettes and wrapping polyhedral packages: New results in computational origami. *Computational Geometry*, 16:105–114, 1999.

[11] R.J. Lang. Treemaker 4.0: A program for origami design, 1998.

[12] E.D. Demaine and T. Tachi. Origamizer: A practical algorithm for folding any polyhedron. *Manuscript*, 2010.

[13] S. Gray, N. Zeichner, M. Yim, and V.Kumar. A simulator for origami-inspired self-reconfigurable robots. In *5th International Meeting of Origami Science, Mathematics and Education*, pages 323–333, 2011.

[14] K. Miura. The science of miura-ori: A review. In Robert J. Lang, editor, *4th International Meeting of Origami Science, Mathematics and Education*, pages 87–100. A K Peters, 2009.

[15] R. Hoffman. Airbag folding: Origami design application to an engineering problem. In *3rd International Meeting of Origami Science, Mathematics, and Education*, Asilomar, CA, March 2001.

[16] C. Cromvik. *Numerical Folding of Airbags Based on Optimization and Origami*. Master's thesis, Chalmers University of Technology and Göteborg University, Sweden, 2007.

[17] Z. You and K. Kuribayashi. A novel origami stent. In *Proceedings of Summer Bioengineering Conference*, Key Biscayne, FL, 2003.

[18] S. Fischer, K. Drechsler, S. Kilchert, and A. Johnson. Mechanical tests for foldcore base material properties. *Composites: PartA*, 2009.

[19] K.E. Evans. Design of doubly curved sandwich panels with honeycomb cores. *Composite Structures*, 17:95–111, 1991.

[20] K. Saito, S. Pellegrino, and T. Nojima. Manufacture of arbitrary cross-section composite honeycomb cores based on origami techniques. *Journal of Mechanical Design*, 136, 2014.

[21] G. Mullineux, J. Feldman, and J. Matthews. Using constraints at the conceptual stage of the design of carton erection. *Mechanism and Machine Theory*, 45(12):1897–1908, 2010.

[22] L. Simon, B. Arnstein, and R. Gurkewitz. *Modular Origami Polyhedra*. Dover, Toronto, Canada, 1999.

[23] R. Gurkewitz and B. Arnstein. *Multimodular origami polyhedra: archimedeans, buckyballs, and duality*. Dover, New York, 2003.

[24] G.W. Hart. Modular kirigami. In *Proceedings of Bridges*, 2007.

[25] ASTM standard f2792. Standard terminology for additive manufacturing technologies.

[26] E. Incorporated. Measurement science roadmap for metal-based additive manufacturing, 2013.

[27] America Makes. Technology roadmap workshop: Next-gen 3dp metal alloys, 2014.

[28] America Makes. Technology roadmap workshop: Next-gen 3dp ceramic and optical materials, 2014.

[29] America Makes. Technology roadmap workshop: Next-gen 3dp polymers, polymer composites, 2014.

[30] America Makes. Technology roadmap workshop: Next-gen 3dp electronic materials, 2014.

[31] CSC. 3d printing and the future of manufacturing, 2012.

[32] T.T. Wohlers. Wohlers report 2012: Additive manufacturing and 3d printing state of the industry: Annual worldwide progress report, 2012.

[33] T.T. Wohlers. Wohlers report 2012: Additive manufacturing and 3d printing state of the industry: Annual worldwide progress report, 2013.

[34] T.T. Wohlers. Wohlers report 2012: Additive manufacturing and 3d printing state of the industry: Annual worldwide progress report, 2014.

[35] C.W. Hull. Apparatus for production of three-dimensional objects by stereolithography, March 1986.

[36] C.R. Deckard. Method and apparatus for producing parts by selective sintering, September 1989.

[37] S.S. Crump. Apparatus and method for creating three-dimensional objects, June 1992.

[38] E.M. Sachs, J.S. Haggerty, M.J. Cima, and P.A. Williams. Three-dimensional printing techniques, April 1993.

[39] J.P. Kruth. Material incress manufacturing by rapid prototyping techniques. *CIRP Annals-Manufacturing Technology*, 40(2):603–614, 1991.

[40] H. Koukka. The rp family tree.

[41] C.B. Williams, F. Mistree, and D.W. Rosen. A functional classification framework for the conceptual design of additive manufacturing technologies. *Journal of Mechanical Design*, 133(12):121002, 2011.

[42] K.J. De Laurentis, F.F. Kong, and C. Mavroidis. Procedure for rapid fabrication of non-assembly mechanisms with embedded components. In *In ASME 2002 international design engineering technical conferences and computers and information in engineering conference*, pages 1239–1245, 2002.

[43] N.A. Meisel, A.M. Elliott, and C.B. Williams. A procedure for creating actuated joints via embedding shape memory alloys in polyjet 3d printing. *Journal of Intelligent Material Systems and Structures*, 2014.

[44] E. Aguilera, J. Ramos, D. Espalin, F. Cedillos, D. Muse, R. Wicker, and E. MacDonald. 3d printing of electro mechanical systems. In *In 25th annual international solid freeform fabrication symposium*, pages 950–961, 2013.

[45] M. Goldberg. Polyhedral linkages. *National Mathematics Magazine*, 16(7):323–332, 1942.

[46] H.F. Verheyen. Expandable polyhedral structures based on dipolygonids. In *Proceedings of 3rd International Conference of Space Structures*, 1984.

[47] H.F. Verheyen. The complete set of jitterbug transformers and the analysis of their motion. *Computers Math Application*, 17(1).

[48] H. Stachel. The heureka-polyhedron. *In Fejes Tóth, G.(ed.): Intuitive Geometry. Colloq. Math. Soc. János Bolyai*, 63:447–459, 1994.

[49] C. Hoberman. Geared expanding structures, 2004.

[50] T. Laliberté and C.M. Gosselin. Polyhedra with articulated faces. In *Proceedings of 12th IFToMM World Congress*, 2007.

[51] G.W. Wei and J. Dai. Synthesis and construction of a family of one-dof highly overconstrained deployable polyhedral mechanisms (dpms). In *Proceedings of ASME 2012 IDETC/CIE*, 2012.

[52] S.T. Griffith. *Growing Machines*. PhD thesis, MIT, MA, USA, 2004.

[53] K.C. Cheung, E.D. Demaine, J. Bachrach, and S.T. Griffith. Programmable assembly with universally foldable strings (moteins). *IEEE Transaction on Robotics*, 27(4):718–729, 2011.

[54] E.D. Demaine, M.L. Demaine, J.F. Lindy, and D.L. Souvaine. Hinged dissection of polypolyhedra. *Lecture Notes in Computer Science*, 3608:205–217, 2005.

[55] E.D. Demaine, M.L. Demaine, D. Eppstein, G.N. Frederickson, and E. Friedman. Hinged dissection of polyominoes and polyforms. *Computational Geometry: Theory and Applications*, 31(3):237–262, 2005.

[56] K. Gilpin, K. Kotay, D. Rus, and L. Vasilescu. Miche: Modular shape formation by self-disassembly. *The International Journal of Robotics Research*, 27(3):345–372, 2008.

[57] Y.G. Ke, L. Ong, W.M. Shih, and P. Yin. Three-dimensional structures self-assembled from dna bricks. *Sience*, 338(6111):1177–1183, 2012.

[58] R.J. Milgram. Surgery with coefficients. *The Annals of Mathematics*, 100(2):194–248, 1974.

[59] P. Schatz. Rhythmusforschung und technik. *Stuttgart: Verlag Freies Geistesleben*, 1998.

[60] D. Sehattsehneide and W. Walker. *M.C.Eseher Kalerdoeycels*. BallantineBooks, NewYork, 1977.

[61] Y. Chen, Z. You, and T. Tarnai. Threefold-symmetric bricard linkages for deployable structures. *International Journal of Solids and Structures*, 42(8):2287–2301, 2005.

[62] E.J. Baker. An analysis of bricard linkages. *Mechanism and Machine Theory*, 15:267–286, 1980.

[63] Y. Chen and Z. You. Spatial overconstrained linkages - the lost jade. *History of Mechanism and Machine Science*, 15:535–550, 2012.

[64] W. Gao, K. Ramani, and R.J. Cipra. Reconfigurable foldable spatial mechanisms and robotic forms inspired by kinetogami. In *Proceedings of the ASME 2012 IDETC/CIE*, Chicago, IL, 2012.

[65] P.N. Sheth and J.J. Uicker. A generalized symbolic notation for mechanisms. *Journal of Engineering for Industry*, 93:102–112, 1971.

[66] P.A. Chebychev. Théorie des mécanismes connus sous le nom de parallélogrammes, 2éme partie. In *Mémoires présentés à l'Académie imperiale des sciences de Saint-Pétersbourg par divers savants*, 1869.

[67] M. Grübler. *Getriebelehre: Eine Theorie Des Zwanglaufes Und Der Ebenen Mechanismen*. Springer, Berlin, 1917.

[68] K.H. Hunt. *Kinematic Geometry of Mechanisms*. Oxford University Press, Oxford, 1978.

[69] H. Lipson and M. Kurman. *Fabricated, the new world of 3D printing*. Wiley, 2013.

[70] K. Vidimče, S.P. Wang, J.R. Kelley, and W. Matusik. Openfab: A programmable pipeline for multi-material fabrication. 32, 2013.

[71] N. Oxman, E. Tsai, and M. Firstenberg. Digital anisotropy: A variable elasticity rapid prototyping platform. 7, 2012.

[72] B.H. Kang, J.T. Wen, N.G. Dagalakis, and J.J. Gorman. Analysis and design of parallel mechanisms with flexure joints. In *In Proceedings of IEEE International Conference on Robotics and Automation*, April 2004.

[73] T. Murata, S. Kurokawa, E. Yoshida, H. Kurokawa, and S. Kokaji. Self-reconfigurable robot-module design and simulation. In *Proceedings of 6th International Conference on Intelligent Autonomous Systems*, pages 911–917, 2000.

[74] S.A. Zotov, M.C. Rivers, A.A. Trusov, and A.M. Shkel. Chip-scale imu using folded-mems approach. *IEEE Sensors*, pages 1043–1046, 2010.

[75] S. Miyashita, S. Guitron, M. Ludersdorfer, C. Sung, and D. Rus. An untethered miniature origami robot that self-folds, walks, swims, and degrades. In *IEEE International Conference on Robotics and Automation (ICRA)*, 2015.

[76] E. Hawkes, B. An, Nadia M. Benbernou, H. Tanaka, S. Kim, E.D. Demaine, D. Rus, and Robert J. Wood. Programmable matter by folding. *Proceedings of the National Academy of Sciences*, 107(28):12441–12445, 2010.

[77] J. Paik, R. Kramer, and R.J. Wood. Stretchable circuits and sensors for robotic origami. In *Proceedings of IEEE/RSJ International Conference on Intelligent Robots and Systems*, San Francisco, CA, 2011.

[78] R.V. Martinez, C.R. Fish, X. Chen, and G.M. Whitesides. Elastomeric origami: programmable paper-elastomer composites as pneumatic actuators. *Advanced Functional Material*, 22:1376–1384, 2012.

[79] M.A.C. Stuart, W.T.S. Huck, J. Genzer, M. Muler, C. Ober, M. Stamm, G.B. Sukhorukov, V.V. Tsukruk I. Szleifer, M. Urban, F. Winnik, S. Zauscher, I. Luzinov, and S. Minko. Emerging applications of stimuli-responsive polymer materials. *Nature Materials*, 9:101–113, 2010.

[80] J. Koh and K. Cho. Omegabot: Crawling robot inspired by ascotis selenaria. In *Proc. IEEE International Conference on Robotics and Automation (ICRA'10)*, pages 109–114, Alaska, USA, 2010.

[81] T. Fukuda and S. Nakagawa. Approach to the dynamically reconfigurable robotic system. In *Proceedings of IEEE International Conference on Robotics and Automation*, volume 3, pages 1581–1586, 1988.

[82] S. Curtis, M. Brandt, G. Bowers, G. Brown, C. Cheung, C. Cooperider, M. Desch, N. Desch, J. Dorband, K. Gregory, K. Lee, A. Lunsford, F. Minetto, W. Truszkowski, R. Wesenberg, J. Vranish, M. Abrahantes, P. Clark, T. Capon, M. Weaker, R. Watson, P. Olivier, M.L. Rilee, and Greenbelt NASA Goddard Space Flight Center. Tetrahedral robotics for space exploration. *Aerospace and Electronic Systems Magazine, IEEE*, 22:22–30, 2007.

[83] S. Murata, E. Yoshida, A. Kamimura, H. Kurokawa, K. Tomita, and S. Kokaji. M-tran: Self-reconfigurable modular robotic system. *IEEE/ASME Transactions on Mechatronics*, 7:431–441, 2002.

[84] M.W. Jorgensen, E.H. Ostergaard, and H.H. Lund. Modular atron: modules for a self-reconfigurable robot. *Intelligent Robots and Systems*, 2:2068–2073, 2004.

[85] R. Pfeifer, M. Lungarella, and F. Lida. Self-organization, embodiment, and biologically inspired robotics. *Science*, 318:1088–1093, 2007.

[86] R.E. Ritzmann, R.D. Quinn, J.T. Watson, and S.N. Zill. Insect walking and biorobotics: A relationship with mutual benefits. *BioScience*, 50(1):23–33, 2000.

[87] C. Ferrell. Robust and adaptive locomotion of an autonomous hexapod. In *Proceedings From Perception to Action Conference*, pages 66–77, 1994.

[88] D.L. Jindrich and R.J. Full. Dynamic stabilization of rapid hexapedal locomotion. *The Journal of Experimental Biology*, 205:2803–2823, 2002.

[89] C.J. Robinson, B. Stucker, A. Lopes, R. Wicker, and J. Palmer. Integration of direct-write (dw) and ultrasonic consolidation (uc) technologies to create advanced structures with embedded electrical circuitry. In *Proc. Proceedings of the 17th Solid Freeform Fabrication Symposium*, pages 60–69, 2006.

[90] J. Casanova, J. Taylor, and J. Lin. Design of a 3-d fractal heatsink antenna. *Antennas and Wireless Propagation Letters, IEEE*, 9:1061–1064, 2010.

[91] S. Castillo, D. Muse, F. Medina, E. MacDonald, and R. Wicker. Electronics integration in conformal substrates fabricated with additive layered manufacturing. In *Proceedings of the 20th Annual Solid Freeform Fabrication Symposium*, pages 730–737, 2009.

[92] F. Medina, A.J. Lopes, A.V. Inamdar, R. Hennessey, J.A. Palmer, B.D. Chavez, and R.B. Wicker. Integrating multiple rapid manufacturing technologies for developing advanced customized functional devices. In *Rapid prototyping & manufacturing 2005 conference proceedings*, pages 10–12, 2005.

[93] K.B. Perez and C.B. Williams. Characterization of in-situ conductive paste extrusion on polyjet substrates. In *International solid freeform fabrication symposium, Austin (TX)*, 2014.

[94] S.B. Kesner and R.D. Howe. Design principles for rapid prototyping forces sensors using 3-d printing. *Mechatronics, IEEE/ASME Transactions On*, 16(5):866–870, 2011.

[95] M. Melzer, D. Karnaushenko, D. Makarov, L. Baraban, A. Calvimontes, I. Mönch, R. Kaltofen, Y.F. Mei, and O.G. Schmidt. Elastic magnetic sensor with isotropic sensitivity for in-flow detection of magnetic objects. *RSC Advances*, 2(6):2284–2288, 2012.

[96] K. Sun, T.S. Wei, B. Ahn, J. Seo, S.J. Dillon, and J.A. Lewis. 3d printing of interdigitated li-ion microbattery architectures. *Advanced Materials*, 25(33):4539–4543, 2013.

[97] E. Malone, M. Berry, and H. Lipson. Freeform fabrication and characterization of zn-air batteries. *Rapid Prototyping Journal*, 14(3):128–140, 2008.

[98] W.M. Wang, T.F.Y. Wang, Z.W. Yang, L.G. Liu, X. Tong, W.H. Tong, J.S. Deng, F.L. Chen, and X.P. Liu. Cost-effective printing of 3d objects with skin-frame structures. *ACM Trans. Graph.*, 32(6):177:1–177:10, November 2013.

[99] L. Lu, A. Sharf, H.S. Zhao, Y. Wei, Q.N. Fan, X.L. Chen, Y. Savoye, C.H. Tu, D. Cohen-Or, and B.Q. Chen. Build-to-last: Strength to weight 3d printed objects. *ACM Trans. Graph.*, 33(4):97:1–97:10, July 2014.

[100] P. Alexander, S. Allen, and D. Dutta. Part orientation and build cost determination in layered manufacturing. *Computer-Aided Design*, 30(5):343 – 356, 1998.

[101] K. Thrimurthulu, P.M. Pandey, and N.V. Reddy. Optimum part deposition orientation in fused deposition modeling. *International Journal of Machine Tools and Manufacture*, 44(6):585 – 594, 2004.

[102] J. Vanek, J.A.G. Galicia, and B. Benes. Clever support: Efficient support structure generation for digital fabrication. *Computer Graphics Forum*, 33(5):117–125, 2014.

[103] J. Dumas, H. Jean, and L. Sylvain. Bridging the gap: automated steady scaffoldings for 3d printing. *ACM Transactions on Graphics (TOG)*, 33(4):98, 2014.

[104] R. Schmidt and N. Umetani. Branching support structures for 3d printing. In *ACM SIGGRAPH 2014 Studio*, SIGGRAPH '14, pages 9:1–9:1, New York, NY, USA, 2014. ACM.

[105] K.L. Hu, S. Jin, and C.C.L. Wang. Support slimming for single material based additive manufacturing. *Computer-Aided Design*, 65(0):1 – 10, 2015.

[106] X. Song, Y. Pan, and Y. Chen. Development of a low-cost parallel kinematic machine for multidirectional additive manufacturing. *Journal of Manufacturing Science and Engineering*, 137(2):021005, 2015.

[107] Y. Pan, C. Zhou, Y. Chen, and J.P. Partanen. Fabrication of conformal ultrasound transducer arrays and horns based on multi-axis cnc accumulation. In *ASME 2011 International Manufacturing Science and Engineering Conference*, pages 39–48. American Society of Mechanical Engineers, 2011.

[108] R. Merz, F.B. Prinz, K. Ramaswami, M. Terk, and L. Weiss. *Shape deposition manufacturing*. Engineering Design Research Center, Carnegie Mellon Univ., 1994.

[109] S. Mueller, S. Im, S. Gurevich, A. Teibrich, L. Pfisterer, F. Guimbretière, and P. Baudisch. Wireprint: 3d printed previews for fast prototyping. In *Proceedings of the 27th Annual ACM Symposium on User Interface Software and Technology*, UIST '14, pages 273–280, New York, NY, USA, 2014. ACM.

[110] S. Mueller, T. Mohr, K. Guenther, J. Frohnhofen, and P. Baudisch. fabrickation: Fast 3d printing of functional objects by integrating construction kit building blocks. In *CHI '14 Extended Abstracts on Human Factors in Computing Systems*, pages 187–188, New York, NY, USA, 2014. ACM.

[111] D. Beyer, S. Gurevich, S. Mueller, H.T. Chen, and P. Baudisch. Platener: Low-fidelity fabrication of 3d objects by substituting 3d print with laser-cut plates. In *In Proceedings of CHI '15*.

[112] C.J. Hansen, R. Saksena, D.B. Kolesky, J.J. Vericella, S.J. Kranz, G.P. Muldowney, K.T. Christensen, and J.A. Lewis. High-throughput printing via microvascular multinozzle arrays. *Advanced Materials*, 25(1):96–102, 2013.

[113] V. Kumar, S. Rajagopalan, M. Cutkosky, and D. Dutta. Representation and processing of heterogeneous objects for solid freeform fabrication. In *IFIP WG5. 2 Geometric Modeling Workshop*, pages 7–9, 1998.

[114] R. Prévost, E. Whiting, S. Lefebvre, and O. Sorkine-Hornung. Make it stand: Balancing shapes for 3d fabrication. *ACM Trans. Graph.*, 32(4):81:1–81:10, July 2013.

[115] N. Umetani and R. Schmidt. Cross-sectional structural analysis for 3d printing optimization. *SIGGRAPH Asia*, page 5, 2013.

[116] M. Alam, C. Mavroidis, N. Langrana, and P. Bidaud. Mechanism design using rapid prototyping. In *Proceedings of the 10th World Congress on the Theory of Machines and Mechanisms*, pages 930–938, 1999.

[117] C. Mavroidis, K.J. DeLaurentis, J. Won, and M. Alam. Fabrication of non-assembly mechanisms and robotic systems using rapid prototyping. *Journal of Mechanical Design*, 123(4):516–524, 2001.

[118] B. Koo, W. Li, J.X. Yao, M. Agrawala, and N.J. Mitra. Creating works-like prototypes of mechanical objects. *ACM Transactions on Graphics (TOG)*, 33(6):217, 2014.

[119] J. Calì, D.A. Calian, C. Amati, R. Kleinberger, A. Steed, J. Kautz, and T. Weyrich. 3d-printing of non-assembly, articulated models. *ACM Trans. Graph.*, 31(6):130:1–130:8, November 2012.

[120] M. Bächer, B. Bickel, D.L. James, and H. Pfister. Fabricating articulated characters from skinned meshes. *ACM Trans. Graph.*, 31(4):47:1–47:9, July 2012.

[121] S. Singare, Y.X. Liu, D.C. Li, B.H. Lu, J. Wang, and S. He. Individually prefabricated prosthesis for maxilla reconstruction. *Journal of Prosthodontics*, 2007.

[122] Z. Wang, Y. Teng, and D.C. Li. [fabrication of custom-made artificial semiknee joint based on rapid prototyping technique: computer-assisted design and manufacturing]. *Zhongguo xiu fu chong jian wai ke za zhi= Zhongguo xiufu chongjian waike zazhi= Chinese journal of reparative and reconstructive surgery*, 18(5):347–351, 2004.

[123] M.Y. Lee, C.C. Chang, and Y.C. Ku. New layer-based imaging and rapid prototyping techniques for computer-aided design and manufacture of custom dental restoration. *Journal of medical engineering & technology*, 32(1):83–90, 2008.

[124] K. Hildebrand, B. Bickel, and M. Alexa. Orthogonal slicing for additive manufacturing. *Computers & Graphics*, 37(6):669–675, 2013.

[125] R.Z. Hu, H.H. Li, H. Zhang, and D. Cohen-Or. Approximate pyramidal shape decomposition. *ACM Transactions on Graphics (TOG)*, 33(6):213, 2014.

[126] U. Chebrolu, P. Kumar, and J.S.B. Mitchell. On finding large empty convex bodies in 3d scenes of polygonal models. In *Computational Sciences and Its Applications, 2008. ICCSA '08. International Conference on*, pages 382–393, June 2008.

[127] K. Ulrich. The role of product architecture in the manufacturing firm. *Research policy*, 24(3):419–440, 1995.

[128] B. Victor. Up and down the ladder of abstraction: A systematic approach to interactive visualization. *Kill Math*, 2011.

VITA

VITA

Wei Gao was born in Shanghai, China on April 24, 1987. He majored in Mechanical Engineering at University of Shanghai for Science and Technology in China, where he received his Bachelor of Science degree in June 2009. During his undergraduate study, he obtained the national patent for invention of the PRC as the first inventor, called "Automobile Chair Auxiliaries for Handicapped People" (filed in 2010). Wei Gao came to Purdue University in August 2009. At Purdue, his research interests include front-end robotic system design and additive manufacturing of functional objects. His research projects involve design, simulation and prototyping of foldable, reconfigurable mechanisms and robotic systems. He also led the project of developing a novel FDM-based 3D printing technique and built a self-contained appliances that allows printing fully-functional objects (customizable products, articulated working models, self-actuated devices). While working on his Ph.D. research project, he also served as an instructor and teaching assistant in several undergraduate and graduate courses, including ME352 and ME553. The following is the list of my publications during my research study at Purdue:

1. W. Gao, Y.B. Zhang, D.C. Nazzetta, K. Ramani, and R.J. Cipra. RevoMaker: Enabling multi-directional and functionally-embedded 3D printing using a rotational cuboidal platform. In Proceedings of User Interface Software and Technology (UIST'15), 2015.

2. W. Gao, Y.B. Zhang, D. Ramanujan, K. Ramani, Y. Chen, C. Williams, C. Wang, Y.C. Shin, S. Zhang, and P.D. Zavattieri. The status, challenges, and future of additive manufacturing in engineering. Computer-Aided Design, *doi* : 10.1016/*j.cad*.2015.04.001, 2015.

3. W. Gao, K. Huo, J.S. Seehra, K. Ramani, and R.J. Cipra. HexaMorph, a reconfigurable and foldable hexapod robot inspired by Origami. IEEE/RSJ International Conference on Intelligent Robots and Systems (IROS'14), 2014.

4. W. Gao, K. Ramani, R.J. Cipra, and T. Siegmund. Kinetogami, a reconfigurable, combinatorial and printable sheet folding. ASME Journal of Mechanical Design, 135(11), 2013

5. C.K. Senthil, K. Ramani, R.D. Sriram, I. Horváth, A. Bernard, R.F. Harik, and W. Gao. The evolution, challenges, and future of knowledge representation in product design systems. Computer-aided design 45, No. 2, 204-228, 2013.

6. W. Gao and K. Ramani, and R.J. Cipra, R.J. Reconfigurable foldable spatial mechanisms and robotic forms inspired by Kinetogami. Proceedings of the ASME 2012 International Design Engineering Technical Conferences, Paper No. DETC2012-71403, Chicago, August, 2012.

7. W. Gao, K. Ramani. Kaleidogami: Multi-Primitive Reconfigurable Artistic Structures. Shape Modeling International, Fabrication and Sculpting Event (FASE), 2012.